

3D PATTERNED CARDIAC TISSUE CONSTRUCT FORMATION USING
BIODEGRADABLE MATERIALS

A THESIS SUBMITTED TO
THE GRADUATE SCHOOL OF NATURAL AND APPLIED SCIENCES
OF
MIDDLE EAST TECHNICAL UNIVERSITY

BY

HALİME KENAR

IN PARTIAL FULFILLMENT OF THE REQUIREMENTS
FOR
THE DEGREE OF DOCTOR OF PHILOSOPHY
IN
BIOTECHNOLOGY

DECEMBER 2008

Approval of the thesis:

**3D PATTERNED CARDIAC TISSUE CONSTRUCT FORMATION USING
BIODEGRADABLE MATERIALS**

submitted by **HALİME KENAR** in partial fulfillment of the requirements for the
degree of **Doctor of Philosophy in Department of Biotechnology, Middle East
Technical University** by,

Prof. Dr. Canan Özgen
Dean, Graduate School of **Natural and Applied Sciences**

Prof. Dr. Gülay Özcengiz
Head of Department, **Biotechnology**

Prof. Dr. Vasıf Hasırcı
Supervisor, **Biological Sciences Dept., METU**

Assoc. Prof. Dr. Gamze Torun Köse
Co-Supervisor, **Genetics and Bioengineering Dept.,
Yeditepe Univ.**

Examining Committee Members:

Prof. Dr. Mesude İşcan
Biological Sciences Dept., METU

Prof. Dr. Vasıf Hasırcı
Biological Sciences Dept., METU

Prof. Dr. Banu Onaral
Biomedical Engineering Dept., Drexel Univ., USA

Prof. Dr. Aykut Özkul
Dept. of Virology, Vet. Med. Fac., Ankara Univ.

Assoc. Prof. Dr. Ayşe Gül Gözen
Biological Sciences Dept., METU

Date: 30.12.2008

I hereby declare that all information in this document has been obtained and presented in accordance with academic rules and ethical conduct. I also declare that, as required by these rules and conduct, I have fully cited and referenced all material and results that are not original to this work.

Name, Last name: Halime Kenar

Signature:

ABSTRACT

3D PATTERNED CARDIAC TISSUE CONSTRUCT FORMATION USING BIODEGRADABLE MATERIALS

Kenar, Halime

Ph.D., Department of Biotechnology

Supervisor: Prof. Dr. Vasif Hasircı

Co-Supervisor: Assoc.Prof. Dr. Gamze Torun Köse

December 2008, 153 pages

The heart does not regenerate new functional tissue when myocardium dies following coronary artery occlusion, or is defective. Ventricular restoration involves excising the infarct and replacing it with a cardiac patch to restore the heart to a more efficient condition. The goal of this study was to design and develop a myocardial patch to replace myocardial infarctions. A basic design was developed that is composed of 3D microfibrinous mats that house mesenchymal stem cells (MSCs) from umbilical cord matrix (Wharton's Jelly) aligned parallel to each other, and biodegradable macroporous tubings to supply growth media into the structure.

Poly(glycerol sebacate) (PGS) prepolymer was synthesized and blended with P(L-D,L)LA and/or PHBV, to produce aligned microfiber (dia 1.16 - 1.37 μm) mats and macroporous tubings. Hydrophilicity and softness of the polymer blends were found to be improved as a result of PGS introduction. The Wharton's Jelly (WJ) MSCs were characterized by determination of their cell surface antigens with flow cytometry and by differentiating them into cells of mesodermal lineage (osteoblasts, adipocytes, chondrocytes). Cardiomyogenic differentiation potential of WJ MSCs in presence of differentiation factors was studied with RT-PCR and

immunocytochemistry. WJ MSCs expressed cardiomyogenic transcription factors even in their undifferentiated state. Expression of a ventricular sarcomeric protein was observed upon differentiation. The electrospun, aligned microfibrinous mats of PHBV-P(L-D,L)LA-PGS blends allowed penetration of WJ MSCs and improved cell proliferation. To obtain the 3D myocardial graft, the WJ MSCs were seeded on the mats, which were then wrapped around macroporous tubings. The 3D construct (4 mm x 3.5 cm x 2 mm) was incubated in a bioreactor and maintained the uniform distribution of aligned cells for 2 weeks. The positive effect of nutrient flow within the 3D structure was significant.

This study represents an important step towards obtaining a thick, autologous myocardial patch, with structure similar to native tissue and capability to grow, for ventricular restoration.

Keywords: Mesenchymal stem cells, Wharton's Jelly, cardiac tissue engineering, cell alignment, 3D scaffold.

ÖZ

BİYOBOZUNUR MALZEMELERDEN ÜÇ BOYUTLU, YÖNLENDİRİLMİŞ KALP KAS DOKUSU OLUŞTURULMASI

Kenar, Halime

Doktora, Biyoteknoloji Bölümü

Tez Yöneticisi: Prof. Dr. Vasıf Hasırcı

Ortak Tez Yöneticisi: Doç. Dr. Gamze Torun Köse

Aralık 2008, 153 sayfa

Kalp, koroner damar tıkanıklığı sonucu ölen veya özürlü olan kalp kası dokusunu yenileme yetisine sahip değildir. Ventriküler restorasyon ölü dokunun kesilip çıkarılması ve kalbin daha verimli çalışır hale getirilmesi için yerine kalp greftinin yerleştirilmesini içerir. Bu çalışmanın amacı, ölü kalp kasının yerine geçebilecek kalp kası grefti tasarlamak ve geliştirmektir. Temel olarak, birbirine paralel yönlendirilmiş kordon dokusu (Wharton Jeli) mezenşimal kök hücreleri (MKHleri) içeren üç boyutlu mikrofiber taşıyıcılar ve bu hücrelere besiyeri sağlayacak biyobozunur makrogözenekli borucuklardan oluşan bir yapı tasarlanmıştır.

Yönlendirilmiş mikrofiber (çap: 1.16 - 1.37 μm) taşıyıcılar ve makro gözenekli borucukların yapımında kullanılmak üzere poli(gliserol sebasat) (PGS) prepolimeri sentezlenmiş ve P(L-D,L)LA ve/veya PHBV ile karışımları oluşturulmuştur. PGS eklenmesi sonucu polimerik karışımların hidrofilisitesinin ve yumuşaklığının arttığı görülmüştür. Wharton Jeli (WJ) MKHleri, akım sitometresi ile hücre yüzey antijenlerinin belirlenmesi ve mezodermal kökenli hücrelere

(osteoblast, adiposit, kondrosit) farklılaştırılmaları yoluyla karakterize edilmiştir. WJ MKHlerin büyüme faktörleri varlığında kalp kası hücrelerine farklılaşma potansiyelleri RT-PCR ve immünohistokimya ile çalışılmıştır. WJ MKHlerinin farklılaştırılmamış halde bile kardiyomyojenik transkripsiyon faktörlerini ürettiği belirlenmiştir. Farklılaşma sonucu ventriküler sarkomer proteini üretimi gözlenmiştir. Elektro-eğirme yöntemiyle hazırlanmış yönlendirilmiş mikrofiber PHBV-P(L-D,L)LA-PGS taşıyıcılar, WJ MKHlerin yapıya nüfuz etmelerine imkan sağlamış ve hücre çoğalmasını geliştirmiştir. Üç boyutlu kalp kası greftinin elde edilmesi amacıyla WJ MKHleri mikrofiber taşıyıcılara ekilmiş ve bu yapılar makrogözenekli borucuklar etrafına sarılmıştır. Üç boyutlu yapı (4 mm x 3.5 cm x 2 mm) biyoreaktör içinde inkübe edilmiş ve iki hafta boyunca yönlendirilmiş hücrelerin homojen dağılımını korumuştur. Besiyerinin üç boyutlu yapının içinden akışının belirgin pozitif etkisi görülmüştür.

Bu çalışma, ventriküler restorasyonda kullanılabilecek, yapıcı doğal dokuya özdeş ve büyüeyebilen, kalın, otolog kalp kası greftinin elde edilmesi yolunda önemli bir adımı teşkil etmektedir.

Anahtar Kelimeler: Mezenşimal kök hücreler, Wharton's Jelly, kalp doku mühendisliği, hücre yönlendirilmesi, 3 boyutlu taşıyıcı.

To my family...

ACKNOWLEDGMENTS

I would like to express my special thanks to my supervisor Prof. Dr. Vasıf Hasırcı for his continuous guidance, encouragement, motivation and support during all the stages of my thesis. I sincerely appreciate the time and effort he has spent to improve my experience during my graduate years.

My deep thanks are to my co-advisor Assoc. Prof. Dr. Gamze Torun Köse for her continuous support, help and encouragement throughout all the stages of my graduate years.

I am also deeply thankful to Prof. Dr. David Kaplan (Tufts U., TERC, Boston, MA) and Prof. Dr. Mehmet Toner (Mass General Hospital, CEM, Boston, MA) for giving an opportunity to study in their labs for a year, for their support to my thesis, leadership and guidance.

I wish to express my sincere gratitude to Prof. Nesrin Hasırcı for her help and guidance in polymer synthesis and characterization.

I am grateful to Prof. Dr. Claudio Migliaresi, Assist. Prof. Dr. Antonella Motta, Erika Bella and Prof. Dr. Heinz Redl and Florian Hildner for giving an opportunity to learn about electrospinning and isolation of Wharton's Jelly at Trento University, Italy and Ludwig Boltzmann Institute, Austria, respectively.

My sincere acknowledgements go to my thesis progress committee members, Prof. Dr. Mesude İşcan and Prof. Dr. Aykut Özkul for their helpful comments and suggestions throughout this thesis.

I would like to thank to Deniz Yücel for being my perfect research partner and invaluable friend, and for the good memories we have.

I would like to express my gratefulness to my special friends Aysel Kızıltay and Tuğba Endoğan for their continuous help in the experiments, for sleepless nights during PGS synthesis, motivation and support.

I deeply thank Dr. Palaniappan Sethu, Dr. Natesh Parashurama, Dr. Kevin King, Dr. Sunitha Nagrath, Dr. Aman Russom, Dr. Utkan Demirci, Dr. Xuanhong Cheng, and Octavio Hurtado from MGH, CEM group and Dr. Akira Matsumoto, Dr. Hyeon Joo Kim and Karmen Preda from Tufts U., TERC for their help in the research carried out in Boston, MA and all the members of METU-BIOMAT group and my special lab mates, Hayriye Özçelik, Albana Ndreu, Pınar Yılgör, Nihan Öztürk, Banu Bayyurt, Arda Buyuksungur, Ozge Karadas, Pınar Zorlutuna, Gizem Altay, Erkin Aydın, Buket Basmanav, Beste Kınıkoğlu, Birsen Demirbağ, Gökhan Bahçecioğlu, Sinem Kardeşler and our special undergrad student Halenur Yavuz for their help and motivation.

I am grateful to Mr. Zeynel Akın, the most qualified technician I have ever seen, for his technical assistance and guidance throughout all my research years, especially for his help in setting up the electrospinning equipment.

My sincere acknowledgments go to Prof. Dr. Yücel Güngen and Mr. Okay Erişöz from Genel Patoloji Merkezi Ltd. (Ankara) for their help in obtaining cryosections of the tissue engineered 3D construct.

I wish to deeply thank my brother Dr. Necmettin Kenar for his continuous encouragement, patience and help in all the stages of my thesis.

This study was supported by METU-BAP 0108 DPT 2006K 120920-20 and FP6 EU Network of Excellence project EXPERTISSUES, and TUBITAK BİDEB Integrated PhD Program (BDP) and these grants are gratefully acknowledged.

Finally, I would like to express my deepest gratitude to my parents, Nesibe Kenar and Ahmet Kenar, for their understanding, patience, continuous support, love and trust, without which it would not be possible to succeed.

TABLE OF CONTENTS

ABSTRACT.....	iv
ÖZ.....	vi
ACKNOWLEDGMENTS.....	ix
TABLE OF CONTENTS.....	xi
LIST OF TABLES.....	xiv
LIST OF FIGURES.....	xv
LIST OF ABBREVIATIONS.....	xix
CHAPTER	
1. INTRODUCTION.....	1
1.1 Heart: The Pump of Life	1
1.2 Myocardial Diseases	4
1.3 Current Procedures Applied for the Treatment of Myocardial Diseases	7
1.3.1 Prosthetic Materials and Biological Patches	10
1.3.2 Limitations of Currently Used Patches	11
1.4 Criteria of An Ideal Patch.....	12
1.5 Myocardial Tissue Engineering: Regenerating Functional Myocardium	14
1.5.1 Cell Sources.....	14
1.5.2 Scaffold Materials, Types and Biomimicry	20
1.5.3 Bioreactors	27
1.5.5 Key issues in myocardial tissue engineering	28
1.6 The Aim, Novelty and the Approach in This Study.....	31
2. METHODS.....	32
2.1 Synthesis of Poly(glycerol sebacate).....	32
2.2 Characterization of PGS.....	32
2.2.1 Molecular Weight Determination by Gel Permeation Chromatography.....	32
2.3 Preparation of Aligned Microfiber Mats Through Electrospinning.....	33

2.4 Preparation of Macroporous Biodegradable Tubings	35
2.5 Characterization of Polymer Blends	37
2.5.1 Mechanical properties	37
2.5.2 Hydrophilicity	37
2.5.3 Gravimetric Determination of PHBV-P(L-D,L)LA-PGS Aligned Fiber Mat Erosion.....	38
2.6 In Vitro Studies	39
2.6.1 Characterization of Human Wharton's Jelly (hWJ) MSCs in Comparison to MSCs from Human Bone Marrow (hBM) (USA).....	39
2.6.2 hWJ MSC Isolation from Umbilical Cord Matrix and Its Culture (TR)	44
2.6.3 Characterization of hMSCs Isolated from Wharton's Jelly	45
2.6.4 Differentiation of hWJ MSCs to Cardiomyocytes	48
2.7 Tissue Engineering on Microfiber Mats.....	50
2.7.1 Morphology of hWJ MSCs Cultured on the Unaligned and Aligned Microfiber Mats	50
2.7.2 hWJ MSC Proliferation on the Aligned Microfiber Mats.....	51
2.8 Tissue Engineering in a Microbioreactor	52
2.8.1 Microbioreactor Design.....	52
2.8.2 Assembly of the 3D Construct	53
2.8.3 Culture of the 3D Construct in the Microbioreactor	54
2.8.4 Analysis of the 3D Constructs Cultured in the Microbioreactor.....	55
3. RESULTS AND DISCUSSION.....	57
3.1 Poly(glycerol sebacate) (PGS) Polymerization.....	57
3.2 Characterization of PGS.....	60
3.2.1 Molecular Weight Determination by Gel Permeation Chromatography	60
3.2.2 DSC Analysis of PGS Prepolymer.....	61
3.3 Aligned Microfiber Mats Prepared Through Electrospinning	62
3.4 The Macroporous Biodegradable Tubings (Hollow fibers)	65
3.5 Characterization of Polymer Blends	68
3.5.1 Mechanical properties	68
3.5.2 Hydrophilicity	69

3.5.3 Gravimetric Determination of PHBV-P(L-D,L)LA:PGS Aligned Fiber Mat Erosion.....	70
3.6 In Vitro Studies	72
3.6.1 Characterization of Wharton's Jelly MSCs and Their Comparison with MSCs from Human Bone Marrow (USA)	72
3.6.2 Characterization of hMSC Isolated from Wharton's Jelly (TR).....	88
3.6.3 Differentiation of hWJ MSCs to Cardiomyocytes	97
3.7. Tissue Engineering on Microfiber Mats.....	102
3.7.1 Morphology of hWJ MSCs Cultured on the Unaligned and Aligned Fiber Mats.....	102
3.7.2 hWJ MSC Proliferation on the Aligned Microfiber Mats.....	105
3.8. Analysis of the 3D Constructs Cultured in the Microbioreactor.....	107
4. CONCLUSIONS.....	121
5. FUTURE PROSPECTS.....	123
REFERENCES.....	125
APPENDICES	
A. MATERNAL CONSENT.....	147
B. GPC DISTRIBUTION PLOTS.....	148
C. FIBER DIAMETERS OF THE MICROFIBROUS MATS.....	149
D. LOAD- EXTENSION CURVE.....	150
E. WJ MSC PROLIFERATION ON ALIGNED FIBER MATS.....	151
CURRICULUM VITAE.....	152

LIST OF TABLES

TABLES

Table 2.1 The types of microfiber mats obtained by electrospinning	35
Table 2.2 Primers used for RT-PCR.....	43
Table 3.1 Average molecular weights and HI values of PGS prepolymer.....	60
Table 3.2 Tensile mechanical properties of nonporous tubings.	69
Table 3.3 Water contact angles of blend films.	70
Table 3.4 Cell surface antigen expression by BM and WJ MSCs.....	76
Table 3.5 ALP activity of P2 bone marrow and Wharton’s Jelly derived MSCs....	77
Table 3.6 ALP activity of human Wharton’s Jelly derived MSCs.	93
Table 3.7 ALP specific activity of hWJ MSCs taken from culture II.	93
Table 3.8 Cardiac transcription factor expression by hWJ MSCs.....	116
Table C.1 Fiber diameters of microfibrinous mats obtained by electrospinning.....	149
Table E.1 hWJ MSC numbers on aligned fiber mats after 1 and 14 days of culture.....	151

LIST OF FIGURES

FIGURES

Figure 1.1 A healthy heart cross-section	2
Figure 1.2 Cell organization and alignment in myocardium.....	3
Figure 1.3 Heart with muscle damage and blocked artery	5
Figure 1.4 Normal heart and heart with ventricular septal defect	6
Figure 1.5 Proposed intracellular transduction pathways generating cardiomyocytes by different growth factors.....	19
Figure 1.6 Scheme of the present major strategies of cardiac tissue engineering...	24
Figure 1.7 Typical electrospinning setup.	26
Figure 2.1 Electrospinning setup used to obtain aligned microfibrinous mats.....	34
Figure 2.2 Scheme of the bifunctional tubing.	36
Figure 2.3 Water contact angle (\square).....	38
Figure 2.4 Schematic presentation of the WJ MSC isolation procedure.....	45
Figure 2.5 Scheme of the microbioreactor.	52
Figure 2.6 Schematic presentation of the method used to form the 3D construct. .	54
Figure 2.7 Scheme of the growth medium perfused culture of the 3D construct in the microbioreactor.	55
Figure 3.1 FTIR spectrum of Glycerol.....	58
Figure 3.2 IR spectrum of Sebacic Acid	59
Figure 3.3 ATR-FTIR spectra of PGS obtained at different time points during polymerization process.....	59
Figure 3.4 DSC thermogram of PGS prepolymer (24h under vacuum).....	61
Figure 3.5 Electrospun PHBV-P(L-D,L)LA with 1% w/w PGS in Chl:DMF (10:1)	62
Figure 3.6 Electrospun PHBV-P(L-D,L)LA with 2% w/w PGS in Chl:DMF (10:1)	63

Figure 3.7 Electrospun PHBV-P(L-D,L)LA with 4% w/w PGS in Chl:DMF (10:1)	63
Figure 3.8 Electrospun PHBV-P(L-D,L)LA with 1% w/w PGS in Chl:DMF (95:5)	64
Figure 3.9 Electrospun PHBV-P(L-D,L)LA with 2% w/w PGS in Chl:DMF (95:5)	64
Figure 3.10 Electrospun PHBV-P(L-D,L)LA with 4% w/w PGS in Chl:DMF (95:5).	64
Figure 3.11 Stereomicroscope images of P(L,DL)LA-PGS tubings.....	65
Figure 3.12 Biodegradable macroporous tubings (Hollow fibers) obtained from 60% salt (particle diameter 70-125 μ m) solution in P(L,DL)LA:PGS (96:4).	66
Figure 3.13 Biodegradable macroporous tubing (Hollow fiber) obtained from 70% salt (particle diameter 70 μ m or less) solution in P(L,DL)LA:PGS (96:4).....	66
Figure 3.14 Stereomicroscope images of bifunctional P(L-D,L)LA:PGS (96:4) tubings	67
Figure 3.15 Biodegradable macroporous tubing (hollow fiber) obtained from P(L-D,L)LA:PGS dissolved in dioxane	68
Figure 3.16 Weight loss from PHBV-P(L-D,L)LA:PGS aligned-fiber mats incubated in PBS at 37 °C for 120 days.....	71
Figure 3.17 Fluorescence micrographs showing MSCs from (a) human bone marrow (P3), and (b) Wharton's jelly (P6).	73
Figure 3.19 Light microscopy images of human MSCs subjected to adipogenic induction medium for 21 days and subsequently stained with Oil Red O.	79
Figure 3.20 Cardiomyocyte specific gene expression in undifferentiated hWJ and hBM MSCs in comparison to the expression at the human myocardial tissue.....	80

Figure 3.21 Expression of cardiac transcription factors in WJ MSCs (P5) and BM MSCs (P3) induced to differentiate into cardiomyocytes in the presence of growth factors..	85
Figure 3.22 Fluorescence microscopic images of (a, c) BM and (b, d) WJ MSCs cultured for 14 days in cardiomyogenic media (B.Ins and VA) and immunostain for α/β MHC (a, b) and α -actinin (c, d)....	87
Figure 3.23 Light micrographs (10x) of primary culture hWJ MSCs grown for 17 days in PM type I (a,c,e), and PM type II (b, d, f) on TCPS.	89
Figure 3.24 hWJ MSCs morphology revealed by fluorescence microscopy.	90
Figure 3.25 Growth curves of hWJ MSCs grown in two different cell culture media: a) PM type I and b) PM type II on TCPS.....	91
Figure 3.26 Light micrographs of (a, c) undifferentiated WJ MSCs and (b, d) WJ MSCs differentiated to bone, subjected to von Kossa staining	94
Figure 3.27 Fluorescence micrographs of undifferentiated WJ MSCs (a, c) and WJ MSCs differentiated to chondrocytes (b, d) subjected to immunostaining for Collagen Type II.....	96
Figure 3.28 Micrographs of undifferentiated WJ MSCs (a, c) and WJ MSCs differentiated to chondrocytes (b, d) subjected to Alcian blue (a, b) and immunostaining for Collagen Type II (c, d).	97
Figure 3.29 Cardiomyogenic gene expression of undifferentiated WJ MSCs grown in Culture I and Culture II.....	98
Figure 3.30 Cardiomyogenic gene expression by WJ MSCs in the presence of differentiation factors.....	99
Figure 3.31 Fluorescence microscopy images of hWJ MSCs cultured for 14 days. in the presence of cardiomyogenic differentiation factors immunostained for ventricular α/β MHC.....	100
Figure 3.32 Morphology of WJ MSCs cultured for 14 days in the presence of cardiomyogenic differentiation factors, revealed by fluorescence microscopy.	101
Figure 3.33 WJ MSC morphology on unaligned (a) and aligned (b) fiber mats...	103
Figure 3.34 WJ MSC distribution and alignment on PHBV-P(L-D,L)LA:PGS mats (1.5 x 3.5 cm ²) after 14 days of culture.	104

Figure 3.35 hWJ MSC attachment on aligned fiber PHBV-P(L-D,L)LA:PGS mats	105
Figure 3.36 hWJ MSC proliferation on aligned fiber PHBV-P(L-D,L)LA and PHBV-P(L-D,L)LA:PGS (98:2) mats within 14 days.....	106
Figure 3.37 The scanning electron micrographs of WJ MSCs grown on aligned fiber PHBV-P(L-D,L)LA:PGS (98:2) mats for 14 days.	108
Figure 3.38 The confocal micrographs of WJ MSCs grown on aligned fiber PHBV-P(L-D,L)LA:PGS (98:2) mats for 14 days.....	108
Figure 3.39 The confocal micrographs of WJ MSCs grown on aligned fiber mats of PHBV-P(L-D,L)LA:PGS (98:2) for 14 days, with an emphasis on nuclear alignment.	109
Figure 3.40 Retraction of an aligned fiber mat as a result of cell growth on it after 14 days of culture.....	110
Figure 3.41 Static culture of the 3D construct.....	111
Figure 3.42 The perfused 3D construct.....	112
Figure 3.43 SEM images of sections from the 3D construct cultured under static conditions for 6 days.....	113
Figure 3.44 SEM images of sections from the 3D construct cultured under medium. perfused conditions for 6 days.	114
Figure 3.45 Confocal microscopy images of sections from the 3D construct cultured under static conditions for 6 days.....	115
Figure 3.46 Acridine Orange stained cryosections of the 3D constructs from the static culture (a, b, c), and perfused culture (d, e, f). a, b, d, e)....	118
Figure 3.47 Phalloidin and DAPI stained cryosections of the 3D construct from static culture (a, b, c), and perfused culture (d, e, f).....	119
Figure B.1 GPC molecular weight distribution plot of PGS prepolymer polymerized under vacuum for 24h (1 st run). (Mw: 16 727 Da).....	148
Figure D.1 Load-Extension Curve of P(L-D,L)LA-PGS (96:4) tubing, with designations for elastic region, strain hardening and failure point.....	150

LIST OF ABBREVIATIONS

Ab	Antibody
ALP	Alkaline phosphatase
APC	Allophycocyanin
bFGF	basic Fibroblast Growth Factor
BM	Bone Marrow
BSA	Bovine serum albumin
CLCs	Cardiomyocyte-like cells
CLSM	Confocal Laser Scanning Microscope
CMs	Cardiomyocytes
DAPI	4,6-diamidino-2-phenylindole
DMF	N,N-dimethyl formamide
DMEM	Dulbecco's Modified Eagle's Medium
DMSO	Dimethyl sulfoxide
DSC	Differential Scanning Calorimetry
E	Modulus of elasticity (Young's Modulus)
ϵ	Strain
FBS	Fetal bovine serum
ECM	Extracellular matrix
FCS	Fetal Calf Serum
FITC	Fluorescein isothiocyanate
GPC	Gel Permeation Chromatography
HDACs	Histone deacetylases
HI	Heterogeneity index
hMSC	Human Mesenchymal Stem Cell
IBMX	Isobutyl-1-methyl xanthine

MHC	Myosin heavy chain
MSC	Mezenchymal Stem Cell
PNIPAAm	Poly(<i>N</i> -isopropylacrylamide)
PBS	Phosphate buffered saline
PCR	Polymerase Chain Reaction
PDMS	Poly(dimethyl siloxane)
PE	Phycoerythrin
PerCP	Peridin chlorophyll-a
PFA	Paraformaldehyde
PGS	Poly(glycerol sebacate)
PHBV	Poly(3-hydroxybutyrate-co-3-hydroxyvalerate)
PM	primary medium
RGD	Arginine-glycine-aspartic acid
RT-PCR	Reverse Transcription –PCR
TCPS	Tissue Culture Polystyrene
THF	Tetrahydrofuran
UTS	Ultimate tensile strength
WJ	Wharton's Jelly

CHAPTER 1

INTRODUCTION

1.1 Heart: The Pump of Life

The heart is the center of the circulation system and distributes blood throughout the body. The function of the heart is vital to supply oxygen and nutrients to, and remove waste products from the body via the blood in order to maintain the balance that is necessary to sustain life (Vander et al., 1994). It beats an average of 100,000 times and pumps 2,000 gallons of blood throughout the vascular system on a daily basis (<http://www.americanheart.org>).

Strong muscular contractions in the ventricles pump blood out of the heart and into the circulatory system (Fig 1.1). These muscular contractions are produced by the muscle tissue that makes up the walls of the ventricles. Healthy heart muscle wall is composed of three layers: a muscular sheet, the myocardium, lined on either side by two collagenous membranes (containing type I and type III collagen and elastin), the endocardium, which is populated by endothelial cells, and the epicardium, also called visceral pericardium (Van de Graaff, 1998). The myocardium is the layer of functional beating muscle that consists of fibroblasts and highly oriented cardiomyocytes (muscle fibers) in a matrix of collagen.

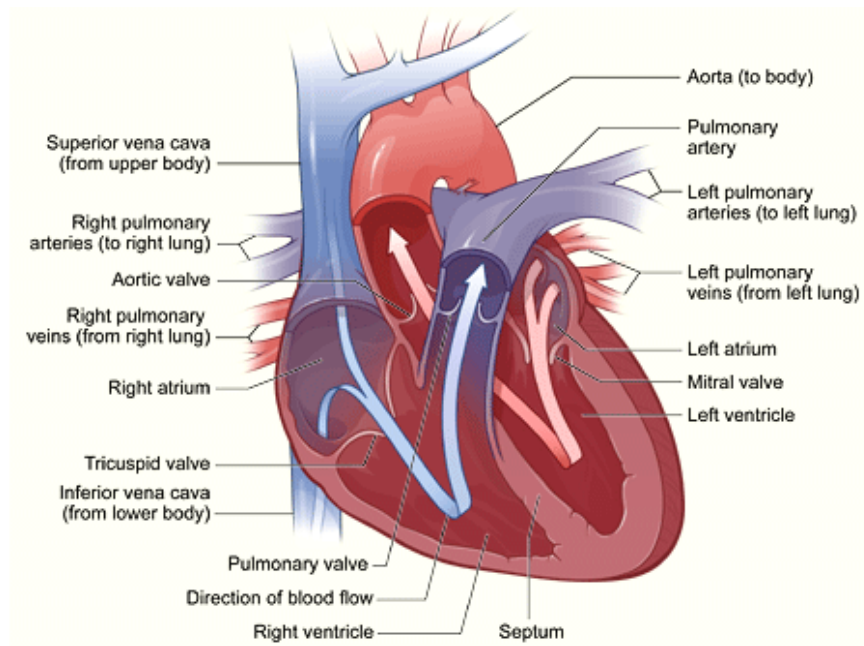


Figure 1.1 A healthy heart cross-section. The blue arrow shows the direction in which oxygen-poor blood flows from the body to the lungs. The red arrow shows the direction in which oxygen-rich blood flows from the lungs to the rest of the body. (http://www.nhlbi.nih.gov/health/dci/Diseases/chd/chd_all.html)

The cardiomyocytes are generally 10–15 μm in diameter and up to 100 μm in length, connected end-to-end in the longitudinal direction (Fig 1.2) and side-to-side in the transverse direction (Parker and Ingber, 2007). The extensive, three-dimensional extracellular matrix (ECM), composed of collagen, elastin bundles and interconnected basement membranes provides a scaffold for cardiomyocytes, fibroblasts and the vasculature to align and build the complex network of the myocardium (Parker and Ingber, 2007). Collagen types I and III are the predominant interstitial collagens in the myocardium that generate structural integrity for the adjoining cardiomyocytes, providing the means by which myocyte shortening is translated into overall ventricular pump function. Basement membrane components include laminin, entactin, fibronectin, collagen type IV, and fibrillin, and proteoglycans include chondroitin sulfate, dermatan sulfate, and heparan sulfate

(Kassiri and Khokha, 2005). The ECM proteins provide the structural foundation for the myocardium, while soluble, matrix-bound, and cell surface proteins deliver molecular cues to the signaling pathways for cardiomyocyte survival and contraction (Kassiri and Khokha, 2005). The cardiomyocytes facilitate conduction of the electrical signals needed to initiate contractile movement in order to pump blood out of the ventricles (Vander et al., 1994). The elementary myocardial functional units are not lone cardiomyocytes but, rather, are multicellular assemblies of these highly oriented cells. The cardiomyocytes are connected with intercalated disks that integrate individual electrical activation and contraction into a pumping action (Fig 1.2). Gap junctions in these intercalated discs allow the action potential to travel through the membranes of the myocytes, thus facilitating signal propagation and a synchronized contractile pulse (Vander et al., 1994). Upon contraction, blood is forced out of the ventricle and into the aorta and coronary arteries, feeding the rest of the body and the heart muscle itself.

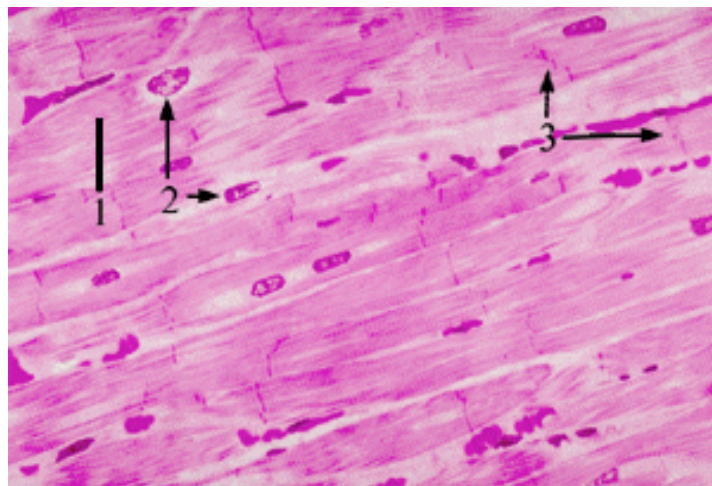


Figure 1.2 Cell organization and alignment in myocardium. 1. cardiac muscle cell; 2. nuclei; 3. intercalated disks. (<http://www.uoguelph.ca/zoology/devobio/210labs/muscle1.html>)

1.2 Myocardial Diseases

Heart failure, stemming from cardiovascular diseases, is the number one cause of death in industrialized countries. About 5 million people in the United States have heart failure, and the number is growing; heart failure contributes to or causes about 300,000 deaths each year (<http://www.nhlbi.nih.gov>). The inhibition of the heart to deliver sufficient blood to meet the body's metabolic requirements will lead to heart failure. The most common causes are coronary artery disease and hypertension (high blood pressure), which damage the myocardium, but damage to any part of the heart's intricate structure can impair cardiac performance and result in heart failure; examples include diseases of the heart valves, the electrical conduction system of the heart, or external pressure around the heart, due to constriction of the pericardial sac in which the heart is sited (Jawad et al., 2007).

When blood flow to the myocardium through coronary arteries is interrupted, the muscle becomes starved of oxygen, a condition termed ischemia, and cells enter a potentially fatal pathway, which can lead to myocardial infarction (death of heart muscle) (Fig 1.3). The early phase postinfarction remodeling involves expansion of the infarct zone, which may result in early ventricular rupture or aneurysm formation. Myocardial infarction typically results in formation of fibrotic scar, which lacks the contractile, mechanical and electrical properties of normal myocardium (Sutton and Sharpe, 2000). An altered and unnatural heart rhythm (arrhythmia) may be experienced. Compensatory mechanisms are activated to assist the heart to maintain cardiac output. This ultimately places an extra burden on the weakened myocardium, eventually leading to end-stage heart failure, with a progressive fall in cardiac output, development of multi-organ failure from reduced perfusion and ultimately death (Jawad et al., 2008).

Physiological and metabolic changes begin within seconds, following arterial occlusion (Kloner and Jennings, 2001, Ferrero, 2006). Shortly after occlusion, adenosine triphosphate (ATP) production in the myocardium switches from an aerobic to an anaerobic mechanism, due to oxygen deficiency and this causes a rapid fall in ATP production. The muscle begins to lose its contractility, due to lack of energy. As anaerobic glycolysis continues, hydrogen ions accumulate

as a byproduct and the intracellular pH of the myocytes decreases causing osmotic flooding of water into the myocytes (Ferrero, 2006). Edema occurs as the heart tissue continues to swell and irreversible damage and cell death occurs in the myocardium. Within weeks to months, scar formation takes place as fibroblasts infiltrate the infarct area and deposit fibrous collagen. As part of the inflammatory response, macrophages, monocytes, and neutrophils migrate to the scarred area and matrix metalloproteinases (MMPs) released from the neutrophils cause further infarct expansion and myocyte collagen degradation (Sutton and Sharpe, 2000).

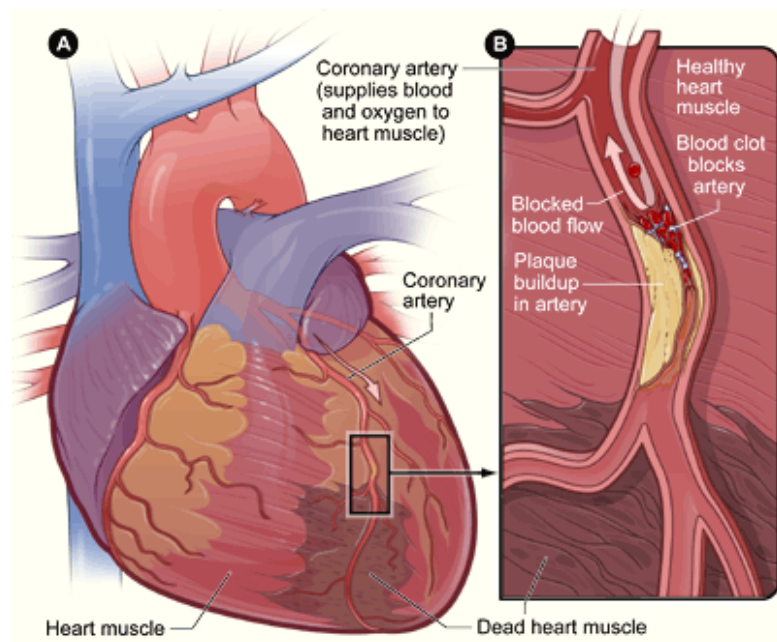


Figure 1.3 Heart with muscle damage and blocked artery. **A** is an overview of the heart and coronary artery showing damage (dead heart muscle) caused by a coronary artery occlusion. **B** shows a cross-section of the coronary artery with plaque buildup and a blood clot (http://www.nhlbi.nih.gov/health/dci/Diseases/HeartAttack/HeartAttack_WhatIs.html).

Congenital heart disease is a considerable problem worldwide, too, affecting approximately 1% of infants (Wu et al., 2006). Congenital heart defects

such as atrial septal defect, ventricular septal defect, double outlet ventricles and hypoplastic left heart syndrome are associated with aplastic, defective or necrotic myocardial structures, where patch closure, correction of the defect or revascularization is usually required (Kofidis et al., 2002). The most common congenital heart defect is the ventricular septal defect (VSD) (Fig 1.4). A VSD can be small or large. A small VSD doesn't cause problems and may often close on its own. Large VSDs cause the left side of the heart to work too hard and increase blood pressure in the right side of the heart and the lungs due to the extra blood flow. The increased work of the heart can cause heart failure and poor growth. If the hole is not closed, the high blood pressure in the lungs can cause the delicate arteries in the lungs to scar, a condition called pulmonary arterial hypertension (http://www.nhlbi.nih.gov/health/dci/Diseases/chd/chd_all.html).

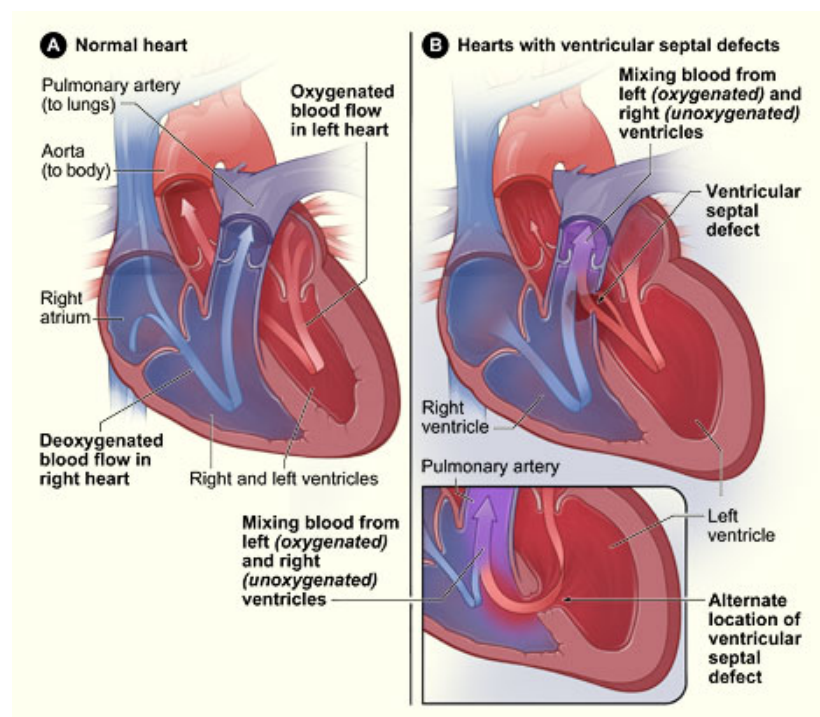


Figure 1.4 Normal heart and heart with ventricular septal defect. **A** shows the normal structure and blood flow in the interior of the heart. **B** shows two common locations for a ventricular septal defect. The defect allows oxygen-rich blood from the left ventricle to mix with oxygen-poor blood in the right ventricle. (http://www.nhlbi.nih.gov/health/dci/Diseases/chd/chd_all.html)

1.3 Current Procedures Applied for the Treatment of Myocardial Diseases

The myocardium can not compensate for the cell loss which occurs during MI, eventually leading to maladaptive left ventricular remodeling and end-stage heart failure (Leor et al., 2006). Following a myocardial infarction, the first step toward improving health is to reperfuse the blocked coronary artery, restoring blood flow to the infarcted region. This primary treatment must be administered as soon as possible in order to minimize ischemic myocardial death. Surgical treatments may be necessary if medications, used as first attempt to dissolve the clot, do not accomplish the desired outcome, or if the infarction has progressed long enough that it has given serious damage to the myocardium. In conditions where the development of an aneurysm, a blood-filled dilation (bulge) of a blood vessel, is a primary concern, surgical intervention is necessary to remove the weak, infarcted region and reconstruct the ventricle. Ventricular reconstruction involves removing the infarcted region of the ventricle and reshaping the heart from a spherical shape, to a more efficient normal (elliptical) shape. This can be done using linear suture technique (direct closure), circular external reorganization or endoventricular circular patch plasty (Dor et al., 2004).

Direct linear closure is a procedure by which the infarcted section of the ventricle is removed, and the remaining heart tissue is sutured together. This procedure provides a method for restoring the size and shape of the infarcted heart however, sometimes there is not enough myocardial tissue to restore the ventricle to the correct dimensions. The Dor procedure, also known as endoventricular patch plasty, has been used since 1984. Infarcted myocardium is removed in this procedure and the heart structure is restored using a patch that is sutured into the opening (Dor et al., 2004). An incision is made in the center of the infarcted area and any thrombi that are present are removed and the infarcted scar is cut out. A balloon is inflated inside the left ventricle and a suture is used to tighten the ventricle to the shape of the balloon. Once the suture is tightened, a patch is sutured in the remaining gap in the myocardium. The use of a patch ensures the restoration of ventricular volume and prevents further ventricular distortion.

Pharmacological therapies can slow the progression to end-stage heart disease, but rarely prevent or reverse progression of the failing state. Currently, the only therapeutic options available to treat patients with terminal end-stage heart failure are heart transplantation or left ventricular assist devices (VADs). However, these two options are not widely available, and have significant limitations of cost. The gold standard is heart transplantation, but organ donors are inadequate and there are complications associated with immune suppressive treatments. While heart transplantation involves the replacement of the whole organ, VADs aim to prevent remodeling and dilation of the left ventricle via unloading the dilated chamber. The first clinical applications of ventricular assist devices merely aimed to support a ventricle failing after an open-heart procedure (postcardiotomy failure) (Vural, 2008). The goal was to support circulation for a few days or weeks, in an expectation of some recovery in myocardial contractility; recovery of the normal response to calcium ions and restoration of the consumed ATP reserves usually require days. The recovery of other systems (such as kidneys) that may be damaged during the low output state also necessitates a sustained, adequate circulation supplying nutrients, oxygen and precursors for repair. In addition to these patients requiring short-term support, there are others who may benefit from long-term circulatory assist: the patients with reversible heart diseases such as myocarditis (bridging to recovery), those waiting for a suitable donor organ (bridging to transplantation) and still others suffering from irreversible, end-stage heart failure who are not transplant candidates for some reason, therefore, in need of permanent mechanical support (destination therapy) (Vural, 2008).

Mechanical circulatory support is an invaluable tool in the care of children with severe refractory cardiac and or pulmonary failure. Two forms of mechanical circulatory support are currently available to neonates, infants, and smaller children, namely extracorporeal membrane oxygenation and use of a ventricular assist device, with each technique having unique advantages and disadvantages (Cooper et al., 2007). Even though exciting progress is being made in the development of ventricular assist devices for long term mechanical support in children, extracorporeal membrane oxygenation remains the mainstay of mechanical circulatory support in children with complex anatomy, particularly

those needing rapid resuscitation and those with a functionally univentricular circulation. Although extracorporeal membrane oxygenation has become a standard of care for many pediatric centers, its use is limited to those patients who require only short term cardiopulmonary support. Over the last few years, substantial progress has been made in pediatric mechanical supports (Duncan, 2006). Ventricular assist devices are being used with increasing frequency in children with cardiac failure refractory to medical therapy for primary treatment as a long-term bridge to recovery or transplantation (Blume et al., 2006). Destination therapy, defined as intracorporeal insertion of a ventricular assist device with the goal of “permanent support”, is currently not an option in children.

Unfortunately, due to the high cost of VADs and the shortage of donor organs (Akins, 2002), many patients die while waiting on the shortlist. Alternatives are therefore required, with cell therapy being a potential option (Jawad et al., 2007). Efforts to regenerate functional myocardial tissue are firstly being pursued through cell grafting by syringe injection directly in the ventricular wall or in the coronary vessels. In particular, over the past few years several teams have claimed that adult stem cells such as bone marrow stem cells can develop into a wide variety of cells, including cardiomyocytes (Orlic et al., 2001). Most studies support the notion that cell engraftment in animal models of myocardial infarction can improve contractile function (Passier and Mummery, 2003), but the mechanism behind this functional improvement remains to be elucidated and there has been no convincing demonstration of implanted haematopoietic or myoblastic adult stem cells taking on the cardiac phenotype (Dengler and Katus, 2002; Murry et al., 2004; Balsam et al., 2004). In addition, the efficacy of cell engraftment is very low as more than 90% of the cell suspension injected is lost and does not engraft. Nevertheless, there are presently several ongoing clinical studies in humans using adult stem cells (e.g. skeletal myoblasts and bone marrow stem cells (BMSC)) to investigate the safety and feasibility of such a cardiac cell therapy (Menasche, 2003; Forrester et al., 2003), despite concerns with timing of cell delivery and occurrence of arrhythmias. The first clinical results are controversial, some reporting improved cardiac function while preserving ventricular geometry and others reporting marginal improvements, and demonstrate the need to better understand stem cell biology and the way to

successfully implant new cells in a diseased tissue. Therefore, the challenges of stem cell treatment for the heart are much more complex than those of bone marrow transplantation for bone marrow failure, especially when the anatomical and physiological interactions of different myocardial cells are considered (Angelini and Markwald, 2005). Much effort is now conveyed to the development of tissue engineering strategies using scaffolds to successfully engraft new cells into the myocardium (Zammaretti and Jaconi, 2004).

Below, the properties of currently marketed patches are mentioned, since they are used nowadays in ventricular restoration, and their limitations discussed to gather information on how far we are from an ideal cardiovascular patch.

1.3.1 Prosthetic Materials and Biological Patches

Although primary repair of congenital structural defects is sometimes possible, implementation of prosthetic replacement grafts has allowed for establishment of anatomic continuity and physiologic restoration in more complicated cases. Repair of complete atrial-ventricular septal defects, augmentation of a hypoplastic, stenotic right ventricular outflow tract, or repair of tetralogy of Fallot often use nonautologous constructs, such as patches (Mirensky et al., 2008). Both synthetic and biological patches are available. Synthetic patches available for clinical use in endocardial patch plasty are made of polyethylene terephthalate (PET) and polytetrafluoroethylene (PTFE), commercially known as Dacron and Teflon, respectively. Gore-Tex® Acuseal Cardiovascular Patch, is a composite material made of expanded PTFE with a middle layer of an elastomeric fluoropolymer, which significantly reduces suture-hole bleeding. The synthetic fibers used in cardiovascular patches can be arranged into either velour, knitted, or woven configurations depending on the desired porosity. DeBakey cardiovascular patches, Hemashield Double Velour Fabrics, HemaPatch Knitted are made of PET. Due to the high porosity of the knitted form, the material needs to be coated with a sealant such as collagen or albumin in order to prevent bleeding through the patch.

Coatings are also sometimes used to improve the suture retention strength and help to induce endothelialization. In addition to these synthetic materials, an ECM derived from pericardium (double walled sac that contains the heart), either autologous or bovine, is also commonly used (Tribak et al., 2008, David and Armstrong, 1998). Bovine pericardium, is treated to remove cells and crosslinked with chemicals such as glutaraldehyde to strengthen the mechanical properties. PeriGuard has improved suturability and handling over synthetic patches, and SJM Pericardial Patch produced with EnCap technology has a proprietary coating that minimizes calcification and promotes endothelial covering.

The wide spread use of these materials is largely due to the fact that they are relatively inert and their interaction with biological surroundings is very predictable.

1.3.2 Limitations of Currently Used Patches

Although the currently available prostheses are adequate for restoring ventricular geometry and maintaining ventricular pressure, and thus may be life saving, they do not actively adapt to the physiological environment and mechanical demands as they represent non-living materials. They have limited durability and are prone to infection, immunologic reactivity, and thrombosis, which often requires repeat operations in the future (Mirensky et al., 2008). When implanted into the immature heart of a child, these materials do not grow with the paediatric patient, which is a disadvantage for the repair of congenital defects. These constructs are also subject to obstructive tissue ingrowths and fibrotic responses with shrinkage and calcification leading to graft failure (Endo et al., 2001). Autologous pericardium is difficult to handle (Mohri et al., 1970, Peter, 1999) while synthetic patches are associated with thromboembolic complications, hemolysis, and infective endocarditis (Shrivastava and Radhakrishnan, 1989, Di Eusanio and Schepens, 2002). Although flexible, strong, and easy to handle, bovine pericardium may be associated with graft calcification and contraction (Pires et al., 1999, Crawford et al., 1986). Upon use of Dacron patches for repair of congenital heart

defects, a scar tissue healing response with contracture of the implant was observed, and this necessitated a reoperation (Barros D'Sa et al., 1980). Dacron grafts were also found to be associated with prosthetic thickening and stiffness (Rittenhouse et al., 1979) and lack of tissue growth in their central region (Barros D'Sa et al., 1980), which may lead to thrombus formation (Mirensky et al., 2008).

1.4 Criteria of An Ideal Patch

The essential characteristics of patch materials were described by Dwight E. Harken (1989) with reference to ideal heart valves as durability, absence of thrombogenicity, resistance to infections, lack of antigenicity, and the potential for growth. To meet these requirements tissue engineering provides a new experimental approach aimed at vital, autologous replacement structures with the capacity of growth.

A recent comprehensive review on myocardial tissue engineering by Jawad et al. (2008) points out the requirements for an ideal tissue engineered myocardial patch. All biomaterials proposed for use in tissue engineered construct should be

1. Biocompatible: Biomaterial must not be rejected or induce an inflammatory response in vivo.
2. Posses mechanical integrity: Biomaterial must enable handling during transplantation. More importantly, mechanical properties should match the host tissue it intends to replace and provide mechanical support during regeneration.
3. Biodegradable: The degradation rate of the biomaterial should match the regeneration rate of the host tissue, and the degradation by-products must be non-toxic and readily removed from the body.
4. Cell 'friendly': Enhance cell adhesion and survival both in vivo and in vitro.
5. Biomimetic: Reflect the extracellular matrix (ECM) of the tissue it intends to replace.

6. Easily accessible: Biomaterial must be easily accessible and designed with acceptable cost.

Other requirements specific for myocardial tissue engineered constructs include the following:

1. It is important that the biomaterial is able to withstand, or even contribute to the continuous stretching/relaxing motion of the myocardium that occurs at each heartbeat, and withstand the ventricular pressure without causing any aneurysmal dilatation.
2. Biomaterial must encourage cell proliferation and differentiation into cardiomyocytes as well as supporting vascular cells.
3. Ideally, biomaterials could encourage cardiomyocyte alignment and maturation in vitro before implantation or in vivo, improving the contractile properties of the graft.
4. Biomaterial must enable electrical integration of engineered graft with the native tissue to allow synchronized beating between the artificial construct and the heart. This requires matched excitability of host and grafted tissue.
5. The construct should house strategies to encourage vascularization to support the survival of grafted cells.
6. The cellular component should not provoke arrhythmia once introduced into the body.
7. The construct should enable surgical simplicity.

An advantage of tissue-engineered patches is the ability to control various properties of the graft, including scaffold degradation time. Utilization of different combinations of polymers and various scaffold preparation techniques enable researchers to develop patches with varying biomechanical and degradation profiles for numerous applications (Mirensky et al., 2008). Although the micro and nanotechnology used to generate the native architecture of complex tissues are premature yet, tissue engineered constructs with higher complexity are on the way

with a hope to get more functional grafts for total elimination of the need for organ transplantation.

1.5 Myocardial Tissue Engineering: Regenerating Functional Myocardium

Ventricular restoration procedures could be enhanced tremendously with the use of an autologous muscle cell-seeded bioengineered patch. Bioengineered muscle grafts may prevent recurrent dilation and improve cardiac function after myocardial repair. Fundamentally, cardiac tissue engineering involves seeding a biodegradable scaffold with muscle cells and allowing tissue formation in vitro before ultimately implanting the graft into the heart. Ideally, the seeded cells will grow into morphologically recognizable tissue before implantation and then integrate and remodel with the host tissue after implantation. Once implanted, the biodegradable scaffold will slowly dissolve and the seeded cells will retain their spatial architecture by synthesizing their own interstitial matrix scaffold (Fedak et al., 2003). The interstitial matrix is a critical mediator of structural support and a key regulator of tissue architecture in vivo. The success of bioengineering heart muscle in vitro will largely depend on the use of an appropriate matrix-like biomaterial capable of providing structural support and organization as well as the molecular cues necessary for functional tissue formation. Cell sources, scaffold types and materials as well as bioreactors used in cardiac tissue engineering studies are reviewed in the following subchapters.

1.5.1 Cell Sources

The negligible ability of adult cardiomyocytes to proliferate has triggered an intense search for progenitor cells that can replace damaged myocardium. It is clear that natural cardiomyocyte regeneration - including differentiation of progenitors residing in the myocardium or the recruitment of stem cells from outside (e.g., from endothelial cells or a niche in the bone marrow) - is

insufficient to overcome cardiomyocyte death in the acutely or chronically damaged heart (Nakamura and Schneider, 2003). Enthusiasm with regeneration from native progenitor pools has encouraged investigators to introduce exogenous cells into damaged heart muscle. Potential of cardiac stem cells resident in the heart, embryonic stem cells, bone marrow stem cells and fetal stem cells (from tissues of umbilical cord) to differentiate into cardiomyogenic lineage either in vivo or in presence of differentiation factors, conditioned media or in co-cultures in vitro have been investigated, but there is still a need for elaboration and improvement in the procedures to be able to obtain high numbers of fully differentiated cardiomyocytes. Since the main concern in myocardial tissue engineering is to show the functionality of the final construct, the majority of in vitro studies involve use of rat neonatal cardiomyocytes or cardiomyocytes derived from embryonic stem cells that are already able to contract.

Almost nothing is known of the molecules or pathways that regulate cardiomyogenic potency of candidate progenitor cells in adults or that stimulate them to differentiate into cardiomyocytes. In contrast, a large body of information is available on embryonic heart induction (Foley and Mercola, 2004). Organ formation requires the precise integration of cell type-specific gene expression and morphological development; both are intertwined in their regulation by transcription factors. Although many transcription factors have been described as regulators of cardiac-specific gene expression, the transcriptional regulation of cardiac morphogenesis is still not well explored (Bruneau, 2002).

Progress has been made in the generation of cardiomyocytes from both embryonic and adult stem cells. Treatment of mesenchymal stem cells (MSCs) isolated from bone marrow (BM) with the DNA demethylating agent 5-azacytidine has been shown to induce multiple new phenotypes including cardiomyocytes (Makino et al., 1999; Hakuno et al., 2002). Xu et al. (2004) showed that 5-azacytidine can promote the differentiation of adult human BM MSCs into a cardiomyocyte-like phenotype, but the process was less than completely specific, as adipocyte-like cells were also observed. It was demonstrated that it is also possible to obtain a specific population of human cardiomyocyte-like cells (CLCs), who express multiple structural and myofibrillar proteins specific to cardiomyocytes, by

using a cardiomyogenic medium without demethylating agents or co-cultures (Shim et al., 2004). However, neither of differentiation attempts of human BM MSCs resulted in beating cardiomyocytes. On the other hand, beating cardiomyocytes were obtained as a result of differentiation of mouse adipose tissue stroma cells in presence of growth factors without addition of 5-azacytidine (Planat-Benard et al., 2004). It has been found also that after 5-azacytidine treatment for 2 weeks, murine BM stromal cells can be differentiated into cardiomyocytes, which formed myotube-like structures and began beating spontaneously (Makino et al., 1999). Studies revealed that transplantation of mouse BM stem cells into an animal model (mouse) of MI attenuates cardiac dysfunction by inducing robust neovascularization and cardiomyogenesis (Orlic et al., 2001). The current dogma is that hBMSCs do not transdifferentiate into contractile cardiomyocytes. This has brought about suggestions that the marginal improvements (e.g. left ventricular ejection fraction) in clinical trials may be due to other factors, such as increased cytokine release and/or formation of more blood vessels (Jawad et al., 2007). BMSCs were found to attenuate left ventricular remodeling after myocardial infarction by preventing cardiomyocyte apoptosis through paracrine mediators (Uemura et al., 2006). Recently, Rosenzweig (2006) reported on the mixed results achieved from BMSC transplantation into patients with infarcted hearts; with Schachinger et al. (2006) reporting the best evidence so far on the success of BMSCs. However, other trials suggesting only mild or no improvement have lessened enthusiasm for the therapeutic use of BMSCs.

Mesenchymal stem cells with a capability to differentiate into cells of mesodermal lineage (osteoblasts, chondrocytes, adipocytes) can be derived from Wharton's Jelly of the human umbilical cord in very high numbers (Weiss et al., 2006, Karahuseyinoglu et al., 2007). Previous studies with Wharton's Jelly MSCs indicate the possibility of their being more primitive relative to BM MSCs (Wang et al., 2004, Weiss et al., 2006). They were investigated for their potential to differentiate into cardiomyocytes by treating them with 5-azacytidine or maintaining them in cardiomyocyte-conditioned medium and it was found that both treatments resulted in expression of the cardiomyocyte markers N-cadherin, cardiac troponin I, connexin 43, α -actinin, and desmin (Wang et al., 2004). Western blots

showed that the newly extracted cells did not express N-cadherin or cardiac troponin I but that both markers were expressed in cells grown in conditioned medium and, to a lesser extent, those grown in 10% FBS. This suggests that FBS provides some differentiating factors, but not to the same extent as cardiomyocyte-conditioned medium. After 5-azacytidine treatment or culture in cardiomyocyte-conditioned media, the cells connected with adjoining cells but did not form myotubes or start spontaneous contraction (Wang et al., 2004). In another recent study by Martin-Rendon et al. (2008), WJ MSCs were found to not respond to cardiomyogenic differentiation with 5-azacytidine at all. The therapeutic potential of human umbilical cord derived stem (UCDS) cells in a rat myocardial infarction model was investigated by Wu et al. (2007), and statistically significant improvement of cardiac function was observed. Some of the UCDS cells expressed cardiac troponin-T, von Willebrand factor, and smooth muscle actin, indicating regeneration of damaged myocardium by cardiomyocytic, endothelial, and smooth muscle differentiation. The capillary and arteriole density were also markedly increased.

Embryonic stem cells (ESCs) derived from blastocyst stage embryos have a potential to differentiate into cells of all the three germ layers - endoderm, mesoderm and ectoderm - but there are some ethical and practical issues (formation of teratoma when implanted to the body in an undifferentiated form, and triggering of immune response) related with their use in humans (Denker, 2006). On the other hand, the obstacles in obtaining beating cardiomyocytes from adult and fetal stem cells makes the idea of using ESCs for both research and therapeutics more attractive. The differentiation of human ESCs into all cardiac cell types (pacemaker, atrial, nodal, Purkinje-like and ventricular cells) have been well characterized in many laboratories (Harding et al., 2007; Kehat et al., 2001, 2002, 2004; Mummery, 2002, 2003).

Cardiomyocyte differentiation could be enhanced by treatment of 3 parent (H1, H7, and H9) hES cell lines and 2 clonal (H9.1 and H9.2) hES cell lines with 5-aza-2'-deoxycytidine. The differentiated cultures could be dissociated and enriched by Percoll density centrifugation to give a population containing 70% cardiomyocytes. The enriched population was proliferative and showed appropriate

expression of cardiomyocyte markers. The beating cells expressed markers characteristic of cardiomyocytes, such as cardiac α -myosin heavy chain, cardiac troponin I and T, atrial natriuretic factor, and cardiac transcription factors GATA-4, Nkx2.5, and MEF-2 (Xu et al., 2002).

Alternatively, co-culture of hESC with a mouse endoderm-like cell line (END-2) resulted in the formation of cardiomyocytes. As early as 6 days after the start of co-culture, beating areas were observed in hESC-END-2 co-cultures, with an optimal cardiac differentiation at 12 days (Mummery et al., 2003), particularly if differentiation is induced in the absence of serum and presence of ascorbic acid (Passier et al., 2005). Differentiation to cardiomyocytes in embryoid bodies (EBs) has been described as ‘spontaneous differentiation’, whereas END-2 cells appear to secrete factors that enhance differentiation of hESC to cardiomyocytes (Mummery et al., 2003). However, it is likely that common factors are involved, as EBs generally also contain a visceral endoderm-like cell population (Mummery et al., 2003). Both spontaneous differentiation of EBs to cardiomyocytes and differentiation of hESC to cardiomyocytes in co-cultures with END-2 cells result in mixed cultures of 3 types of cardiomyocytes: atrial, ventricular and nodal. It is possible to determine the type of cardiomyocyte by action potential characterization (He et al., 2003). In hESC-END-2 co-cultures, 85% of cardiomyocytes were of ventricular type (Mummery et al., 2003). The electromechanical integration of hESC derived cardiomyocytes with the host myocardium both in vitro and in vivo has successfully demonstrated the potential of these cells for use in cell therapy. Laflamme et al. (2005) reported the formation of human cardiac tissue in athymic rat hearts by injecting an enriched population of hESC derived cardiomyocytes by the fourth week. Leor et al. (2005) compared undifferentiated hESCs and hESC derived cardiomyocytes and showed that both can survive when transplanted into normal or infarcted hearts of nude rats. However, neither type contributed to new myocardium formation, and some possible teratoma formation was observed indicating the importance of undifferentiated cell elimination prior to transplantation.

Understanding of cardiac developmental pathways may be of enormous strategic benefit in devising or refining cellular therapies for the heart; it may be

even possible to eliminate use of cell co-cultures or extracts of animal cells in in vitro induction of cardiogenesis. Several classic growth factors such as members of TGF- β superfamily (especially BMPs), IGF I, insulin, FGF and erythropoietin (EPO) have been identified to promote heart development via activation of the MAP kinase, the PI-3 kinase and the PLC- γ 1 pathways (Fig 1.5). Activation of the signal molecules after growth factor-receptor association results in an expression of transcriptional factors such as FOG-2, GATA-4, and Nkx-2.5 that are essential for cardiac development (Sachinidis et al., 2002).

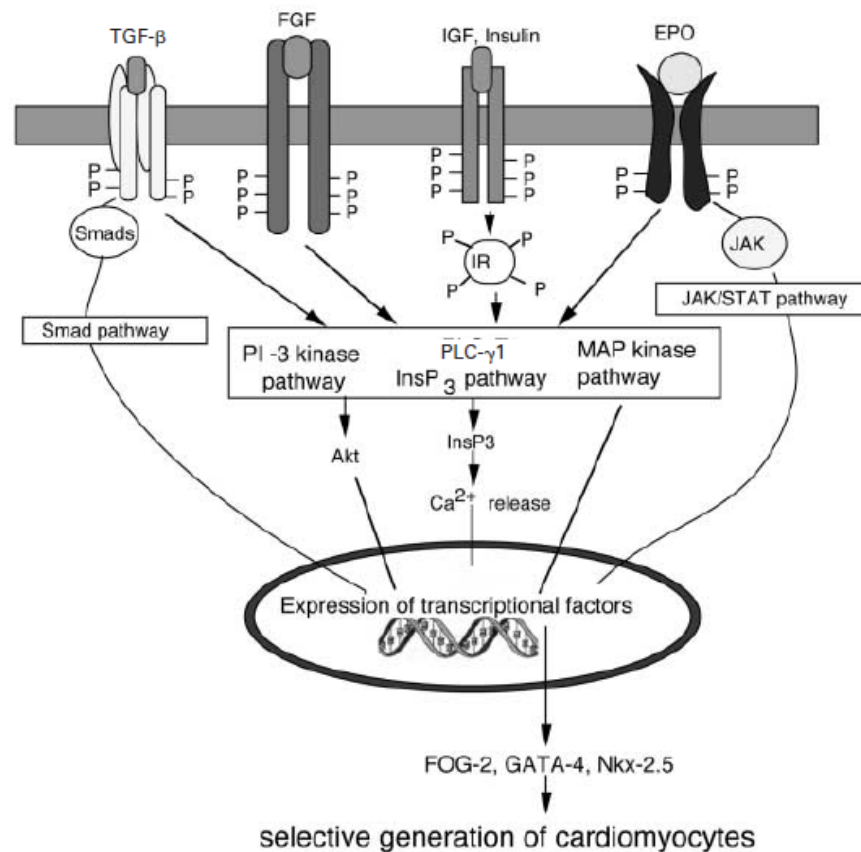


Figure 1.5. Proposed intracellular transduction pathways generating cardiomyocytes by different growth factors (Sachinidis et al., 2002).

Differentiation of adult or fetal stem cells to functional cardiomyocytes in vitro is still under investigation and besides the types of growth factors used, the variations in concentration, timing and/or combinatorial effects of the growth factors should be considered as parameters that may affect the outcome. It will also be important to identify specific factors that control maturation, proliferation and electrical characteristics of the stem cells.

1.5.2 Scaffold Materials, Types and Biomimicry

Polymers, both natural and synthetic, are the largest class of engineered biomaterials used today for myocardial tissue reconstruction. They are available in a wide variety of compositions and properties. One of the first materials used for tissue engineering of the heart was based on synthetic, hydrolytically degradable biocompatible polymers composed of polylactic acid (PLA), polyglycolic acid (PGA) and their copolymer polylactic-co-glycolic acid (PLGA) (Zund et al., 1997). Subsequently, researchers realized that the mechanical properties of the material used had to be adapted to the elastic properties of the heart tissue. Therefore, most research focused on the use of hydrogels made of different synthetic and/or natural polymers. Promising results in the development of collagen (the major constituent of the cardiac ECM) -based grafts or ‘patches’ containing beating cardiomyocytes were obtained (Akhyari et al., 2002; Kofidis et al., 2002, 2003; Zimmermann et al., 2002, 2003, 2004). These studies comprised the application of cardiomyocyte-seeded collagen strings that were cyclically stretched, thus providing patches with improved morphology and contractile function. Zimmermann et al. (2004) demonstrated that these collagen patches could survive and beat for up to eight weeks after engraftment on the heart of immunosuppressed rats. Fedak et al. (2003) seeded human pediatric heart cells on Gelfoam patches and subjected them to a mechanical stretch regimen. Mechanical stretch resulted in the synthesis and formation of an organized, healthy matrix by the seeded cells, consistent with normal myocardium. Radisic et al. (2004) applied electrical signals designed to mimic those in the native heart to rat cardiomyocytes seeded onto Ultrafoam collagen

sponges using Matrigel, and were successful in inducing synchronous contractions. These data suggest that heart cells retain the capacity to form cardiac-like tissue when provided with appropriate environmental cues. Poor mechanical properties, the lack of structural stability, and large degree of swelling (approximately 30% immediately following hydration in culture medium (Radisic et al., 2003)), however, may hamper clinical applications of collagen sponges. Similar approaches and results were obtained using alginate-based scaffolds by Leor et al. (2000) and Dar et al. (2002). After implantation into the infarcted rat myocardium, the alginate-biografts were shown to stimulate intense neovascularization and to attenuate left ventricular dilatation and failure, compared with control rat hearts (Leor et al., 2000). P4HB is another natural polymer considered for use in cardiovascular tissue engineering due to its suitable elastic property, but it degrades very fast (after 8 weeks) in vivo (Sodian et al., 2000, Hoerstrup et al., 2000). Poly(ϵ -caprolactone) (PCL) and poly(glycerol sebacate) (PGS) are synthetic elastic polymers with a potential use in cardiovascular tissue engineering, too (Wang et al., 2002, Klouda et al., 2008). PCL has a relatively slow degradation rate (more than 2 years), compared to PGS (totally absorbed in 60 days in vivo) (Wang et al., 2002), and this is the main disadvantage of PCL use as the scaffold material (Yang et al., 2001). PGS have been used to produce sponges and is shown to support vascularization after 2 weeks, when implanted on the infarcted myocardium (Radisic et al., 2006, 2008). Microfabrication techniques were used to create an accordion-like honeycomb microstructure in poly(glycerol sebacate), which yields porous, elastomeric three-dimensional (3D) scaffolds with controllable stiffness and anisotropy (Engelmayr et al., 2008). These scaffolds with cultured neonatal rat heart cells demonstrated utility through closely matched mechanical properties compared to native adult rat right ventricular myocardium, heart cell contractility inducible by electric field stimulation, and greater heart cell alignment than isotropic control scaffolds. PGS, being a thermosetting polymer, has been limited to cast structures. However a recent work reported on feasibility of obtaining PGS nanofibers in random non-woven mats by coaxial core/shell electrospinning (Yi and LaVan, 2008). Composites of natural and synthetic polymers were also developed; for example, sponges based on ϵ -caprolactone-co-L-lactide reinforced with knitted

poly-L-lactide fabric (PCL-PLLA), gelatin or PGA. Using rat aortic smooth muscle cells, an increased colonization of the right ventricular outflow tract was obtained using gelatin or PCL-PLLA, but not with PGA-reinforced grafts (Ozawa et al., 2002). Park et al. (2005) obtained a composite scaffold for cardiac tissue engineering from poly(dl-lactide-co-caprolactone), poly(dl-lactide-co-glycolide) (PLGA), and type I collagen that showed markedly improved construct cellularity, presence of cardiac markers, and contractile properties upon their culture with heart cell as compared with PLGA and Ultrafoam controls.

The most fascinating approach to the regeneration of heart has been proposed by Shimizu and co-workers (2002, 2003, 2006), who used materials only as a means to create electrically communicating three-dimensional cardiac tissue layers. In this case, cells were adhered on tissue-culture plates previously coated with poly(N-isopropylacrylamide) (PNIPAAm), a temperature-sensitive polymer. At 37 °C PNIPAAm is hydrophobic, enabling cell adhesion and access to the binding sites offered on this modified surface; at a lower temperature such as 32 °C, the surface becomes hydrophilic and inappropriate for cell adhesion due to the rapid hydration and swelling of PNIPAAm. Using poly(vinylidene difluoride) (PVDF) membranes, which are hydrophobic, the detaching cell layers can be collected and handled, providing up to four conducting layers of synchronously beating cardiomyocytes. When these patches were implanted on rats with induced myocardial infarction, an improved myocardial contractility was observed, concomitant with the appearance of a vascular network within a few days after implantation. The thickness limit for layered rat cardiomyocyte sheets was found to be 80 μm (3 layers) in subcutaneous implantation, however, multistep transplantation of the triple-layer grafts on top of each other with several-day intervals created ~1 mm thick myocardium with a well-organized microvascular network (Kikuchi et al., 2006). In addition to that, neonatal rat cardiomyocyte sheets were sequentially wrapped around a resected adult rat thoracic aorta, to obtain 6-layered myocardial tube, and transplanted in place of the abdominal aorta of athymic rats. Four weeks after transplantation, the myocardial tubes demonstrated spontaneous and synchronous pulsations independent of the host heartbeat (Sekine et al., 2006). By this way it was demonstrated that functional

myocardial tubes that have the potential for circulatory support can be created with cell sheet engineering. Very recently it was shown by the same research group that co-cultured endothelial cells (ECs) formed cell networks, which were preserved during the sheet harvest, within the cardiomyocyte sheets. After layering of 3 cardiac cell sheets to create 3-dimensional myocardial tissues, these patch-like tissue grafts were transplanted onto infarcted rat hearts. Four weeks after transplantation, recovery of cardiac function could be significantly improved by increasing the EC densities within the engineered myocardial tissues. Blood vessels originating from the engineered EC-positive cardiac tissues bridged into the infarcted myocardium to connect with capillaries of the host heart (Sekine et al., 2008). In vitro engineering of 3-dimensional cardiac tissues with preformed EC networks that can be easily connected to host vessels can contribute to the construction of myocardial tissue grafts with high potential for cardiac functional repair. Figure 1.6 summarizes three of the major approaches to cardiac engineering, based on the use of collagen, hydrogel and multiple layers (Zammaretti and Jaconi, 2004).

Several groups have reported that cells grown in three-dimensional (3D) context more closely resemble the in vivo cells, both morphologically and in their molecular regulation (Armstrong et al., 2000; Cukierman et al., 2001). This has been found to be particularly true for cardiac myocytes (Bursac et al., 1999; Carrier et al., 1999). Cardiac cultures grown as aggregates or “organ cultures” were found to respond to mitogenic signals quite differently from those cultured in 2D context (Armstrong et al., 2000).

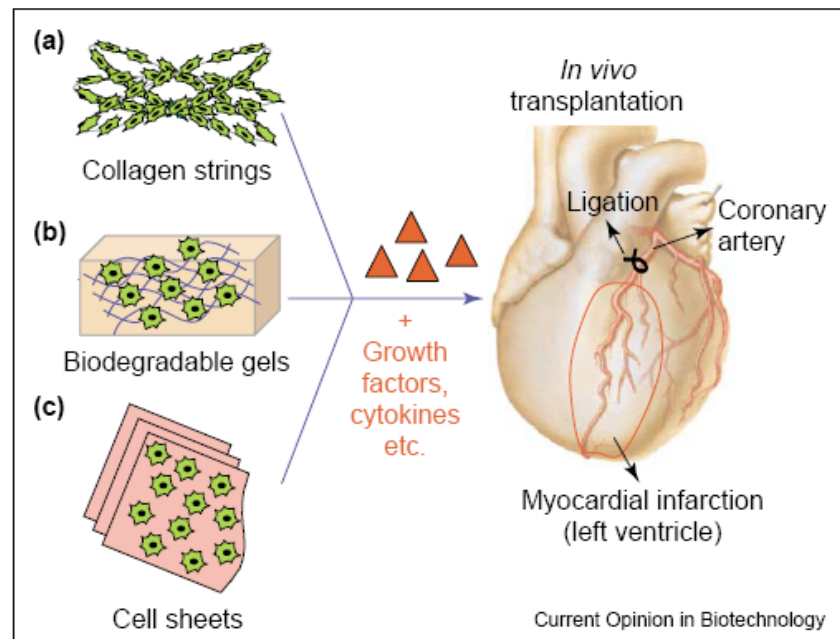


Figure 1.6 Scheme of the present major strategies of cardiac tissue engineering using (a) collagen strings, (b) biodegradable gels or (c) cardiac cell sheets. The incorporation of growth factors (triangles) may have a crucial role to support cell differentiation, engraftment and survival, both within the scaffolds and in vivo, thus improving the overall cardiac function (Zammaretti and Jaconi, 2004).

Cardiac myocytes are responsive to the geometry of their environment (Evans et al., 2003), too. It was shown that cardiomyocytes can align parallel to micron range fibers (Zong et al., 2005). Electrospun mats with oriented fibers from PLLA and PLGA were utilized by Zong et al. (2005), to assess scaffold effects on primary cardiomyocyte attachment, structure and function. The primary cardiomyocytes (CMs) had a preference for relatively hydrophobic surfaces (PLLA), where they aligned in the direction of fibers and developed mature contractile machinery (sarcomers). It was shown with this study that nano- and microstructured electrospun non-woven scaffolds provide both flexibility and guidance for CM growth and can be successfully applied to obtain structurally and functionally competent cardiac tissue constructs. 2-3 cell layers thick aligned cardiomyocytes were obtained on biodegradable, elastomeric polyurethane films

patterned by microcontact printing of laminin lanes (McDevitt et al., 2003). In addition, dense, highly aligned monolayers of patterned cardiomyocytes were able to contract the thin, solvent-cast polyurethane films. With these studies it was shown that it is possible to mimic the anisotropic, i.e. aligned, organization of cardiomyocytes on two dimensional scaffolds that can be considered also as 3D in micron scale. However, these still need to be developed into thick tissue grafts to be able to offer a realistic solution for cardiac tissue replacement. Electrospun mats of poly(epsilon-caprolactone) with random, unaligned, fiber orientation were seeded with cardiomyocytes by Ishii et al. (2005) and stacked with the purpose of generating a 3D cardiac graft. 5 layers of these mats were successfully overlaid to form a 3D graft without any incidence of core ischemia. The individual layers adhered intimately, morphological and electrical communication between the layers was established, and synchronized beating was also observed. This study demonstrated the feasibility of obtaining a 3D cardiac graft from 2D cell sheets residing on nanofibers that mimic the native structure of ECM.

The area of tissue engineering has been driven by biomimicry-inspired design of materials to recreate the natural three-dimensional environment for better cell and tissue growth (Hubbell, 2003). An important aspect of these efforts is to mimic the fibrillar structure of the ECM, which provides essential guidance for cell organization, survival and function. Only recently, success has been reached in developing biomaterials with sub-micron fibers and morphological similarity to the ECM, thus possibly providing an innate setting for cell assembly and growth. Electrospinning has emerged as a simple yet versatile method in manufacturing such biomaterials out of synthetic (Kim et al., 2003; Zong et al., 2003) or natural (Matthews et al., 2002; Huang et al., 2001) polymers. Recently, electrospun nonwoven nanofiber membranes have been demonstrated in multiple biomedical applications, including the production of scaffolds for tissue engineering, wound healing, drug delivery, and medical implants (Kim et al., 2003; Boland et al., 2001; Xu et al., 2004; Min et al., 2004; Khil et al., 2003; Jia et al., 2002; Zong et al., 2004). The attraction of electrospun biomaterials in the context of tissue engineering is manifested in several ways. First, very high surface area-to-volume ratio and high porosity can be achieved for better cell incorporation and perfusion. Second, the

process allows for control of structure at the nano-, micro- and macro-scales for flexible tissue design. It has been suggested that nanofibrous ECM-mimicking features may improve cellular response and biocompatibility because of the morphological similarities to the three-dimensional ECM protein fiber network (Li et al., 2002). Third, the electrospinning process is versatile, since it offers the ability to incorporate multiple polymers and bioactive ingredients (Fang and Reneker, 1997); it can also be used to enhance mechanical properties of the obtained nanofibrous materials compared to solid-walled equivalents (Kim and Reneker, 1999).

One attractive feature of electrospinning is the simplicity and inexpensive nature of the setup; the typical electrospinning setup consists of a syringe pump, a high voltage source, and a collector (Fig 1.7). During the electrospinning process, a polymer solution is held at a needle tip by surface tension. The application of an electric field using the high-voltage source causes charge to be induced within the polymer, resulting in charge repulsion within the solution. This electrostatic force opposes the surface tension; eventually, the charge repulsion overcomes the surface tension, causing the initiation of a jet. As this jet travels, the solvent evaporates and an appropriate collector can be used to capture the polymer fiber, either in random or aligned fashion (Pham et al., 2006).

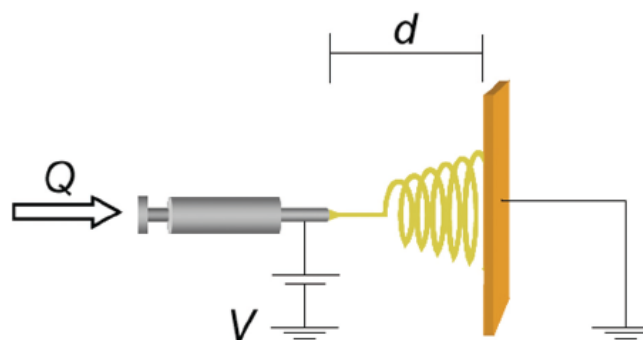


Figure 1.7 Typical electrospinning setup. Q , flow rate; d , distance between plate and needle; V , applied voltage (Pham et al., 2006).

1.5.3 Bioreactors

The bioreactor provides three-dimensional tissue developing in vitro with appropriate biochemical mass transport (e.g., oxygen and growth factors) and mechanical stimulation (e.g., tension/compression and shear stress), mimicking conditions present in vivo. Bioreactor conditions affect cell viability and proliferation, ECM content and the architecture in the engineered tissue. The ability of producing a 3D myocardial tissue comprising more than a few layers of muscle is the main advantage of using a bioreactor. Several different bioreactors have been suggested for cardiac constructs: static or mixed flask bioreactors, where constructs are suspended in a cultivation medium; rotating vessel bioreactors, where constructs are suspended in a medium that has a constant rotational flow; and finally perfusion cartridge bioreactors, where constructs are perfused at interstitial velocities, comparable to blood flow in native tissue (Jawad et al., 2008). Researchers are constantly striving to design an improved bioreactor. Many different geometries, portraying various patterns of fluid dynamics, have been suggested (Leor et al., 2005). Currently, the negative aspect of bioreactors is their restricted ability to supply an adequate amount of nutrients to a tissue of thickness greater than approximately 100 μm , or less than 10 cell layers thick (Leor et al., 2005). This limitation causes weak cellular integrity and short duration of contractility, as well as nonhomogeneous seeding, as a result affecting tissue function and cellular viability (Vunjak-Novakovic et al., 2006). Although the purpose of these bioartificial tissues is primarily for scientific studies, researchers also intend to improve their in vitro designs and eventually use them for cardiac repair. Carrier et al. (2002) and Radisic et al. (2006) demonstrated the importance of oxygen on engineered cardiac grafts to overcome the limitation of producing a 100 μm thick new tissue. They found that, by increasing the oxygen concentration supply to the in vitro construct, an improved engineered cardiac muscle was produced. Using a perfusion bioreactor, cardiac muscles could be optimally cultured within a scaffold as thick as 0.5 cm (Radisic et al., 2004). Kofidis et al. (2003) who obtained 8-mm-thick cardiomyocyte/ collagen constructs using a continuous perfusion of the scaffold through a core vessel, introduced an interesting method of providing

oxygenation within the scaffold. Not only did this system allow oxygenation during in vitro culture, but perfusion of the construct after implantation might also be possible after connection of this core vessel to the host vascular system (Giraud et al., 2007).

1.5.5 Key issues in myocardial tissue engineering

Several issues will have to be resolved to improve the complexity and function of engineered myocardium: (1) high numbers of cardiac myocytes need to be made available; (2) the survival rate of cardiac myocytes in a three-dimensional environment needs to be improved; (3) the size of three-dimensional myocardium needs to be increased; (4) engineered myocardium must develop appropriate force (Zimmermann et al., 2006). The choice of biomaterial, cell source and suitable environment for cells to proliferate and differentiate in vitro before implantation remain obstacles in the field (Jawad et al., 2008). The allocation of sufficient amounts of cardiac myocytes to engineer thick myocardium seems possible with appropriate embryonic or adult stem cells, and applications of growth factors or growth factor providing cells, culture under hyperbaric oxygen, and induction of vascularization to resolve the problems of low cell survival and seeding efficiency (Zimmermann et al, 2006).

The maximal size and thickness of engineered heart muscle will critically depend on oxygen and nutrient supply. Perfusion in vitro may improve the metabolic supply and could be achieved by induction of angiogenesis or vasculogenesis. The angiogenesis may be induced by embedding continuously perfused, functional vessels into engineered heart muscles leading to sprouting of capillaries from the vessel into the construct. This approach ideally establishes a vascular bed that could subsequently be surgically connected to the recipient vasculature.

An important task for cardiac tissue engineers in the future is certainly to identify more and ultimately all factors including optimal concentrations and time windows in which specific factors have to be present during culture. So far,

growth factors are mostly applied by addition of xenogenic sera which is not compatible with human applications. Other factors that can improve structure and function of engineered myocardium are mechanical and electrical stimulation (Zimmermann et al., 2006).

There is a need to go back one step and address the heart's unique structure, the aligned architecture of cardiomyocytes together with cardiac fibroblasts, to generate a patch capable of synchronous contraction. Micro and macro-vascularization will be of paramount importance too. Nanobiology and biomaterials science will provide new impetus to this emerging field (Kofidis, 2008).

None of the so far developed methods to construct engineered myocardium yields autologous graft material and all implantation studies have been performed in the presence of immune suppressants or in nude rats and mice. Autologous tissues would without doubt be preferable. This may in fact be possible with adult stem cell-derived cardiac myocytes or with ES-cells that are derived from the inner cell mass from somatic nuclear transfer derived blastocysts.

Limitations to take myocardial tissue engineered construct further into clinical trials are inevitable still. The proposed materials, which use animal-derived products, add another layer of complication to the testing and approval process for clinical application. Although many biomaterials, with varying compositions and properties, are continually being suggested for myocardial tissue engineering, the current challenge is to focus investigations on the already available materials of proved biocompatibility in order to improve their performance towards clinical trials. Furthermore, at what stage of development cells should be used remains to be determined: whether immature cells which could further proliferate in vivo or mature cardiomyocytes with the properties of adult myocytes. In addition, the question remains as to whether cardiomyocytes alone should be introduced into the region or rather a multi-type culture consisting of cardiomyocytes, endothelial and fibroblastic cells to further enhance neovascularization. Moreover, whether the cellular constructs need to be cultured in vitro over a period before introducing into the myocardium or implantation should occur immediately after cell seeding remains questionable. Attachment of the material is another challenge, given the

strong and repetitive forces generated during myocardial contraction. Compressive forces upon constructs placed within the muscle, or stretching of suture sites, will be experienced in every heartbeat. Although many groups have provided evidence of the beneficial effects of myocardial tissue engineering in vitro and in vivo (animal models), the mechanism behind this functional improvement is yet to be elucidated (Jawad et al., 2008). Improved clinical protocols and minimally invasive routes of stem cell and tissue administration will be necessary to render myocardial restoration a true first-line therapy.

The vision to create whole organs in the lab is impressive. If successful it may offer salvation to patients with so far incurable disabling diseases including heart failure. Replacing a heart with an engineered heart seems an unlikely option in the near future. However, restoring or at least enhancing heart muscle function by grafting of tissue engineered myocardium seems foreseeable and may not only be applicable in older patients with heart failure but also in children with congenital malformations. Ultimately, tissue engineering based myocardial regeneration may be an attractive alternative to heart transplantation and other surgical interventions to rebuild the heart (Zimmermann et al., 2006).

1.6 The Aim, Novelty and the Approach in This Study

The aim of this study was to produce a tissue engineered, 3D myocardial construct that is similar to native tissue in cell organization and cell-to-cell interactions.

Human MSCs from umbilical cord matrix (WJ), known to have the capability to differentiate into cells of myocardium (cardiomyocytes, endothelial cells and smooth muscle cells) *in vivo*, were used for the first time as the cell component in a myocardial patch, in order to obtain a graft applicable to humans. Initially microfiber mats were used to align MSCs and then stacked up to create a 3D structure that allows cell-to-cell interaction. Small diameter macroporous biodegradable tubings that penetrated the myocardial patch were used to supply growth media to the cells in a similar way to that *in vivo*. The whole project represents an attempt towards generating a well perfused, thick myocardial patch.

Human WJ MSCs and BM MSCs were characterized and compared by flow cytometry for their surface antigens, for their capability to differentiate into cells of mesodermal lineage (osteoblasts, adipocytes), and their potential to differentiate into cardiomyocytes. The preliminary part was carried out in the USA (MGH and Tufts U., Boston, MA, as a collaborative work with Deniz Yücel). A prepolymer of PGS, an elastomer, was synthesized and blended for the first time with PHBV and P(L-DL)LA, to increase their softness and hydrophilicity, to obtain a biodegradable material with more suitable mechanical properties for cardiac tissue engineering. Aligned microfibrinous mats were obtained by electrospinning of the blend and hWJ MSCs were grown on them to obtain aligned cell sheets. 3D constructs were produced by wrapping the cell seeded, aligned-fiber mats around macroporous tubings prepared from a P(L-DL)LA:PGS blend. The 3D construct was cultured in a microbioreactor by perfusing growth media through the macroporous tubings to feed the cells in the fibrous mat layers. The construct was cultured for two weeks in the presence of cardiomyogenic differentiation factors and was analyzed for cell viability (MTS test), cell distribution and preservation of alignment (fluorescence microscopy), and for differentiation to cardiomyocytes (RT-PCR and immunocytochemistry).

CHAPTER 2

METHODS

2.1 Synthesis of Poly(glycerol sebacate)

The procedure used by Wang et al. (2002) was modified to synthesize the poly(glycerol sebacate). A 250 mL three-neck flask equipped with a N₂ inlet, and thermometer adapter was charged with anhydrous glycerol and sebacic acid (1:1 mole ratio). N₂ was bubbled through the mixture while it was heated to 120°C with constant stirring. The reaction was maintained at 120°C under N₂ for 24 h, then the N₂ was disconnected, the set was connected to a vacuum line and the reaction was continued at 120°C for 24 h. Polymer formation was followed by FTIR spectra of the reaction mixture at different times during the polymerization process.

2.2 Characterization of PGS

2.2.1 Molecular Weight Determination by Gel Permeation Chromatography

Determination of PGS prepolymer molecular weight and its change during polymerization was studied by Gel Permeation Chromatography (Polymer Laboratories (UK), PL-GPC 220 with tetrahydrofuran (THF) column). The analysis was carried out by dissolving samples in THF, with flow rate of 1 mL/min at 30 °C. The Polystyrene Universal Calibration method was used for evaluation of the results.

2.2.2 Differential Scanning Calorimetry (DSC) Analysis

DSC thermogram of the PGS was obtained under nitrogen atmosphere by using DuPont 2000 Differential Scanning Calorimeter at a heating rate of 10 °C/min in the temperature range between -50 °C and 100°C.

2.3 Preparation of Aligned Microfiber Mats Through Electrospinning

Poly(3-hydroxybutyrate-co-3-hydroxyvalerate) (PHBV, MW: 222.2 kDa), containing 5% 3-hydroxyvalerate from Sigma-Aldrich Co. (USA), P(L-D,L)LA (70:30, i.v.: 5.5-6.5 dl/g) from Boehringer-Ingelheim (Germany), and poly(glycerol sebacate) (PGS) (polymerized for 24h under vacuum, MW: 9929 Da) produced in our lab were blended using Chloroform (Chl) : N,N-dimethyl formamide (DMF) (10:1 or 95:5 v/v) as the solvent. Biodegradable aligned fiber mats of PHBV-P(L-D,L)LA-PGS blends with different PGS content were prepared by electrospinning.

The home-made electrospinning set up used in this study consisted of a high voltage supply (Gamma High Voltage Research, Ormond Beach, FL, USA), a syringe pump (New Era Pump Systems, NE 1800), a 10 mL syringe capped with a blunt end-needle, and a grounded frame collector (Fig 2.1).

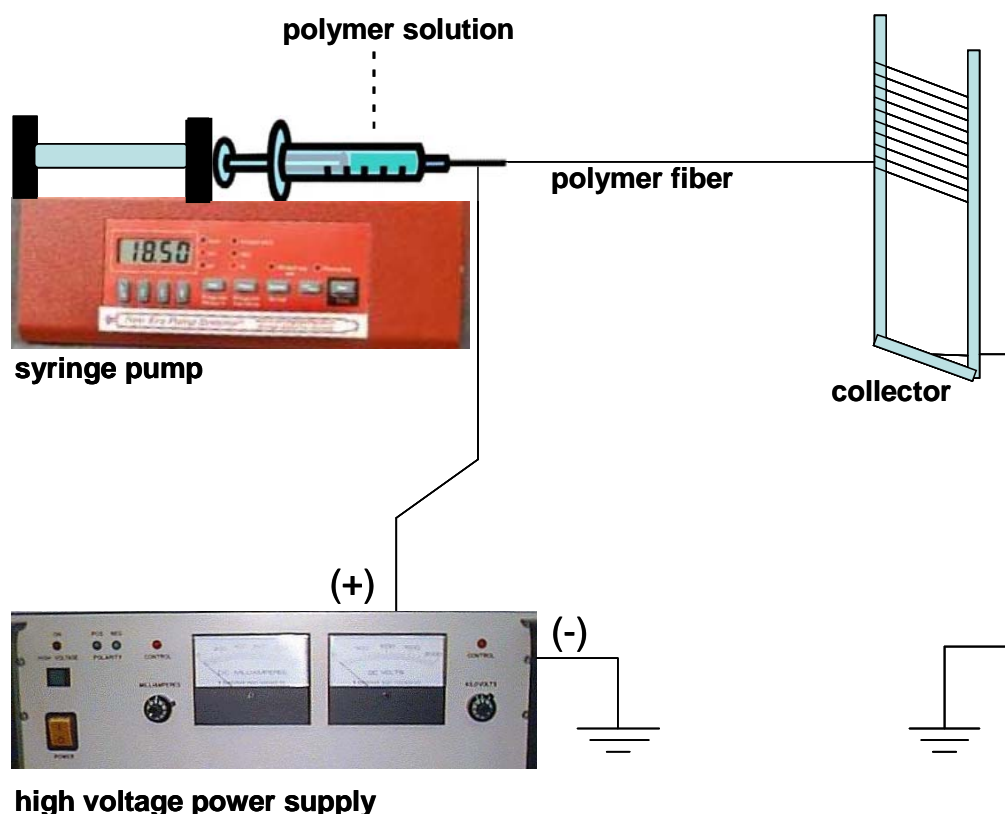


Figure 2.1 Electrospinning setup used to obtain aligned microfibrinous mats.

The experimental parameters were fine tuned until a good Taylor cone shape and a continuous thin polymer jet were obtained. Conditions were optimized to have minimum fiber fusion and minimum bead formation.

PHBV-P(L-D,L)LA (1:1 w/w) solution (5%) with varying PGS content (1, 2, or 4% w/w) in Chl:DMF (10:1) was electrospun at a flow rate of 30 $\mu\text{L}/\text{min}$ at 18 kV and a needle tip to receiver metal frame distance of 24 cm.

PHBV-P(L-D,L)LA solution (5%) that contained 0, 1, 2, or 4% w/w PGS in Chl:DMF (95:5) (here the DMF concentration was decreased by half in order to minimize fiber stickiness), was electrospun to obtain aligned fiber mats applying the same conditions. Unoriented fiber mats were prepared from 5% PHBV-P(L-D,L)LA and 5% PHBV-P(L-D,L)LA with 2% w/w PGS, too.

The types of microfiber mats obtained are summarized in Table 2.1.

Table 2.1 The types of microfiber mats obtained by electrospinning.

		Samples							
Parameter Varied		Unaligned Fiber Mats	Aligned Fiber Mats						
Solvent Composition	Chl:DMF 10:1		+	+	+				
	Chl:DMF 95:5	+				+	+	+	+
PGS Content	No PGS in polymer blend	+				+			
	1% PGS in polymer blend		+				+		
	2% PGS in polymer blend	+		+				+	
	4% PGS in polymer blend				+				+

2.4 Preparation of Macroporous Biodegradable Tubings

A 96:4 (w/w) blend of P(L,DL)LA (70:30) with PGS (polymerized for 24h under vacuum, MW: 9929 Da) was prepared in chloroform and coated on a glass rod and on a silver wire by dip coating and dried in the hood to test for feasibility of obtaining a tubing that can be demolded in water from the rod and the wire mechanically.

In order to obtain a macroporous tubing, the same blend was prepared and salt granules of 70-125 μm or less than 70 μm in diameter were added to obtain a salt concentration of 60% (w/v) and 70% (w/v), respectively. These blends were dip coated on stainless steel wires and after drying in the hood, the resultant biodegradable tubings were demolded in deionized water, dried and studied under SEM (QUANTA 400F Field Emission SEM).

For preparation of a bifunctional tubing with both nonporous and macroporous regions, the same blend of P(L,DL)LA with PGS was prepared in chloroform and coated on a section of the wire by dip coating and dried in the hood prior to coating the remaining part for the macroporous portion. A more practical method was developed to obtain the porous structure. P(L-D,L)LA-PGS solution was prepared in dioxane and coated on the remaining uncoated part of the stainless steel wire and subsequently frozen at $-80\text{ }^{\circ}\text{C}$ and freeze dried to obtain the macroporous part. After the freeze drying, the resulting biodegradable tubings were demolded in water and observed under stereomicroscope (Nikon SMZ 1500) and with SEM. Schematic presentation of the bifunctional tubing is given in Figure 2.2.

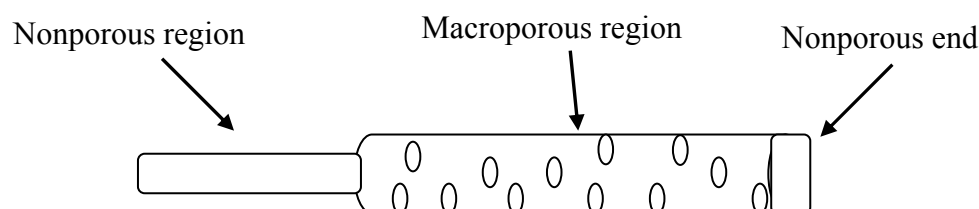


Figure 2.2 Scheme of the bifunctional tubing.

2.5 Characterization of Polymer Blends

2.5.1 Mechanical properties

The tensile tests of nonporous tubings obtained from P(L-D,L)LA and P(L-D,L)LA-PGS (96:4 w/w) were performed at room temperature (20 °C) with a Lloyd LRX 5K Mechanical Tester, controlled by a computer running program (WindapR). First samples were wetted in water overnight at 37 °C and then strained at room temperature. The biodegradable tubings (length 50 mm) were attached to the holders (gauge length: 10 mm) of the instrument. A constant extension rate of 10 mm/min was applied.

The tensile strength was obtained from equation $\sigma = F/A$, where σ is the tensile strength (MPa), F is the maximum load applied (N) before rupture, and A is the initial cross-sectional area (mm²) of the specimen. The load-deformation curve was converted to stress–strain curve, where stress is the load applied per unit area (F/A) and strain is the deformation per unit length ($(l-l_0)/l_0$). Slope of the straight line region (elastic region of the stress-strain curve) is accepted as the Young's Modulus of the specimen. The tests were repeated at least four times for each sample and the average values of Young's Modulus and tensile strength were calculated.

2.5.2 Hydrophilicity

Contact angle of a liquid droplet is the angle formed between the surface and the tangent to the droplet at the point it touches the surface (Fig 2.3). Contact angle indicates the strength of the weak interactions between the liquid and the first monolayer of the material. Small contact angles show a strong interaction between the liquid and the surface. In this study surface hydrophilicities of the polymer films were determined with deionized triple distilled water by a contact angle goniometer equipped with high-performance image processing system (KSV-CAM200, USA).

Water contact angles of blend films were recorded and average values obtained. For each sample at least 6 contact angle measurements were carried out.

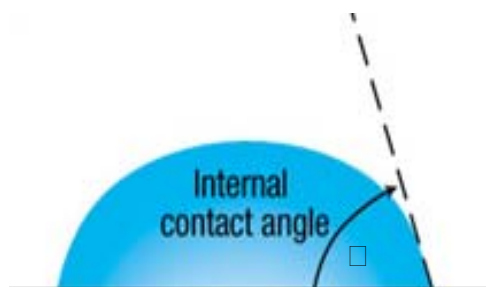


Figure 2.3 Water contact angle (□)

2.5.3 Gravimetric Determination of PHBV-P(L-D,L)LA-PGS Aligned Fiber Mat Erosion

For the degradation study, aligned fiber PHBV-P(L-D,L)LA-PGS mats with 1, 2 and 4% PGS were weighed (30-40 mg) and sterilized under UV C for 15 min each side. The mats were transferred into 50 mL Corning test tubes containing phosphate buffer (30 mL, pH 7.4, 10 mM, 100 U/mL penicillin and 100 µg/mL streptomycin) and incubated at 37 °C with 50 rpm rotation speed for 4 months. On days 10, 30, 60, 90 and 120 the mats were washed 3 times with distilled H₂O, dried in a vacuum oven for 48h and weighed. After every measurement, the incubation was continued within the starting PBS solution. The samples were studied in duplicate and all measurements were expressed as means of remaining weight.

2.6 In Vitro Studies

2.6.1 Characterization of Human Wharton's Jelly (hWJ) MSCs in Comparison to MSCs from Human Bone Marrow (hBM) (USA)

This study focused on the determination of the capacity of mesoderm originated MSCs to differentiate to cardiac cells, which are derived from mesoderm. A broader investigation of cardiomyogenic lineage markers expressed by human MSCs in their undifferentiated state may help reveal their potential to differentiate to cardiomyocytes and to determine the genes whose expression should be induced to obtain the target mature cells. Immunophenotypic characterization in addition to osteogenic and adipogenic differentiation of WJ MSCs with respect to BM MSCs and assessment of cardiomyogenic lineage markers of both cell types were carried out.

2.6.1.1 Culture of MSCs from Bone Marrow and Wharton's Jelly

Human BM MSCs were obtained from whole bone marrow aspirates from male donors of 25 years of age (Clonetics-Poietics, Walkersville, MD) as previously described (Chen et al., 2003). They were plated at 8–10 mL aspirate/cm² on 185 cm² tissue culture flasks and cultivated until confluence (12–14 days) in 40 mL of expansion medium consisting of Dulbecco's modified Eagle's medium (DMEM) supplemented with 10% fetal calf serum (FCS), 100 U/mL penicillin, 100 µg/mL streptomycin, 1 ng/mL of basic fibroblast growth factor (bFGF) (all from InVitrogen), and 0.1 mM nonessential amino acids (Sigma). MSCs were grown in a humidified tissue culture incubator at 37 °C with 5% CO₂. MSCs were selected on the basis of their ability to adhere to the tissue culture polystyrene (TCPS). After 5 days in culture the medium was replaced to get rid of the non-adherent hematopoietic cells, and afterwards the medium was changed twice per week. The

primary culture MSCs were subsequently detached using 0.05% trypsin/EDTA, and frozen in liquid nitrogen in FCS containing 8% dimethyl sulfoxide (DMSO) to be used later. The MSCs were thawed and cultured until confluence in the expansion medium on TCPS to obtain Passage 1, and subsequently Passage 2 cells with a plating density of 5×10^3 cells/cm².

Human WJ MSCs isolated from umbilical cord matrix (Friedman et al., 2007) were kindly provided by Dr. Hans Klingemann (Tufts University, New England Medical Center, MA, USA), and cultured under the same conditions as BM MSCs mentioned above.

Human BM and WJ MSCs at passage (P) 2, 3 and 4 were used for the characterization studies. Both cell types were stained with Alexa Fluor 546 Phalloidin (Invitrogen) for actin filaments and with Hoechst 33342 (Invitrogen) for their nuclei, and examined via fluorescence microscopy for morphological analysis.

2.6.1.2 Flow Cytometric Analysis of hMSCs

Specific surface antigens of BM MSCs and WJ MSCs (P2, P3, and P4) were analyzed by flow cytometry. Cell surface markers investigated were hematopoietic lineage markers (CD34, CD45), adhesion integrins (CD49d, CD106), MSC markers like SH2 (CD105), SH3 (CD73), CD44, CD29 and CD90, immunogenic antigens (HLA-ABC (MHC class I), HLA-DR (MHC class II)), and the early endothelial progenitor cell marker CD133. The cell surface markers were visualized using peridin chlorophyll-a (PerCP)-conjugated anti-CD49d, CD29, HLA-DR, fluorescein isothiocyanate (FITC)-conjugated anti-CD105, CD44, CD45, and phycoerythrin (PE)-conjugated anti-CD106, CD73, CD34, allophycocyanin (APC)-conjugated CD90, HLA-ABC and CD133. All antibodies were purchased from BD Biosciences except anti-CD105 (Serotec) and anti-CD133 (Miltenyi Biotech). To stain the MSCs, the cells were detached with trypsin, pelleted (ca. 10^5 cells), and resuspended in 1% BSA in PBS before addition of fluorochrome conjugated monoclonal antibodies. After incubation for 45 minutes at 4°C, the cells

were fixed with 1% paraformaldehyde (PFA), and analyzed in a FACSCalibur flow cytometer (BD Biosciences), using CellQuest software (BD Pharmingen). An isotype control was included in each experiment; specific staining was measured from the cross point of the isotype graph with the particular antibody graph, and positive cells were counted.

2.6.1.3 Osteogenic Induction of hMSCs

In order to differentiate the hMSCs into osteoblasts, to prove that they are mesenchymal stem cells, the cells from both sources at P2 were seeded at 5×10^3 cells/well into 24-well plates in the expansion medium. After 1 day of incubation, the MSCs were cultured in DMEM medium containing 10% FCS, 100 U/mL penicillin, 100 μ g/mL streptomycin, 0.1mM nonessential amino acids, 10 nM dexamethasone, 50 μ g/mL ascorbic acid, and 10 mM β -glycerophosphate for 21 days in an incubator at 37°C, and the medium was refreshed twice a week. The control samples were cultured under the same conditions in the absence of osteogenic supplements: dexamethasone, ascorbic acid and β -glycerophosphate. After 21 days of culture, differentiation of the cells to osteoblasts was proved by alkaline phosphatase (ALP) activity assay. Briefly, the cells were lysed with 0.2% (v/v) Triton X-100 and the homogenate was incubated with the AMP buffer (Sigma) and the substrate p-nitrophenyl phosphate (Sigma) at 37°C for 1h. The reaction was stopped with 0.2 M NaOH and then the concentration of p-nitrophenol, the product of the enzymatic activity, was measured spectrophotometrically at 405 nm. A calibration curve of p-nitrophenol at 37 °C was used to determine the enzyme activity in units of micromole substrate converted to product per minute.

2.6.1.4 Adipogenic Induction of hMSCs

Human MSCs at P2 were plated at 5×10^3 cells/well in 24 well plates, and cultured in expansion medium for 1 day. To induce adipogenic differentiation, and again to prove that they are mesenchymal stem cells, the cells were grown in DMEM supplemented with 10% FCS, 100 U/mL penicillin, 100 mg/mL streptomycin, 0.1mM nonessential amino acids and adipogenic stimulants consisting of 0.5 mM 3-isobutyl-1-methyl xanthine (IBMX), 1 μ M dexamethasone, 5 μ g/mL insulin, and 50 μ M indomethacin, for 21 days (Mauney et al., 2005). MSC control cultures were maintained similarly in parallel without adipogenic stimulants. All MSC cultures were maintained in an incubator at 37°C and medium change was carried out twice a week. To detect intracellular fat deposition, the cells were fixed with paraformaldehyde and stained with Oil Red-O for 45 min with a filtered 60% Oil Red-O solution in PBS, prepared from a stock solution of 0.07 g Oil Red-O powder in 20 mL of isopropanol. The background formed due to Oil Red-O staining was removed by washing the culture with PBS, and then the photomicrographs of cells were obtained with a light microscope.

2.6.1.5 Cardiomyogenic Potential of hMSCs

2.6.1.5.1 Gene Expression of MSCs Analyzed by Reverse Transcription –PCR

Total RNA was isolated from human MSCs (BM and WJ at P2, P3 and P4) and human myocardial tissue using NucleoSpin RNA II kit (Clontech, BD Biosciences) and stored at -80°C. The cDNA was synthesized, and then amplified with Polymerase Chain Reaction (PCR) using OneStep RT-PCR kit (Qiagen). The mRNA obtained from normal human myocardium extract (kindly provided by Dr. Richard Patten from Tufts U.-NEMC, Boston, MA) was used as positive control.

PCR was performed in a 20 μ L reaction solution composed of 4 μ L of 5x Qiagen OneStep RT-PCR buffer (with 12.5 mM MgCl₂), 0.8 μ L of dNTP mix (having 10 mM of each dNTP), 0.8 μ L of OneStep RT-PCR Enzyme Mix (composed of Omniscript Reverse Transcriptase, Sensiscript Reverse Transcriptase, and HotStarTaq DNA Polymerase), 0.5 μ L of RNase inhibitor, 2 μ L of forward and reverse primers (0.4 μ M), and variable volumes of template RNA (30 ng) and RNase free water. The RT-PCR conditions were as follows: 30 min at 50°C, 15 min at 95°C followed by 30 cycles of 94°C for 30 s, 55°C for 30 s, and 72°C for 30 s, and final extension for 10 min at 72°C. Primer sequences (forward, reverse) and lengths of the amplified products are listed in Table 2.2. β -Actin was analyzed as a housekeeping gene. The PCR products were size fractionated by 2% agarose gel electrophoresis, stained with ethidium bromide, and visualized by UV illumination.

Table 2.2 Primers used for RT-PCR

Gene	Primer Sequence (Forward-Reverse)	Product Size (bp)
Housekeeping gene β -Actin	5'-AACGGTGAAGGTGACAGCA-3' 5'-TGTGTGGACTTGGGAGAGG-3'	202
GATA binding protein 4 (GATA4)	5'-ATCCAAACCAGAAAACGGAAG-3' 5'-GGGAGACGCATAGCCTTGT-3'	297
NK2 transcription factor related, locus 5 (Nkx 2.5)	5'-ATGGTATCCGAGCCTGGTAG-3' 5'-ATAATCGCCGCCACAAAC-3'	211
Myocyte enhancer factor 2A (MEF 2A)	5'-CAATGCCGACTGCCTACAA-3' 5'-AACTGCCCTCCAGCAACA-3'	166
Myocyte enhancer factor 2C (MEF 2C)	5'-CCAGGCAGCAAGAATACGAT-3' 5'-AACCCAGACAGAGATGACAGGT-3'	227
Myocyte enhancer factor 2D (MEF 2D)	5'-GGCAACAGCCTAAACAAGGTC-3' 5'-GGTGGTGAGCGAATGAGTAGA-3'	210
T-box 5 (Tbx5)	5'-GCGGATGTTTCCCAGTTACA-3' 5'-CAGGTGGTTGTTGGTGAGC-3'	253
Zinc finger protein friend of GATA 2 (FOG-2)	5'-CCAGGCTTCCTCAAATGG-3' 5'-TGTGGTCGTCTTCGTGCT-3'	170

2.6.1.5.2 Induction of Differentiation to Cardiomyocytes

hBM MSCs (P3) and hWJ MSCs (P5), approximately 90% confluent, were trypsinized and then seeded on 24 well TCPS plates in DMEM medium (10%FCS, 1% Pen/Strep, nonessential amino acids) supplemented with either bovine insulin (100 µg/mL) or bovine insulin (100 µg/mL) and valproic acid (2 mM). The medium was refreshed 2 times a week. After 14 days of growth in the particular differentiation medium, cells were studied by RT-PCR and immunocytochemistry.

Immunocytochemistry was carried out using standard protocols. Cell nuclei were counterstained with 4,6-diamidino-2-phenylindole (DAPI). Antibodies (Ab) and dilutions were as follows: α -actinin, monoclonal, 1:500 (Sigma); ventricular α/β myosin heavy chain (MHC) (Biocytex Biotech), monoclonal, 1:10. Following overnight incubation of primary Ab at 4 °C, fluorescent labeled secondary Ab were applied for 45 minutes at RT, and the samples were examined with fluorescence microscope.

2.6.2 hWJ MSC Isolation from Umbilical Cord Matrix and Its Culture (TR)

Human Wharton's Jelly MSCs (WJ MSCs) were isolated from umbilical cord matrix. Human umbilical cords were collected from full-term births with informed consent of the mother (APPENDIX A) after either caesarean section or normal delivery and aseptically stored at 4°C in sterile saline until processing. The interval between collection and isolation of WJ MSCs was at most 24h. To isolate WJ MSCs, the cords were rinsed several times with sterile saline and cut into 2- to 4-cm lengths, the vessels were stripped manually from cord segments and the wall of the cords was cut open. The explants were transferred to 6-well plates containing either DMEM low glucose/Ham F-12 (1:1) with 10% fetal bovine serum, 100 U/mL penicillin, 100 µg/mL streptomycin, and 1 ng/mL of basic fibroblast growth factor (bFGF) or α MEM/Ham F-12 (1:1) with 2% fetal bovine serum, 100 U/mL penicillin

and 100 µg/mL streptomycin. They were left undisturbed for 2 weeks to allow migration of cells from the explants. WJ MSCs were fed 3 times a week and passaged and cryopreserved. Schematic presentation of the cell isolation procedure is given in Figure 2.4.

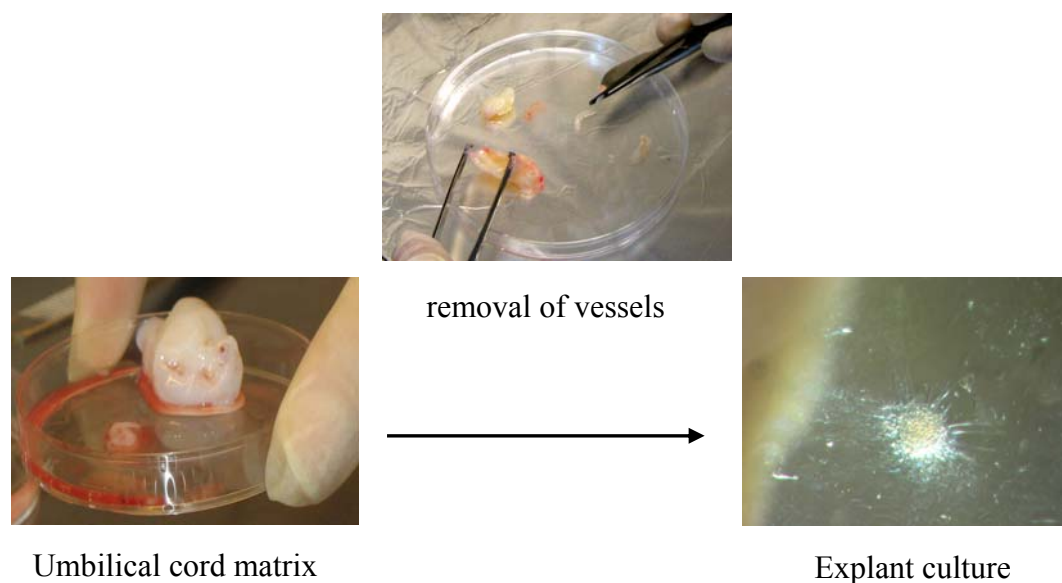


Figure 2.4 Schematic presentation of the WJ MSC isolation procedure.

2.6.3 Characterization of hMSCs Isolated from Wharton's Jelly

2.6.3.1 Cell Growth Kinetics: Doubling Time Determination

WJ MSCs isolated as in Section 2.6.2 and grown until 2nd passage on TCPS were trypsinized and counted. The cell suspension was diluted to 1×10^4 cells/mL and 1 mL was seeded into each well of the 24-well plate. The plate was incubated at 37 °C in a CO₂ incubator for 24 h and the cell number in three of the

wells was determined with MTS test. 500 μ L of DMEM Low Glu with 10% MTS/PES was applied on cells in a well and the plate was incubated at 37°C in the CO₂ incubator for 2h, and finally 200 μ L aliquots were taken from the wells and absorbance was determined at 490 nm using an Elisa Plate Reader (Molecular Devices (USA), Model Maxline). Cell numbers were calculated using a calibration curve that was prepared using the same protocol. Cell number determination in triplicates was repeated on days 2, 3, 4, 6, 8 and 10. The medium of the wells was changed twice a week.

2.6.3.2 Osteogenic Induction of hWJ MSCs

In order to differentiate the hMSCs into osteoblasts, to prove that they are mesenchymal stem cells, the cells at P3 were seeded at 5×10^3 cells/well into 24 well plates in the expansion medium. After 1 day of incubation, the MSCs were cultured in DMEM medium containing 10% FCS, 100 U/mL penicillin, 100 μ g/mL streptomycin, 10 nM dexamethasone, 50 μ g/mL ascorbic acid, and 10 mM β - glycerophosphate for 14 days in an incubator at 37°C, and the medium was refreshed twice a week. The control samples were cultured under the same conditions but without the osteogenic supplements dexamethasone, ascorbic acid and β -glycerophosphate. After 14 days of culture, differentiation to osteoblasts was shown by alkaline phosphatase (ALP) activity assay. Briefly, the cells were washed with PBS and lysed with 0.3 mL Tris buffer (10mM, pH 7.5, 0.2% Triton X-100). The samples were freeze-thawed three times, sonicated (5 min, 25 W) on ice and centrifuged (2000 rpm, 10 min) to get rid of large particles. ALP activity of cells was determined from the supernatant using an ALP kit (Randox). The supernatant was incubated with the substrate p-nitrophenyl phosphate (Sigma) at 37°C for 2 h. The reaction was stopped with 0.2 M NaOH and then the concentration of p-nitrophenol, the product of the enzymatic activity, was measured spectrophotometrically at 405 nm. A calibration curve of p-nitrophenol at 37 °C was used to

determine the enzyme activity in units of “nanomole substrate converted to product per minute”. Samples were studied in triplicate.

Von Kossa staining was done to demonstrate deposits of calcium-phosphate minerals by the osteoblasts. In this method, the cells were fixed with 4% formaldehyde for 15 min at room temperature, then rinsed with distilled water and treated with a 1% silver nitrate solution for 20 min under UV C. Unreacted silver was removed with 5% sodium thiosulfate for 5 min and the samples were rinsed several times with distilled water prior to observation with a light microscope. Samples were studied in triplicate.

2.6.3.3 Chondrogenic Induction of hWJ MSCs

Passage number 3 WJ MSCs seeded in 24-well plates as 5×10^3 cells/well were supplied with a chondrogenic medium: DMEM High Glucose medium with 50 $\mu\text{g/mL}$ ascorbic acid, 1% non-essential amino acids, 5 $\mu\text{g/mL}$ bovine insulin, 10 nM dexamethasone, and 5 ng/mL TGF $\beta 1$, that either contained 15% FCS or did not. The cells were grown in this chondrogenic medium for 14 or 21 days, with a medium change twice a week. At the end of the culture period, the cells were fixed with 4% formaldehyde for 15 min at room temperature and stored in PBS at 4 °C until staining.

For Alcian Blue staining, 0.1 g of Alcian Blue was dissolved in 10 mL of 3% acetic acid solution (pH 2.5). The cells were washed with distilled H_2O , incubated in Alcian Blue solution for 30 min at room temperature and washed with distilled H_2O before examination with light microscope.

For immunostaining, the fixed cells were rinsed 3 times with PBS and incubated in 100 mM glycine for 15 min (to saturate reactive PFA groups). The samples were washed again 3 times with PBS and incubated in 0.1% Triton X-100 (in PBS, 10 mM) for 5 min. After rinsing 3 times with PBS the background was blocked with 1% BSA containing PBS (10 mM) solution at 37 °C for 30 min. Next, the samples were left for 1 h in the 0.1% BSA solution that contained the primary

Ab (anti-Collagen Type II, 1:100) at 37°C. The cells were washed 3 times with PBS and incubated with the secondary Ab (Alexa Fluor 488 labeled, 1:100 in PBS) for 1 h at 37 °C. After rinsing 3 times with 0.1% Triton X-100 (in PBS), the samples were counterstained with DAPI for their nuclei and observed under fluorescence microscope (Olympus IX 70, Japan).

2.6.4 Differentiation of hWJ MSCs to Cardiomyocytes

2.6.4.1 Gene Expression of Undifferentiated hWJ MSCs Analyzed by RT-PCR

Total RNA was isolated from undifferentiated human WJ MSCs (at P3) using NucleoSpin RNA II kit (Clontech, BD Biosciences) and stored at -80°C. The cDNA was synthesized, and then amplified with PCR using OneStep RT-PCR kit (Finnzymes RobusT II). PCR was performed in a 20 µL reaction solution with 2.5 mM MgCl₂ for Nkx 2.5 and 1.5 mM for all other genes. The RT-PCR conditions were as follows: 45 min at 48°C, 2 min at 94°C followed by 30 cycles of 94°C for 30 s, 55°C for 30 s, and 72°C for 1 min, and final extension for 10 min at 72°C. Amount of template RNA used was 30 ng/reaction. Primer sequences (forward, reverse) and lengths of the amplified products were the same ones given in Table 2.2, except GATA4; GATA4 had 5'-AACGGAAGCCCAAGAACC-3' forward primer sequence, 5'-AGAGGACAGGGTGGATGGA-3' reverse primer sequence, and the expected length of PCR product was 246 bp. β-Actin was analyzed as a housekeeping gene. The PCR products were size fractionated by 2% agarose gel electrophoresis, stained with ethidium bromide, and visualized by UV illumination.

2.6.4.2 Influence of Cardiomyogenic Differentiation Factors on hWJ MSCs

The Wharton's Jelly MSCs cultured in the α MEM/Ham F-12 (1:1) supplemented with 2% fetal bovine serum, 100 U/mL penicillin and 100 μ g/mL streptomycin were grown until the P3 and then detached from the flask by trypsinization and 5×10^3 cells/well were seeded into collagen Type I coated 24-well plates to study differentiation to cardiomyocytes. The primary medium (PM), which served as negative control consisted of DMEM High Glu with 10% FCS, 1% non-essential amino acids and 1% antibiotics (Pen/Strep). Media composition of the four experimental groups were as follows: 1) PM only, 2) PM supplemented with 2 mM Valproic acid (VA), 3) PM supplemented with 100 μ g/mL bovine insulin (B. Ins) and 2 mM VA, and 4) PM supplemented with 100 μ g/mL B. Ins, 1 ng/mL interleukin 1-beta (IL 1 β) and 2 mM VA. The cells were cultured for 14 days and analyzed by immunostaining and RT-PCR for cardiomyogenic differentiation.

2.6.4.2.1 Gene Expression Analysis by RT-PCR

Total RNA was isolated from WJ MSCs exposed to cardiac differentiation factors using Qiagen RNeasy Kit and stored at -80°C. The cDNA was synthesized, and then amplified with PCR using OneStep RT-PCR kit (RobusT II, Finnzymes). PCR was performed in a 20 μ L reaction solution with 2.5 mM MgCl₂ for Nkx 2.5 and 1.5 mM for GATA4 and beta actin, whose primer sequences and PCR product sizes were mentioned in section 2.6.4.1. The RT-PCR conditions were the same as mentioned in section 2.6.4.1, too. β -Actin was analyzed as a housekeeping gene. The PCR products were size fractionated by 2% agarose gel electrophoresis, stained with ethidium bromide, and visualized by UV illumination.

2.6.4.2.2 Immunostaining for ventricular α/β MHC

The fixed cells were rinsed 3 times with PBS and incubated in 100 mM glycine for 15 min (to saturate reactive PFA groups). The samples were washed again 3 times with PBS and incubated in 0.1% Triton X-100 (in PBS, 10 mM) for 10 min. After rinsing 3 times with PBS the background was blocked with 1% BSA containing PBS (10 mM) solution at 37 °C for 30 min. Next, the samples were left for 1h in the 0.1% BSA solution that contained the primary Ab α/β MHC (1:10 dilution) at 37°C. The cells were washed 3 times with PBS and incubated with the secondary Ab (Alexa Fluor 532 labeled, 1:100 in PBS) for 1h at 37 °C. After rinsing 3 times with PBS, and counterstaining cell nuclei with DAPI, the samples were observed under fluorescence microscope.

2.7. Tissue Engineering on Microfiber Mats

2.7.1 Morphology of hWJ MSCs Cultured on the Unaligned and Aligned Microfiber Mats

Electrospun blends of PHBV-P(L-D,L)LA and PHBV-P(L-D,L)LA with 2% w/w PGS were tested for their suitability for attachment and alignment of WJ MSCs. Third passage WJ MSCs fed with α MEM/Ham F-12 (1:1) with 2% fetal bovine serum, 100 U/mL penicillin and 100 μ g/mL streptomycin were detached from the flask surface with trypsin, and 7.5×10^3 cells in 500 μ L of α MEM/Ham F-12 (1:1) with 10% fetal bovine serum, 1% non-essential amino acids, and 100 U/mL penicillin and 100 μ g/mL streptomycin were seeded on the UV sterilized 1×1 cm² mats. The cells were cultured on the mats at 37 °C in the CO₂ incubator for 5 days and then samples were fixed in 4% PFA for fluorescence microscopy examination.

The fibrous mats were stained with FITC-labeled Phalloidin (Sigma) in order to observe the orientation of cytoskeletal actin filaments, and the cell nuclei

were counterstained with DAPI. Samples were washed twice with PBS (10 mM, pH 7.4) and fixed in formaldehyde solution (4%) for 30 min at room temperature. The samples were again washed twice with PBS and the cells were permeabilized with 0.1% Triton X-100 solution for 5 min at room temperature. After washing with PBS, samples are incubated at 37°C for 30 min in 1% BSA containing PBS solution in order to block the non-specific binding. After washing with 0.1% BSA, FITC-labeled Phalloidin (1:100 dilution in 0.1% PBS-BSA from stock of 0.1 mg/mL) was added and samples were incubated for 1 h at 37°C. Finally, the samples were washed with 0.1% BSA solution (in PBS) and counterstained with DAPI solution (diluted 1:1000 in PBS) for 10 min at room temperature and washed with PBS. The samples were transferred on microscope slides and observed using fluorescence microscope of a CLSM (Leica DM 2500, Germany) under 488 nm filter for phalloidin and under 330-385 nm filter for DAPI.

Nile red was used to stain the fibers of mats to show the fiber orientation. A stock of 0.5 mg Nile red per mL of acetone was prepared and 50 μ L of this stock was added to 50 mL of 75:25 (v/v) glycerol-water to obtain the final staining concentration of the dye. The staining solution was transferred on the dry mats and after 15 min they were observed under 532 nm filter of a fluorescence microscope (Olympus IX 70, Japan).

2.7.2 hWJ MSC Proliferation on the Aligned Microfiber Mats

Upon obtaining confluent monolayers, third passage WJ MSCs fed with α MEM/Ham F-12 (1:1) with 2% fetal bovine serum, 100 U/mL penicillin and 100 μ g/mL streptomycin were detached from the flask surface with trypsin, resuspended in α MEM/Ham F-12 (1:1) with 10% FCS, 1% non-essential amino acids and 100 U/mL penicillin and 100 μ g/mL streptomycin to 6×10^4 cells/mL, and 3×10^4 cells were seeded on PHBV-P(L-D,L)LA and PHBV-P(L-D,L)LA:PGS (98:2) parallel fiber-mats with $1 \times 1 \text{ cm}^2$ area that were either unmodified or collagen type I adsorbed (from 40 μ g/mL collagen solution). Cell seeded mats were incubated at 37°C in the CO₂ incubator for 1 and 14 days and cell number on the mats was

determined with MTS test at these time points. Briefly the mats were transferred into freshly prepared 500 μL of DMEM Low Glu with 10% FBS and 10% MTS/PES, in a new 24-well plate and the plate was incubated at 37°C in the CO₂ incubator for 2 h, and finally 200 μL aliquots were taken from the wells and absorbance was determined at 490 nm using an Elisa Plate Reader (Molecular Devices (USA), Model Maxline). Cell numbers were calculated using a calibration curve that was prepared using the same protocol.

2.8. Tissue Engineering in a Microbioreactor

2.8.1 Microbioreactor Design

A poly(dimethyl siloxane) (PDMS) chamber with 1x1.5x1 cm³ volume was prepared by using a PMMA mold. The PDMS prepolymer-catalyst mixture (10:1 by weight) was poured on the PMMA mold and it was polymerized at 60°C. Resulting PDMS chamber was removed mechanically from the mold.

Two inlets and one outlet were drilled through the PDMS wall and Tygon tubings inserted for medium infusion through the chamber (Fig 2.5).

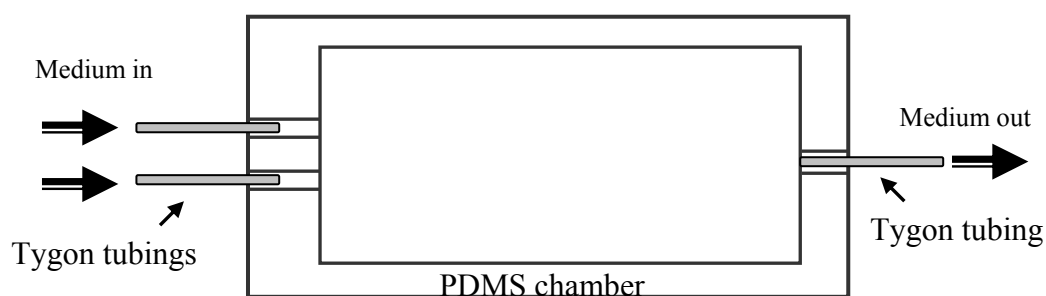


Figure 2.5 Scheme of the microbioreactor (top view).

2.8.2 Assembly of the 3D Construct

Electrospun parallel fiber PHBV-P(L-D,L)LA-PGS (98:2) mats were seeded with undifferentiated cells, cultured for 14 days and finally rolled around macroporous region of the biodegradable tubings to obtain a 3D construct. It was designed as such to be able to send the cell growth medium through the tubings to feed the cells residing within the layers of 3D aligned fiber mats.

In the preliminary trial, the electrospun parallel fiber PHBV-P(L-D,L)LA-PGS (98:2) mats ($3.5 \times 6 \text{ cm}^2$) were placed in sterile petri plates of 10 cm diameter, sterilized under UV C light for 15 min each side, coated with Collagen Type I as done previously and then seeded with 6×10^5 WJ MSC cells (from 10^5 cells/mL cell suspension) and cultured for 14 days in α MEM/Ham F-12 (1:1) with 2% fetal bovine serum, 100 U/mL penicillin and 100 $\mu\text{g/mL}$ streptomycin medium in the CO_2 incubator. Media was refreshed twice a week. The aligned fiber mats with WJ MSCs grown on them for 14 days were wrapped around macroporous portion of UV sterilized biodegradable tubings, so that the fibers are parallel to the main axis of the tubings, to form a 3D construct (Fig 2.6). One mat was rolled around one tubing and then rolled together with one half rolled mat around another tubing.

In the second application, the electrospun parallel fiber PHBV-P(L-D,L)LA-PGS (98:2) mats ($3.5 \times 6 \text{ cm}^2$) were placed in sterile petri plates of 10 cm diameter, sterilized under UV light, coated with Collagen Type I and seeded with 3×10^5 WJ MSC cells (from 2×10^5 cells/mL cell suspension) and cultured for 14 days in α MEM/Ham F-12 (1:1) with 10% fetal bovine serum, 1% non-essential amino acids, and 100 U/mL penicillin and 100 $\mu\text{g/mL}$ streptomycin medium in the CO_2 incubator. Media was refreshed twice a week. The aligned fiber mats with WJ MSCs grown on them for 14 days were wrapped around macroporous portion of UV sterilized biodegradable tubings like it was mentioned previously but this time with Collagen Type I gel among the mat layers.

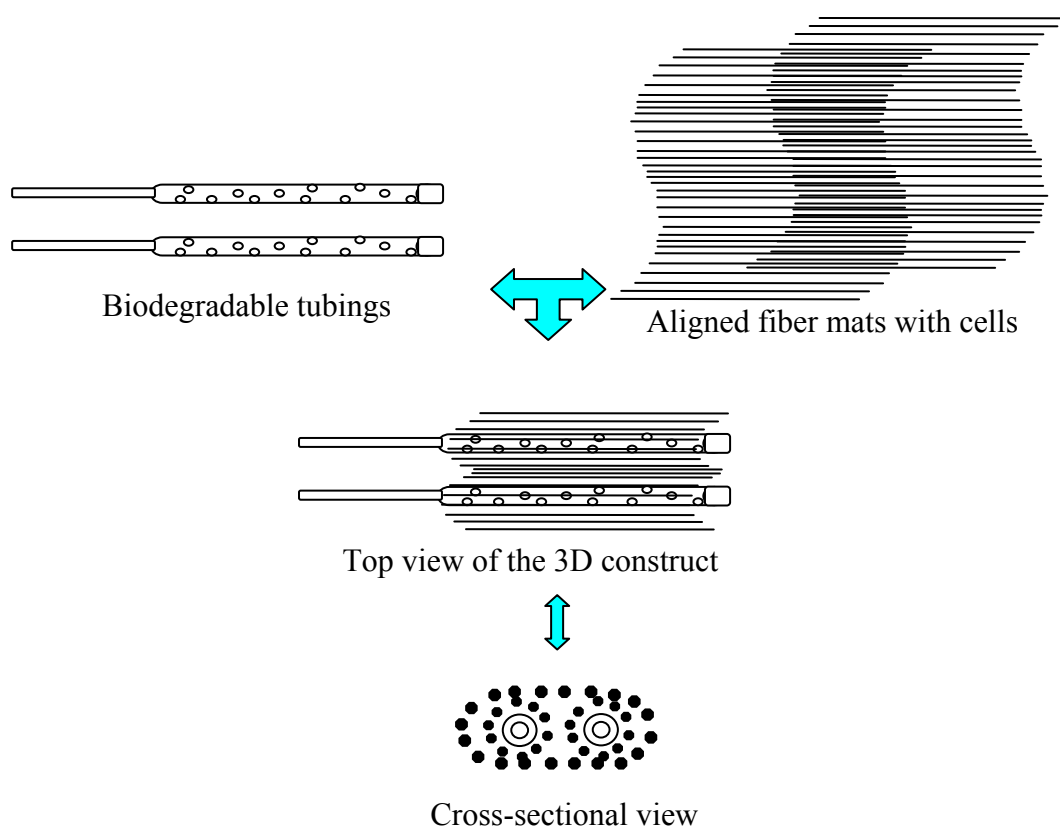


Figure 2.6 Schematic presentation of the method used to form the 3D construct.

2.8.3 Culture of the 3D Construct in the Microbioreactor

To assemble the 3D construct in the microbioreactor, the PDMS chamber and a glass cover were sterilized under UV C for 15 min. The Tygon tubings were sterilized by flushing 70% EtOH through them and inserted in the inlet and outlet holes of the PDMS chamber. The 3D constructs were placed in the PDMS chambers full of media. A glass slide was placed as a cover on the chambers.

In the preliminary trial, one of the two cultures started was kept static and medium was perfused through the biodegradable tubings of the other culture. The media of the both chambers was refreshed every other day. In order to perfuse

media through the biodegradable tubings of 3D construct in the perfused chamber, its biodegradable tubings (the nonporous portion) were inserted to the inner side of the chamber inlets (Fig 2.7). A total of 250 μL medium was perfused through the 3D construct in this chamber at a rate of 100 $\mu\text{L}/\text{h}$ every other day. Both constructs were cultured for 6 days.

In the second application, cardiac differentiation medium (DMEM High Glu with 10% FCS, 1% non-essential amino acids, 1% Pen-Strep, 100 $\mu\text{g}/\text{mL}$ B. Ins, 1 ng/mL IL 1 β and 2 mM VA) was applied to the 3D constructs in the static and medium perfused cultures for 14 days, while media of the chambers was refreshed every third day. A total of 250 μL medium was perfused through the 3D construct in the medium perfused chamber at a rate of 100 $\mu\text{L}/\text{h}$ every third day. Both constructs were cultured for 14 days.

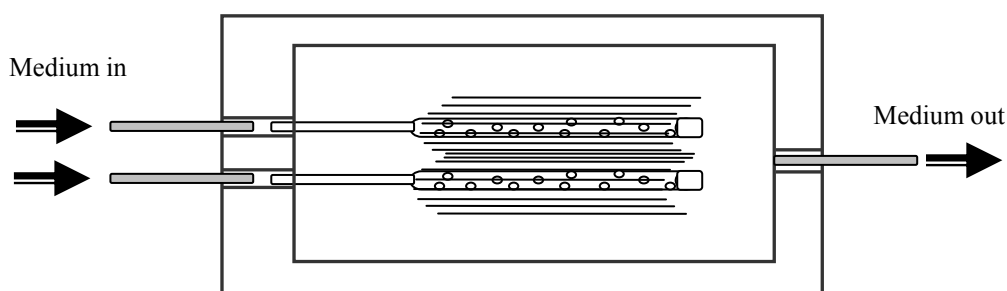


Figure 2.7 Scheme of the growth medium perfused culture of the 3D construct in the microfluidic device.

2.8.4 Analysis of the 3D Constructs Cultured in the Microfluidic Device

In the preliminary trial, after 6 days of culture the constructs were washed with PBS and fixed with 2.5% glutaraldehyde in 0.1 M, pH 7.4 cacodylate buffer for 45 min at room temperature. Prior to SEM analysis, the constructs were washed with distilled H_2O , frozen at $-80\text{ }^{\circ}\text{C}$ and gross-sectioned with a scalpel in their frozen state. Finally the sections were dried at room temperature, and some

were coated with Cd-Au to examine with SEM. The remaining sections were stained with Acridine Orange in order to visualize the cells in the construct with confocal microscope (Leica DM 2500, Germany). The constructs were washed with PBS (10 mM, pH 7.2) and then stained with acridine orange (6 $\mu\text{g/mL}$) for 10 min at room temperature and washed with PBS before the microscopic examination at 488 nm.

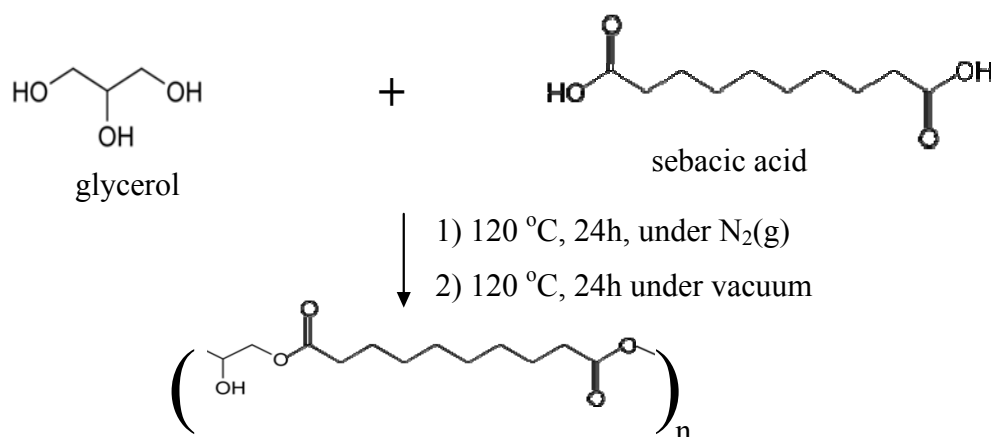
In the second application of 3D construct, after 14 days of culture both constructs were cut with a scalpel into 1 cm-long 3 pieces. One of the pieces was transferred into a cell lysis buffer for further RNA isolation and RT-PCR analysis. Cardiac specific gene expression of differentiated cells in both cultures was analyzed with RT-PCR. The second piece was embedded in OCT for further cryosectioning prior to immunostaining. The 20 μm thick longitudinal sections of the engineered tissues, obtained by cryosectioning, were immunostained for ventricular α/β MHC and also stained with Acridine Orange and FITC-Phalloidin for evaluation of cell alignment with confocal microscopy. The third piece was subjected to MTS for cell number determination.

CHAPTER 3

RESULTS AND DISCUSSION

3.1 Poly(glycerol sebacate) (PGS) Polymerization

Polymer formation was followed by obtaining ATR-FTIR spectra of the monomer mixture at different times during the polymerization process. These spectra were compared to those of monomers: glycerol (Fig 3.1) and sebacic acid (Fig 3.2). The polycondensation reaction of sebacic acid and glycerol to yield poly(glycerol sebacate) is as follows:



This reaction yielded a transparent, almost colorless viscous liquid that solidifies to a whitish sticky material when cooled to room temperature at the end of 48h polymerization. The resulting prepolymer features hydroxyl groups directly attached to the backbone. The intense C=O stretch at 1740 cm^{-1} in ATR-FTIR spectrum confirms the formation of ester bonds (Fig 3.3). Decrease in –OH stretch at $3400\text{--}3450\text{ cm}^{-1}$ due to decrease in glycerol amount in the monomer mixture is also an indication of polymerization (Fig 3.3).

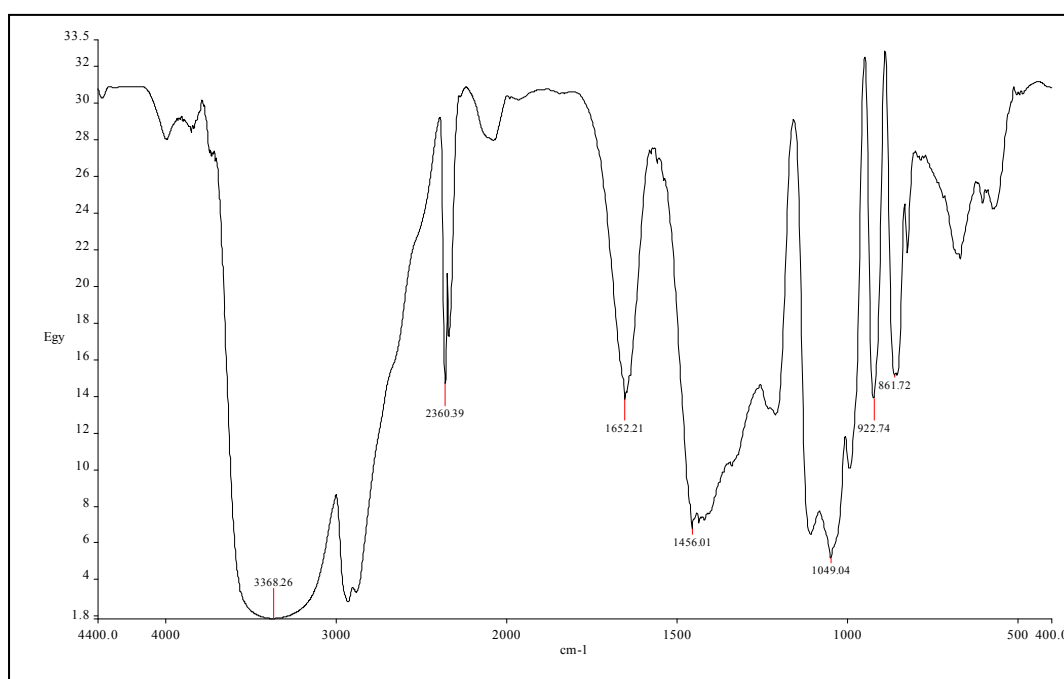


Figure 3.1 FTIR spectrum of Glycerol

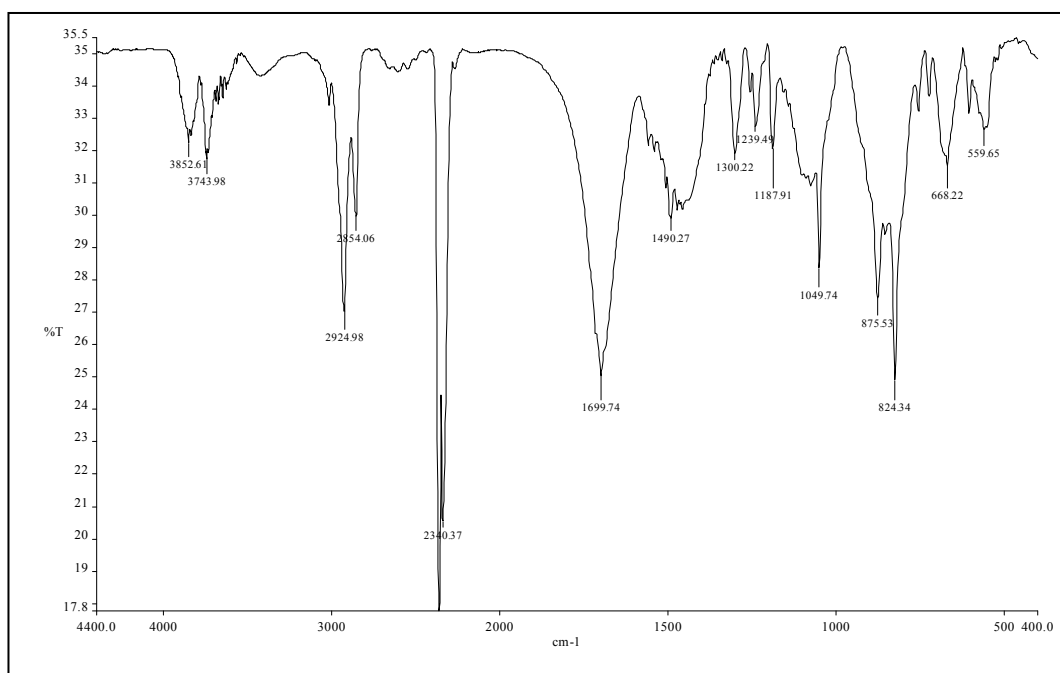


Figure 3.2 IR spectrum of Sebacic Acid

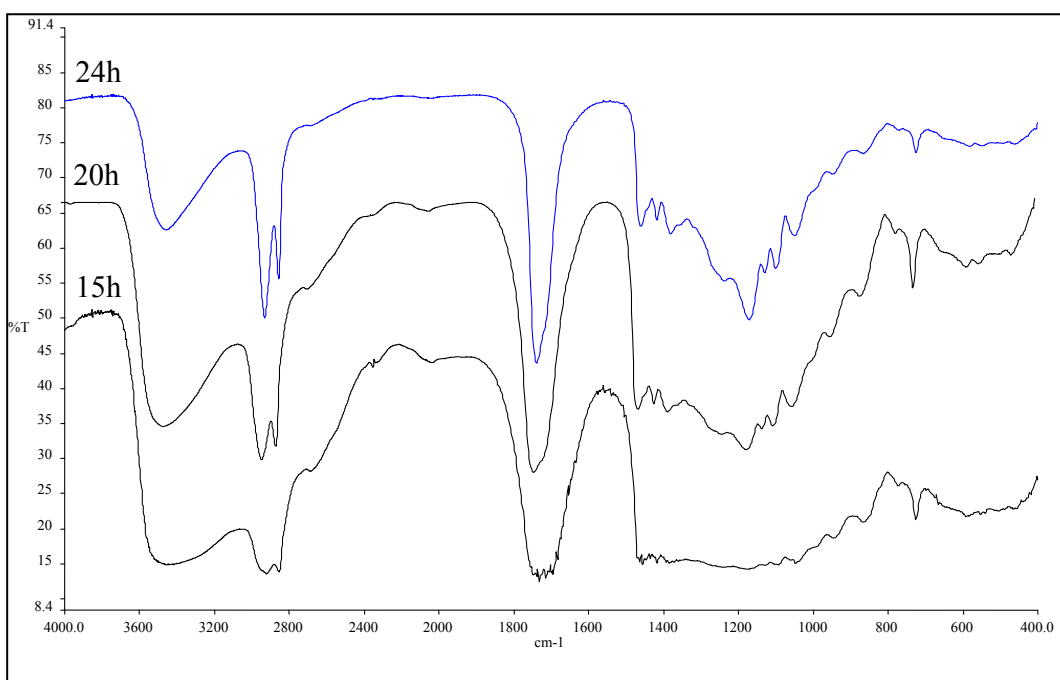


Figure 3.3 ATR-FTIR spectra of PGS obtained at different time points during polymerization process. From bottom to top: 15h, 20h, and 24h polymerization under vacuum.

3.2 Characterization of PGS

3.2.1 Molecular Weight Determination by Gel Permeation Chromatography

The molecular weight (MW) increase of PGS prepolymer during polymerization process was determined by gel permeation chromatography (GPC). The resulting data are tabulated in Table 3.1. GPC chromatograms showed that the molecular weight of the prepolymer increased during the polymerization. Solubility of PGS prepolymer in THF decreased with increase in polymerization time and branching; after 31h of polymerization under vacuum, the prepolymer became insoluble in THF as a result of extensive branching. Branching of PGS was observed as an increase in heterogeneity index (HI), i.e. polydispersity. The molecular weights of the prepolymer obtained at the end of 24h-polymerization under vacuum at two different runs differed significantly (16 727 Da vs. 9929 Da), which points out to the effect of vacuum that needs to be kept constant in order to obtain reproducible molecular weights during polymerization. The molecular weight distribution plot of PGS prepolymer (24h vacuum, 1st run) is given in Appendix B.

Table 3.1 Average molecular weights and HI values of PGS prepolymer.

Run	Sample	M _n (g/mol)	M _w (g/mol)	HI
1	PGS prepolymer (15h vacuum)	3111	8009	2.5743
1	PGS prepolymer (24h vacuum)	4350	16727	3.8446
2	PGS prepolymer (24h vacuum)	5470	9929	1.8151

3.2.2 DSC Analysis of PGS Prepolymer

Differential Scanning Calorimetry (DSC) of PGS showed two endothermic peaks at 3.16 °C and 36.06 °C. These were interpreted as two melting points by Wang et al. (2002). No other changes, glass transition or crystallization temperatures, were observed in the temperature range between -50 and +100 °C (Figure 3.4). Based on these interpretations the prepolymer appears to be totally amorphous at 37 °C.

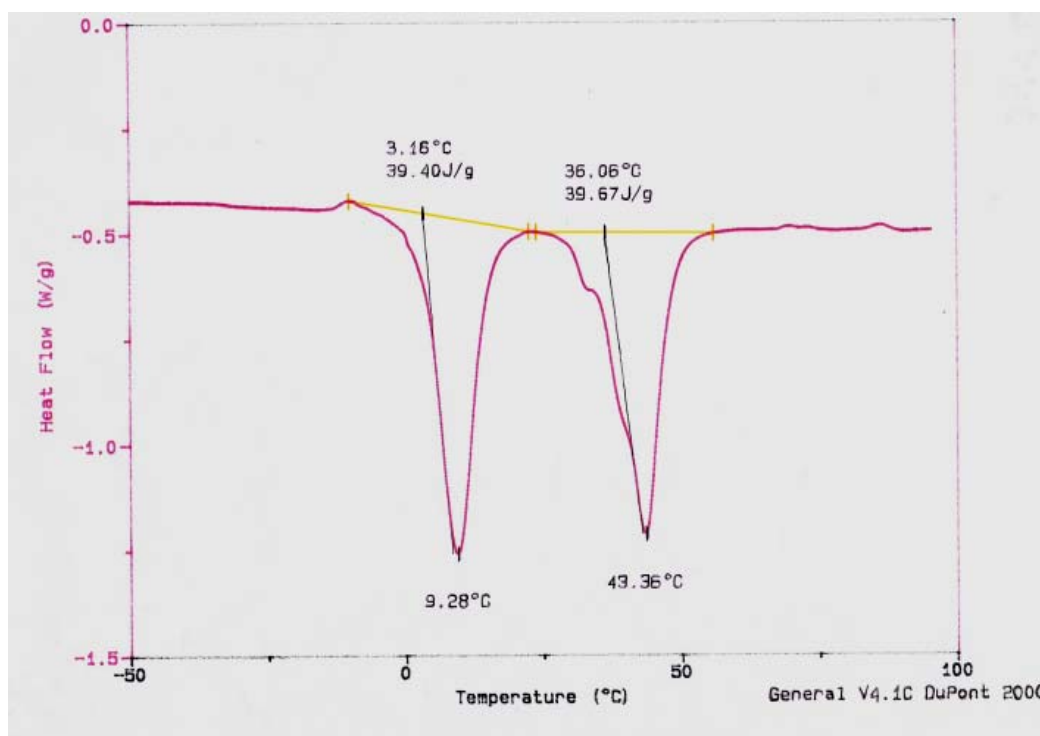


Figure 3.4 DSC thermogram of PGS prepolymer (24h under vacuum).

3.3 Aligned Microfiber Mats Prepared Through Electrospinning

Biodegradable polyesters like P(L-D,L)LA and PHBV are biocompatible polymers widely used as materials for scaffold preparation in tissue engineering applications. However, their high hydrophobicity and lack of flexibility (elasticity) restrict their use in this field. It is necessary to have polymers with higher flexibility for use in the engineering of soft tissues, like heart, since cardiac cells need to retract and extend on the surface to function properly. PGS, being a hydrophilic and low molecular weight polymer can serve as a plasticizer, and was blended with these polymers to augment their hydrophilicity and softness, in order to make them suitable for cell attachment and contraction.

PHBV-P(L-D,L)LA-PGS blends were used to obtain micron-size aligned fiber mats, through electrospinning. PHBV-P(L-D,L)LA solution (1:1, 5% w/v) with varying concentrations of PGS (1% w/w PGS (Fig 3.5), 2% w/w PGS (Fig 3.6), or 4% w/w PGS (Fig 3.7)) in Chl:DMF of 10:1 volumetric ratio was electrospun with an expectation to obtain more flexible mats with increase in PGS concentration. Some fusion was observed among the fibers.

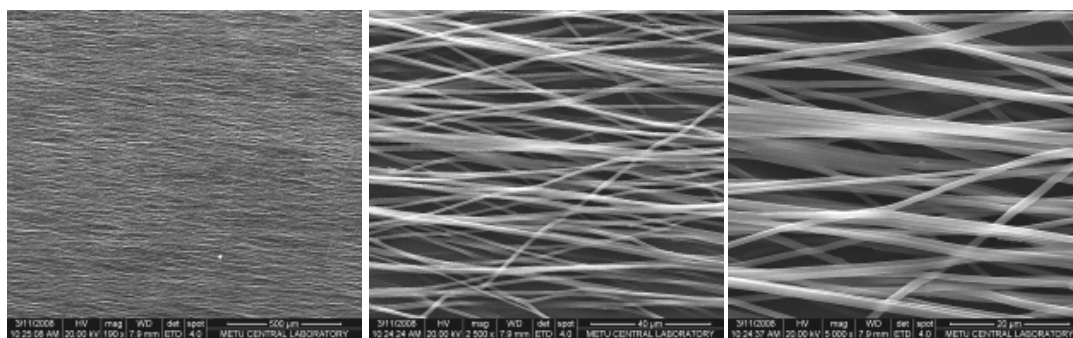


Figure 3.5 Electrospun PHBV-P(L-D,L)LA with 1% w/w PGS in Chl:DMF (10:1). Magnification: left: x 190, middle: x2500, right: x5000.

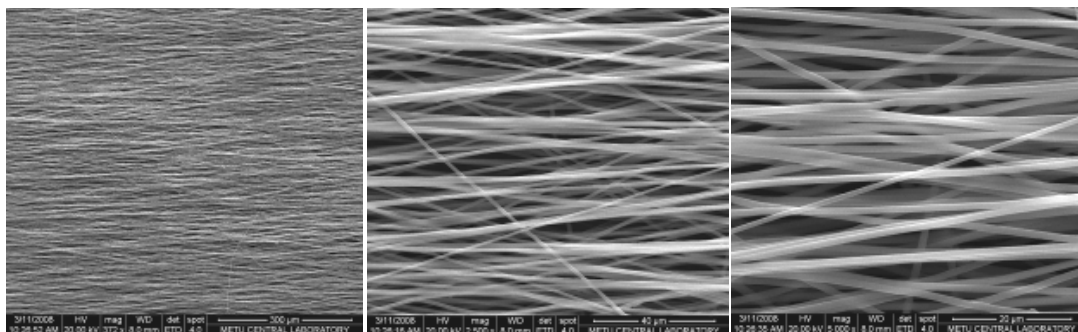


Figure 3.6 Electrospun PHBV-P(L-D,L)LA with 2% w/w PGS in Chl:DMF (10:1). Magnification: left: x372, middle: x2500, right: x5000.

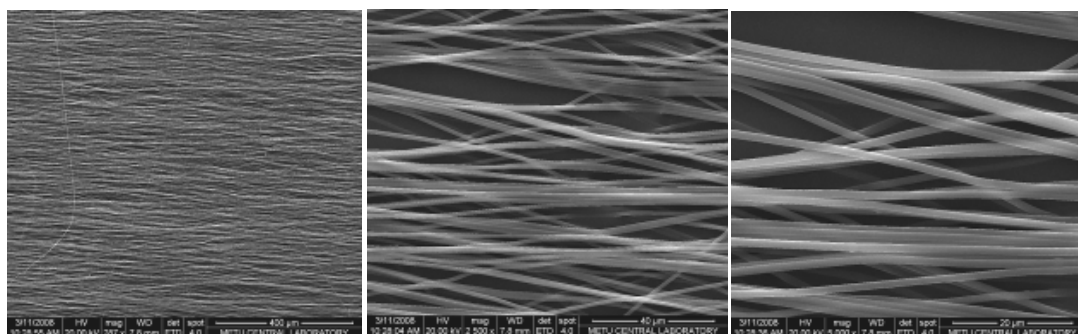


Figure 3.7 Electrospun PHBV-P(L-D,L)LA with 4% w/w PGS in Chl:DMF (10:1). Magnification: left: x287, middle: x2500, right: x5000.

Changing the solvent composition by decreasing the DMF concentration by half (Chl:DMF (95:5 v/v)) under the same production conditions led to a decrease in fiber fusion (Figs 3.8, 3.9 and 3.10), which will allow a more uniform cells penetration within the mat, and was found to be more useful for further use of fibers in cell culture studies, where residual DMF may have had adverse effects on cell viability. Decrease in DMF concentration caused a slight increase in fiber diameter. Fiber diameters in the range of 1.16 - 1.37 μm were obtained (Appendix C).

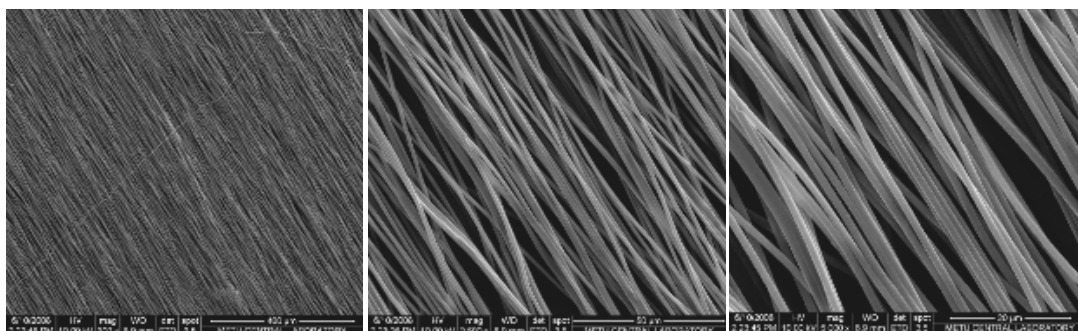


Figure 3.8 Electrospun PHBV-P(L-D,L)LA with 1% w/w PGS in Chl:DMF (95:5). Magnification: left: x300, middle: x2500, right: x5000.

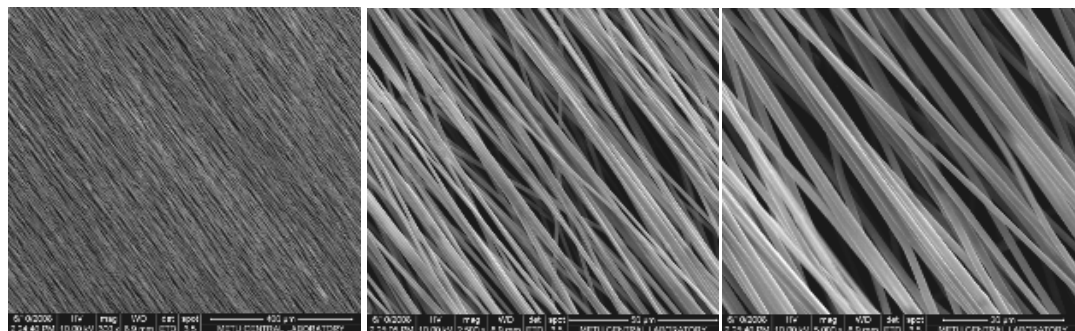


Figure 3.9 Electrospun PHBV-P(L-D,L)LA with 2% w/w PGS in Chl:DMF (95:5). Magnification: left: x300, middle: x2500, right: x5000.

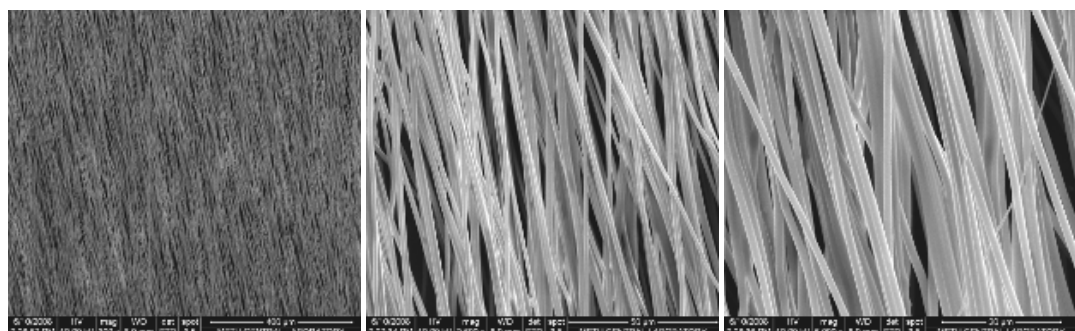


Figure 3.10 Electrospun PHBV-P(L-D,L)LA with 4% w/w PGS in Chl:DMF (95:5). Magnification: left: x300, middle: x2500, right: x5000.

Increase in PGS content in the polymer blend did not cause a significant change in fiber diameter, however as PGS content increased to 4%, occurrence of fiber fusions increased even at low DMF concentrations. Orientation of the fibers parallel to each other was more pronounced in the initial layers of the mat and this decreased as the mats became thicker. Mats with $12 \pm 3 \mu\text{m}$ thickness were obtained.

3.4 The Macroporous Biodegradable Tubings (Hollow fibers)

Stereomicrographs of the tubings produced using a 96:4 w/w blend of P(L,DL)LA (70:30) with PGS (MW: 9929 Da) revealed that the tubings had a uniform central hole (Fig 3.11). They were flexible, also a very crucial property for artificial vessels.

To make the biodegradable tubings permeable, the particulate leaching method was used to obtain a spongy, macroporous tubing with interconnected pores. Salt particles of 70-125 μm or less than 70 μm diameter were added to P(L,DL)LA-PGS (96:4 w/w) blend and dip coated on stainless steel wires to obtain a sponge with pores the same size with the salt particles (Figs 3.12 and 3.13).

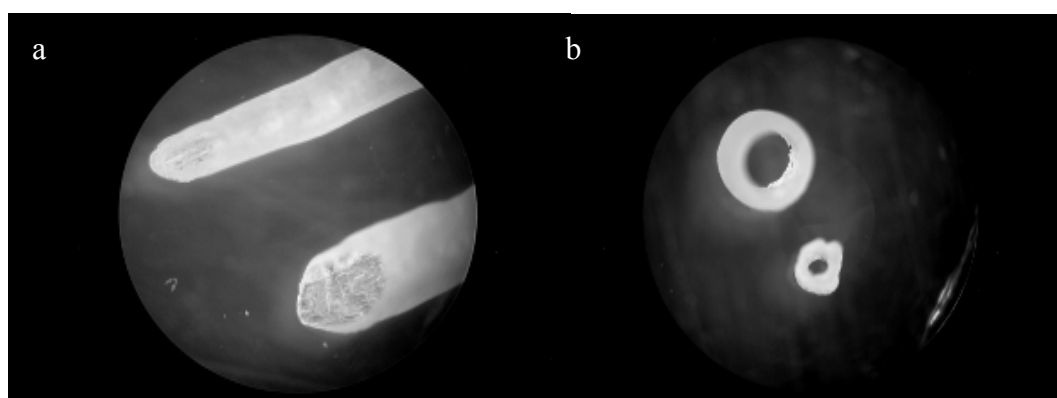


Figure 3.11 Stereomicroscope images of P(L,DL)LA-PGS tubings produced by using a glass rod (dia: 1 mm) and a silver wire (dia: 0.3 mm). Magnification: x19.

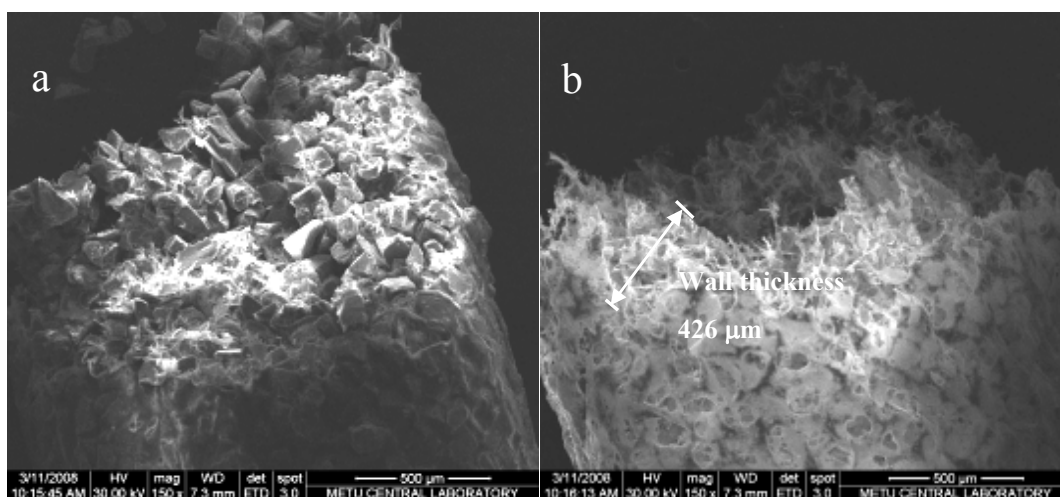


Figure 3.12 Biodegradable macroporous tubings (Hollow fibers) obtained from 60% salt (particle diameter 70-125 μm) solution in P(L,DL)LA:PGS (96:4) : tubing before (a) and after (b) salt leaching.

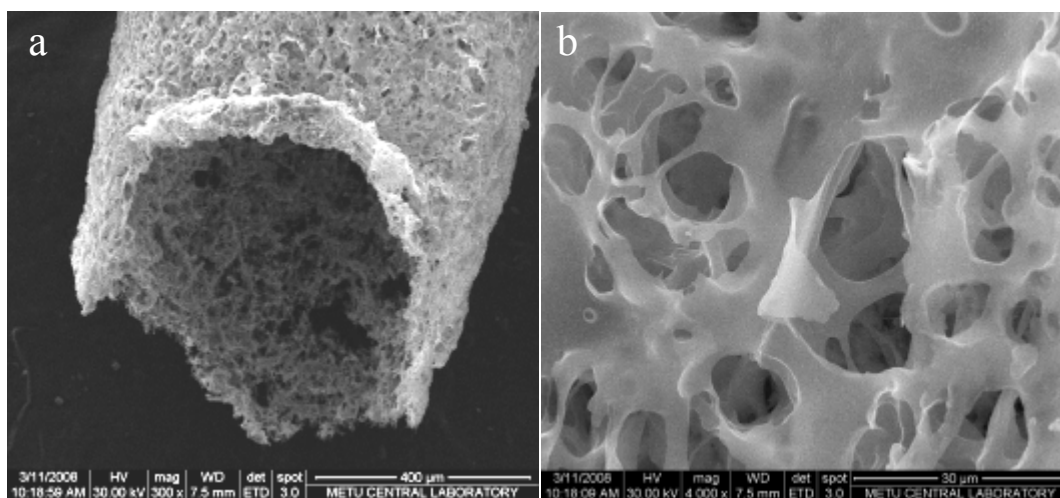


Figure 3.13 Biodegradable macroporous tubing (Hollow fiber) obtained from 70% salt (particle diameter 70 μm or less) solution in P(L,DL)LA:PGS (96:4): a) the tubing after salt leaching, b) a closer look at the wall of the tubing.

Although being a useful method to obtain the macroporous tubings, due to the high evaporation rate of chloroform and the difficulty in getting intact tubings

with uniform thickness, an alternative method was developed to obtain the macroporous structure. P(L-D,L)LA-PGS solution was prepared in dioxane, an organic solvent with low evaporation rate at room temperature, and coated on the stainless steel wire and subsequently frozen at -80 °C and freeze dried.

Hybrid tubings with both nonporous and macroporous regions were obtained by first dip coating the polymer in chloroform at room temperature, and after drying it completely, by dip coating the remaining, polymer-free, portion of the stainless steel wire with P(L-D,L)LA-PGS in dioxane and subsequent freeze drying. Stereomicrographs of the tubings, which had both porous and nonporous regions, were obtained (Fig 3.14). The cross-section of the tubing wall (Fig 3.15b) examined with SEM revealed the interconnectivity of the porous structure.

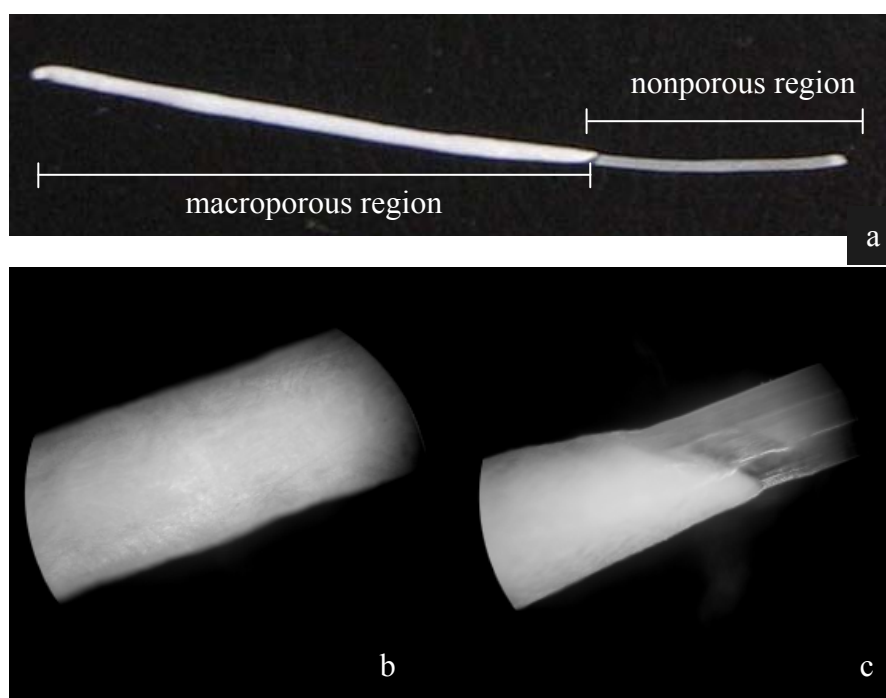


Figure 3.14 Stereomicroscope images of bifunctional P(L-D,L)LA:PGS (96:4) tubings obtained by using a stainless steel wire (dia: 0.5 mm). a) the whole tubing , b) porous region, c) transition region between the porous and nonporous parts (x10).

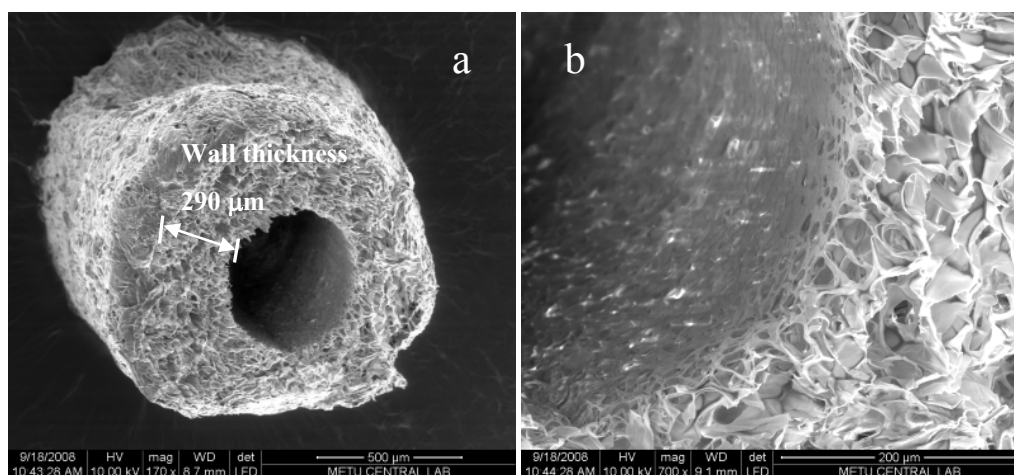


Figure 3.15 Biodegradable macroporous tubing (hollow fiber) obtained from P(L-D,L)LA:PGS dissolved in dioxane: a) the tubing, b) a closer look at the cross-section of the tubing wall.

3.5 Characterization of Polymer Blends

3.5.1 Mechanical properties

Modulus of elasticity (Young's Modulus, E), ultimate tensile strength (UTS) and strain (ϵ) for P(L-D,L)LA and P(L-D,L)LA-PGS (96:4 w/w) nonporous tubings were calculated as given in Table 3.2.

The elastic modulus, UTS and strain values for P(L-D,L)LA nonporous tubings were found to be higher than their P(L-D,L)LA -PGS (96:4 w/w) counterparts. The PGS prepolymer used as the blending material had a low molecular weight, and thus was expected to act as a plasticizer among the P(L-D,L)LA molecules. The results were in agreement with our expectations. E decreased upon use of PGS due to decrease in association among the P(L-D,L)LA molecules, making the structure less crystalline. The higher UTS value of P(L-D,L)LA tubings can be attributed to the better association among crystalline regions in the absence of any plasticizer molecule. Two separate Young's Modulus values

were obtained for both P(L-D,L)LA and P(L-D,L)LA-PGS tubings. Polymers are ductile materials, which deform reversibly up to a certain degree (observed as the elastic region of the stress-strain curve) and then yield and flow under the applied force until it begins to harden under load (strain hardening) and finally fail (Appendix D). In Table 3.2 the 1st value for E represents the Young's Modulus in the elastic region, and the 2nd E represents the Young's Modulus in the strain hardening region.

Table 3.2 Tensile mechanical properties of nonporous tubings.

Sample	UTS (MPa)	E (MPa)		ε (%)
		1 st	2 nd	
P(L-D,L)LA	24.2 ± 13.4	96.49 ± 38.81	2.01 ± 1.28	750.5 ± 43.6
P(L-D,L)LA-PGS (96:4 w/w)	9.3 ± 1.4	48.71 ± 9.09	0.90 ± 0.22	629.5 ± 40.0

UTS: Ultimate tensile strength, E: Young's Modulus, ε: Strain,

3.5.2 Hydrophilicity

Surface hydrophilicities of the polyester blends, P(L-D,L)LA:PGS (96:4) and P(L-D,L)LA-PHBV:PGS (98:2), used for preparation of the tubings and aligned fiber mats, respectively, were studied with contact angle goniometry. PGS, with -OH groups in its structure, was expected to increase the hydrophilicities of the polymer blends. Addition of PGS to P(L-D,L)LA (4%) caused a little decrease in the water contact angle (from 87 to 82), but the 2% PGS in the P(L-D,L)LA-PHBV blend did not affect the surface hydrophilicity (Table 3.3).

Table 3.3 Water contact angles of blend films.

Film Sample	Water Contact Angle (Degree)
P(L-D,L)LA	86.98 \pm 2.45
P(L-D,L)LA:PGS (96:4)	81.98 \pm 1.30
P(L-D,L)LA-PHBV	87.67 \pm 1.97
P(L-D,L)LA-PHBV:PGS (98:2)	87.61 \pm 1.58

3.5.3 Gravimetric Determination of PHBV-P(L-D,L)LA:PGS Aligned Fiber Mat Erosion

The rate and mode of degradation of the polymers influence their mechanical properties, service life, and the response of the biological system towards them. Erosion of PHBV-P(L-D,L)LA:PGS aligned fiber mats with 1, 2 and 4% (w/w) PGS content was studied in PBS at 37 °C via gravimetry. Theoretically, PGS with its low molecular weight (9929 Da) and its hydrophilicity was expected to leave the blend structure with time by dissolution and may be also with hydrolysis. On the other hand, PHBV and P(L-D,L)LA were high molecular weight polyesters and since they are hydrophobic in nature they were not expected to dissolve out or hydrolyze rapidly, especially in the absence of any hydrolytic enzymes. P(L-D,L)LA (70:30) cages were shown to maintain mechanical strength for at least 6 months during degradation studies in vitro (Smit et al., 2007). Holland et al. (1990) studied in vitro degradation of PHBV20 (20% HV content) in pH 7.4 buffer at 37°C in which the weight of the sample remained almost unchanged for about 400 days. PHBV (5% HV content) used in this study is more crystalline and is expected to degrade even more slowly. In this study, shortening of the long degradation durations was aimed by blending with PGS, because when PGS leaves, more polymer surface will be exposed to the hydrolytic medium. As expected,

weight loss of the PHBV-P(L-D,L)LA:PGS aligned fiber mats was not much and was observed to be higher in samples with higher PGS content (Fig 3.16). Cracks were observed in the mat structure, especially at the edges and some in fibers, in the mats with 2 and 4% PGS starting from the 3rd month. Crack formation was more noticeable in thinner mats.

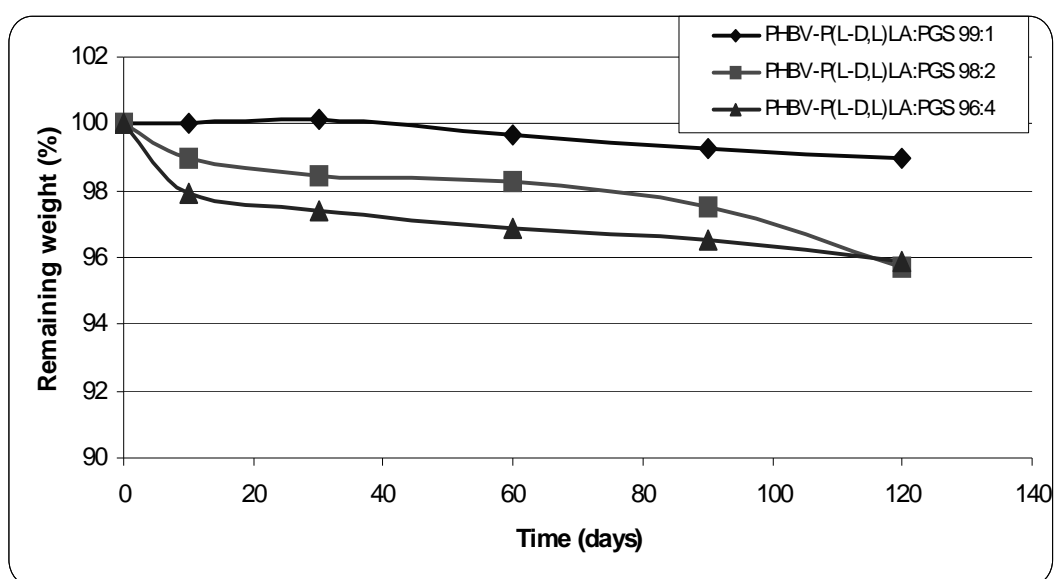


Figure 3.16 Weight loss from PHBV-P(L-D,L)LA:PGS aligned-fiber mats incubated in PBS at 37 °C for 120 days (n=2).

These all indicate that it is possible to increase the erosion rate of the parallel fiber mats by increasing the PGS content of the polymer blend used in fiber production.

3.6 In Vitro Studies

3.6.1 Characterization of Wharton's Jelly MSCs and Their Comparison with MSCs from Human Bone Marrow (USA)

Human BM MSCs and WJ MSCs were characterized in terms of their cell surface markers and their capability to differentiate into cells of mesodermal lineage (osteoblasts, adipocytes), to prove their mesenchymal origin. As the main focus of this study, the early cardiomyocyte specific gene expression of these cells was determined and they were grown under particular culture conditions to induce their differentiation into cardiomyocytes.

3.6.1.1 Morphology of hBM MSCs and hWJ MSCs in Culture

Human BM and hWJ MSCs were grown until confluent on TCPS according to standard protocols for MSCs. MSCs derived from both sources displayed spindle-shape or flat-polygonal fibroblastic morphology (Fig 3.17). Bone marrow derived MSCs formed a distinct monolayer, whereas Wharton's Jelly MSCs were able to form spherical cell clusters. Other differences between the two cell types were that those derived from WJ were more heterogeneous and usually larger in size compared to hBM MSCs.

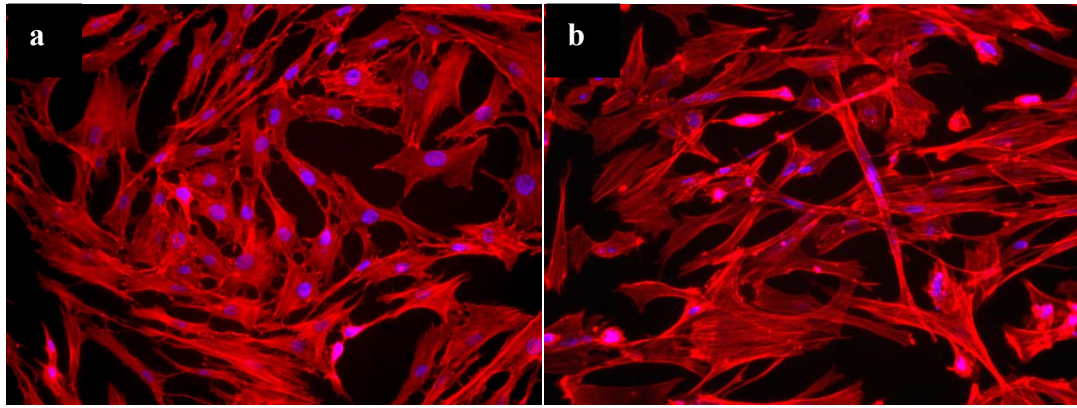


Figure 3.17 Fluorescence micrographs showing MSCs from (a) human bone marrow (P3), and (b) Wharton's jelly (P6). Both cell types presented a fibroblast-like morphology (x200). Red: F-actin stained with Rhodamine-Phalloidin. Blue: cell nuclei stained with Hoechst 33342.

3.6.1.2 Immunophenotype Analysis of MSCs by Flow Cytometry

For the characterization of hBM and hWJ MSCs, specific cell surface antigens were analyzed by flow cytometry. Positive cells were counted and compared with the signal of the corresponding immunoglobulin isotypes (Fig 3.18). Cell surface antigen expression is summarized in Table 3.4. The cells derived from both sources were negative for hematopoietic markers CD34, CD45, and strongly positive for MSC markers, like CD105, CD73, CD44 and CD90. This profile, which is in agreement with the literature (Weiss et al., 2006, Wang 2004, Bieback et al., 2004, Pittenger and Martin, 2004), indicated that these cell populations were composed of mesenchymal stem cells.

The staining pattern of hWJ MSCs differed from that of hBM MSCs in terms of several surface markers: significantly lower percentage of hWJ MSCs stained for CD105 as passage number increased from 2 ($p=0.034$) to 4 ($p=0.007$) (shown also by Weiss et al., 2006), the number of cells positive for CD106 was significantly low considering all passages, and a significant difference was observed in expression of CD44 at P4. Although CD29 expression by hBM MSCs was

significantly lower, this antigen was found to be present on hBM MSCs obtained from another donor in amounts comparable to that of WJ MSCs (data not shown). BM MSCs were found to be moderately positive for the vascular cell adhesion molecule CD106, also implicated in atherosclerosis, as expected according to several recent studies (Bieback et al., 2004, Pittenger and Martin, 2004).

No significant difference was observed in the expression of CD49d, CD90, CD73, CD45, CD34, HLA-ABC, and CD133 by both cell types.

hWJ MSCs were negative for HLA DR, unlike hBM MSCs, regardless of passage number, and this is in agreement with the results of Weiss et al. (2006). There was a significant decrease in expression of this antigen by hBM MSCs as passage number increased, though. In the literature there is a controversy about the expression of HLA-DR antigen by hBM MSCs; it was shown to be expressed in the study by Portmann-Lanz et al. (2006), it was found to be absent in the studies of some others (Wagner 2005, Bieback et al., 2004, Xu 2004), and was stated to be inducible in another study (Pittenger and Martin, 2004). The absence of HLA-DR in hWJ MSCs in this study implies that these cells will be less prone to immune rejection in case of allogenic transplantation, because it is known that HLA-DR antigens are responsible for triggering humoral immune response (Burlingham et al., 2000).

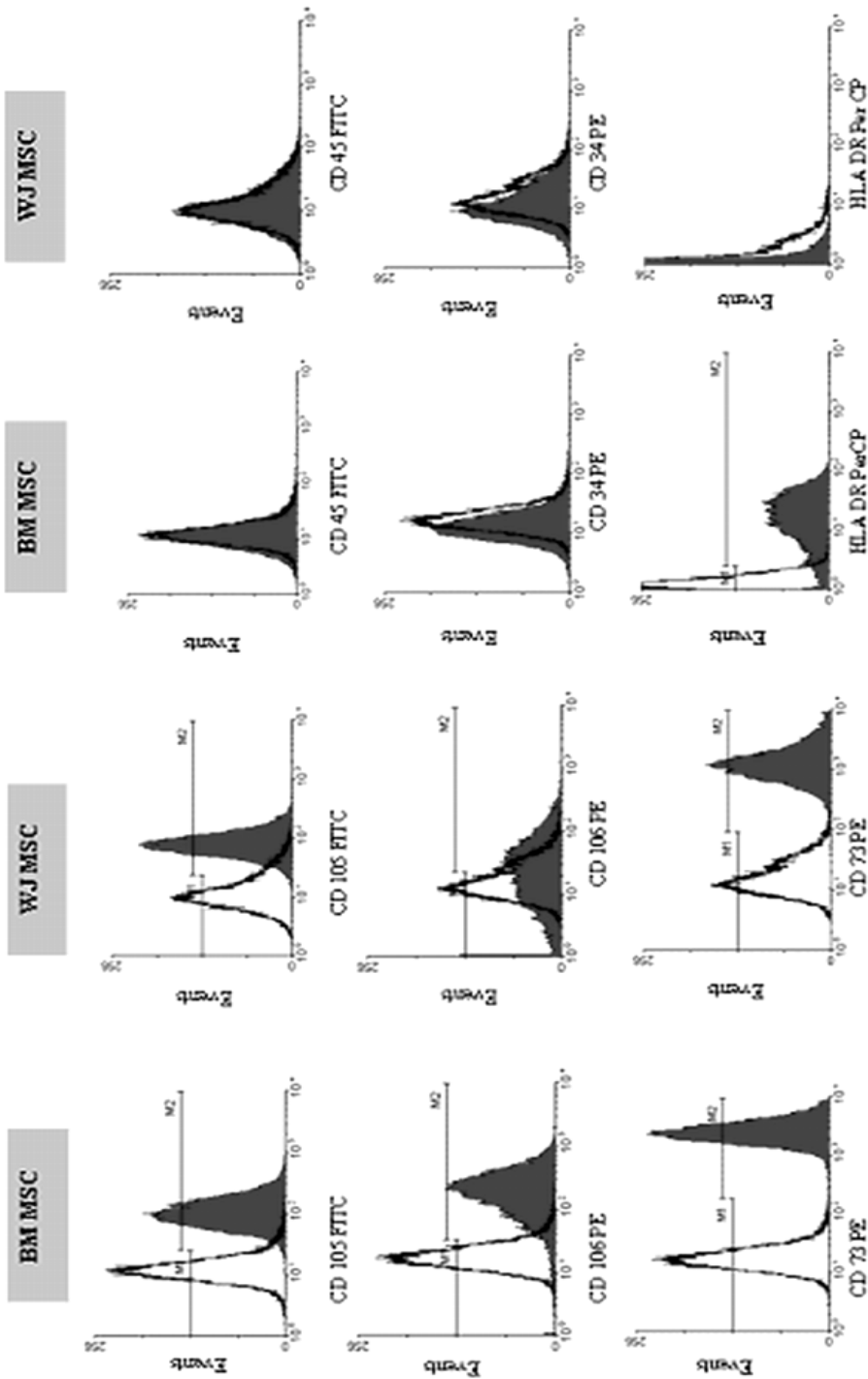


Figure 3.18 Determination of immune phenotype of human BM and WJ MSCs. Fraction of absolute positives at M2 region was determined by subtracting number of cells of isotype control at that region from the number of positively labeled cells. Representative histograms are demonstrated (solid). The respective histogram of isotype control is shown as a black line (with colorless interior).

Table 3.4 Cell surface antigen expression by BM and WJ MSCs.

Surface Antigen	BM MSC %*			WJ MSC %*		
	P2	P3	P4	P2	P3	P4
CD105	98.2 ± 0.2	96.3 ± 2.1	91.2 ± 4.0	97.2 ± 0.1	85.6 ± 14.4	55.8 ± 1.1
CD106	83.4 ± 13.6	79.5 ± 12.8	63.5 ± 9.2	22.4 ± 13.6	11.1 ± 15.7	0.0 ± 0.0
CD49d	0.7 ± 0.5	0.0 ± 0.0	0.0 ± 0.0	17.4 ± 9.9	10.2 ± 3.3	6.1 ± 2.3
CD90	99.9 ± 0.0	99.8 ± 0.2	99.8 ± 0.0	99.8 ± 0.1	100.0 ± 0.0	93.5 ± 8.6
CD44	98.2 ± 0.8	96.7 ± 1.8	95.3 ± 0.3	87.2 ± 7.8	91.1 ± 7.0	80.6 ± 3.0
CD73	99.9 ± 0.2	100.0 ± 0.0	99.0 ± 0.1	92.7 ± 9.7	99.1 ± 1.3	96.3 ± 2.5
CD29	36.0 ± 7.5	40.3 ± 13.8	31.0 ± 1.8	91.6 ± 8.8	92.8 ± 3.5	70.0 ± 29.6
HLA-ABC	99.8 ± 0.1	99.7 ± 0.2	98.5 ± 0.0	93.0 ± 9.8	99.6 ± 0.1	98.1 ± 2.0
CD45	0.3 ± 0.4	1.0 ± 1.4	0.0 ± 0.0	0.0 ± 0.0	0.0 ± 0.0	0.0 ± 0.0
CD34	0.0 ± 0.0	0.0 ± 0.0	0.0 ± 0.0	0.0 ± 0.0	0.0 ± 0.0	0.0 ± 0.0
HLA-DR	89.3 ± 1.8	78.9 ± 8.1	67.1 ± 1.6	0.0 ± 0.0	0.0 ± 0.0	0.0 ± 0.0
CD133	0.0 ± 0.0	0.0 ± 0.0	0.0 ± 0.0	0.0 ± 0.0	0.0 ± 0.0	0.0 ± 0.0

*Percentage of positive cells; the data present the average of two independent experiments.

3.6.1.3 Osteogenic Differentiation of hMSCs

Alkaline phosphatase is an extracellular enzyme secreted by osteoblasts during the early stages of mineralization. Although the precise mode of action for ALP is still unclear, it has the ability to hydrolyze phosphate from various compounds and thus helps to supply the inorganic phosphate necessary for the nucleation of hydroxyapatite crystals during mineralization. Level of this enzyme has been routinely used in in vitro studies as an indicator of osteoblastic differentiation. ALP activity of cell lysates obtained in this study was determined spectrophotometrically by the detection of the enzyme product at the end of 1h following the start of the reaction at 37 °C. The results were expressed as μmol of substrate converted to product/min/sample (Table 3.5), using the calibration curve for the enzymatic product, and ALP activities of BM MSCs and WJ MSCs were considered as comparable with each other since the osteogenic cultures were initiated with the same cell number.

Table 3.5 ALP activity of P2 bone marrow and Wharton's Jelly derived MSCs.

Cell Type	Sample No	*ALP Activity after 21 days of osteogenic induction
hBM MSCs	1	361.25
	2	338.46
hWJ MSCs	1	12.66
	2	1.60

*ALP Activity: μmoles of substrate consumed per min

ALP activity was observed in cell lysates from both hBM and hWJ MSCs induced for osteogenic differentiation. Bone marrow derived MSCs showed

significantly higher ALP activity (349.86 ± 16.11 $\mu\text{moles/min}$) than WJ MSCs (7.13 ± 7.82 $\mu\text{moles/min}$). This can be attributed to the hBM's being already committed to enter the osteoblastic lineage.

3.6.1.4 Adipogenic Differentiation of hMSCs

Human MSCs from both sources demonstrated a change in their morphological features during the time course of adipogenic induction from a spindle-shaped fibroblastic morphology to a relatively spherical cell phenotype in comparison to untreated controls (Fig 3.19). The adipogenic differentiation was shown with cells which stained positive by Oil Red-O for lipid droplets. The change in cell morphology to spherical was observed in MSCs from both sources, but increase in lipid production, as oil vesicles, was more apparent in hBM derived MSCs than in hWJ MSCs. The higher level of lipid accumulation might demonstrate that hBM MSCs can be in a later stage in mesodermal lineage compared to hWJ MSCs, so they show a stronger commitment to become adipocytes under the present induction conditions. In the literature there are several studies on differentiation of MSCs from hBM and hWJ to adipocytes. Compared with bone marrow MSCs, Karahuseyinoglu et al. (2007) demonstrated that UC stromal cells are capable of forming premature adipocytes bearing smaller multilocular lipid droplets. In contrast, Baksh et al. (2007) found that UC stromal cells generated significantly more fat-containing cells than bone marrow MSCs by day 21, while Lu et al. (2006) reported no significant adipogenic difference between these two cell types. Our findings are more similar to the outcomes of Karahuseyinoglu et al. (2007), and the different experimental results of the mentioned groups suggest the effect of interindividual differences.

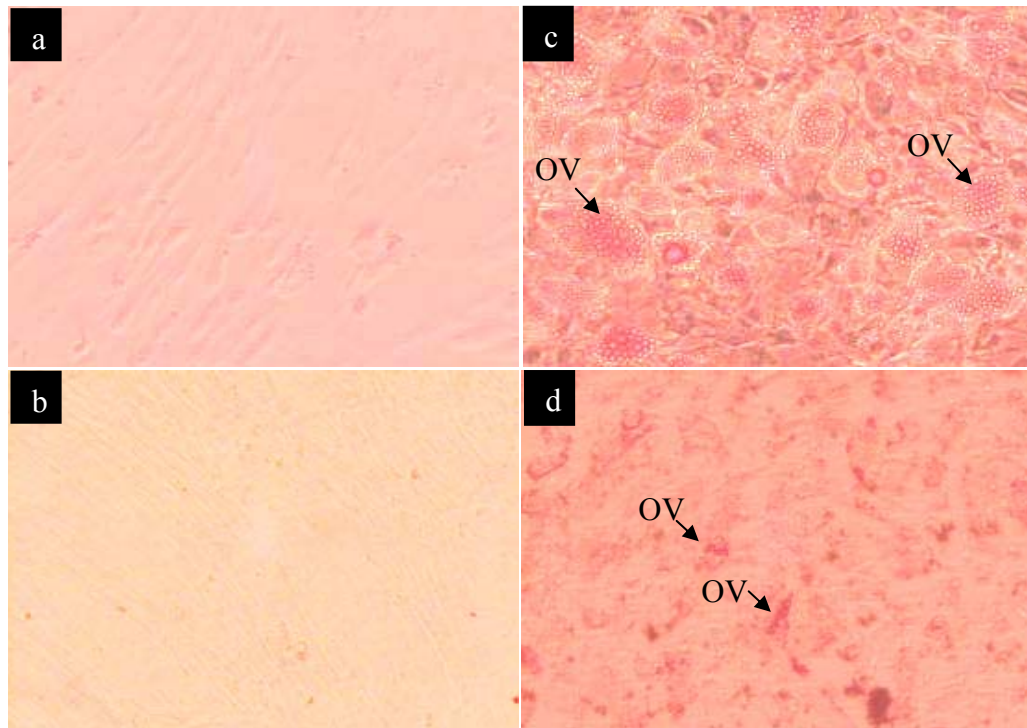


Figure 3.19 Light microscopy images of human MSCs subjected to adipogenic induction medium for 21 days and subsequently stained with Oil Red O. Controls: (a) BM MSCs and (b)WJ MSCs; MSCs subjected to adipogenic differentiation: (c) BM MSCs and (d) WJ MSCs (x20). The arrows show the oil vesicles (OV) formed upon adipogenic differentiation.

3.6.1.5 Cardiomyogenic Potential of hMSCs

3.6.1.5.1 Gene Expression Analysis of Undifferentiated hMSCs by RT-PCR

Undifferentiated BM and WJ MSCs were analyzed for their expression of cardiac specific markers. PCR primers for these markers were designed de novo, so they were proven to be specific for the mRNA of interest by using mRNA extract from human adult myocardium (Fig 3.20). The single bands obtained at the

expected size by RT-PCR analysis showed that our primer design and PCR conditions were optimized successfully. All cardiac related transcripts were detected in the human adult myocardial tissue.

The RT-PCR results revealed that human BM and WJ MSCs expressed MEF 2A, MEF 2C, MEF 2D and FOG-2 in high amounts and Nkx 2-5 and Tbx5 in low amounts. Tbx5 expression was detected in passage numbers 2 and 3 of WJ MSCs, but not at P4. BM and WJ MSCs differ in FOG-2 expression; WJ MSCs expressed higher levels.

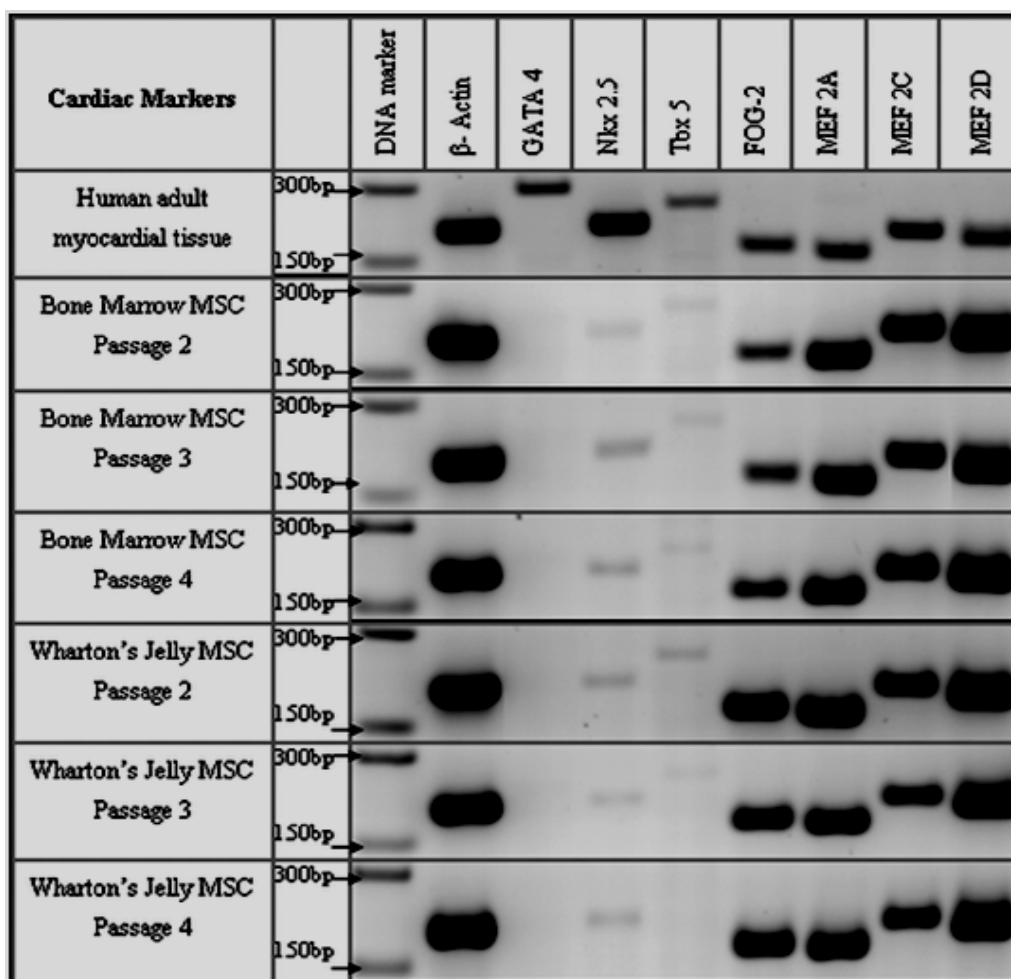


Figure 3.20 Cardiomyocyte specific gene expression in undifferentiated hWJ and hBM MSCs in comparison to the expression at the human myocardial tissue.

The particular roles of growth factors involved in embryonic cardiac development are not clearly known, but most of the genes whose expression is necessary for cardiogenesis and normal cardiac function have been identified. Cardiac myogenesis and morphogenesis are regulated by interconnected networks of transcription factor genes (Bruneau, 2002). Factors that play central roles in all muscle lineages, as the MADS-box proteins SRF and Mef2A/B/C/D positive pathways, participate in these networks, in addition to more cardiac-restricted factors like Nkx2.5/2.6, GATA4/5/6, Tbx2/5/20, Hand1/2, Irx1/2/3/4, CITED1/2, COUPTFII, Hey1/2, Pitx2 and myocardin (Solloway and Harvey, 2003). Expression of Nkx2.5, GATA4, Tbx5, Mef2A/C/D and FOG2 transcription factors by hWJ and BM MSCs were investigated in this study.

GATA4 expression in human bone marrow MSCs has been identified by Bayes-Genis et al. (2005), however, this could not be observed in the present study neither with BM MSCs, nor with WJ MSCs. This contradictory result can be attributed to the cell growth medium composition. GATA4, 5, and 6 subfamily of transcription factors are co-expressed with the homeoprotein Nkx 2.5 in the precardiac mesoderm during the earliest stages of its specification and are known to be important determinants of cardiac gene expression (Brewer et al., 2005). Employment of P19 CL6 mouse embryonic carcinoma cells as a model to investigate the temporal order of the expression of these transcription factors demonstrated that when these cells are induced to differentiate to a cardiogenic lineage, the expression of GATA4 and GATA6 is up-regulated prior to the transcriptional activation of Nkx 2.5 (Brewer et al., 2005). GATA4 can be detected in the precardiac mesoderm where it precedes the expression of the earliest cardiac differentiation markers, such as contractile protein genes and natriuretic peptide genes (Charron and Nemer, 1999). It is the predominant transcript in cardiomyocytes at all stages of the development. In fact, both the *in vivo* and *in vitro* studies suggest that GATA4 is required for proliferation and/or migration of cardiac cells or for early mesoderm-endoderm interactions (Charron and Nemer, 1999). GATA4 transcripts are detected throughout the myocardium and endocardium where they are present at a high level in the postnatal heart (Heikinheimo et al., 1994).

Until the present study there were no reports in the literature on the expression of the principal cardiac transcription factor Nkx 2.5 in MSCs of human adult BM or WJ. Nkx 2.5 function is essential for the commitment of mesoderm into the cardiac muscle lineage (Jamali et al., 2001). In mice, Nkx2.5 is required for the terminal differentiation of cardiac myocytes that includes the establishment or maintenance of a ventricular gene expression program (Lyons et al., 1995, Tanaka et al., 1999, Bruneau et al., 2000).

Tbx5 was expressed by P2, P3 and P4 BM MSCs and P2 and P3 WJ MSCs, while its RNA could not be detected in P4 WJ MSCs using 30 ng of total RNA. During embryonic development, it is expressed initially throughout the cardiac mesoderm in its earliest stages, but at mid gestation its expression is restricted to the atria and left ventricle, where it has critical functions (Bruneau et al., 1999, Liberatore et al., 2000). By late gestation and adulthood, however, low levels of Tbx5 transcripts can be detected equally in both the left and right ventricles in mice and humans (Bruneau, 2002, Hatcher et al., 2000). Lack of Tbx5 results in severely hypoplastic atria and left ventricle (Bruneau et al., 2001) and overall ventricular differentiation is impaired in Tbx5-deficient embryos (Bruneau, 2002).

In addition to their separate contributions to cardiac development, interaction of the cardiac transcription factors was found to be important. Nkx 2.5 physically interacts with Tbx5 and GATA4 to synergistically activate transcriptional target genes (Durocher and Nemer, 1998, Charron and Nemer, 1999, Bruneau et al., 2001, Hiroi et al., 2001). Tbx5 and Nkx 2.5 were found to have a specific role in regulating the genes involved in conduction system function, such as cx40 (Bruneau et al., 2001, Kasahara et al., 2001). ANF and cx40 have been identified as *in vivo* targets of Nkx2.5 and Tbx5 (Tanaka et al., 1999, Bruneau et al., 2001). Considering these vital interactions among the critical cardiac transcription factors, it is possible to conclude that together with Nkx 2.5 expression, the presence of regular Tbx5 transcripts at a basal level in MSCs would provide a greater potential to differentiate into functional cardiomyocytes, the main unsolved issue, under suitable induction conditions.

In this study, the zinc finger transcription factor FOG-2 was expressed by both BM and WJ MSCs. FOG-2 functions as negative regulator of transcription via interactions with GATA proteins (Svensson et al., 2000, Fossett and Schulz, 2001). A N-terminal domain of FOG-2 (amino acids 1–247) that is both necessary and sufficient to repress GATA4-dependent transcription from cardiac promoters, has been identified (Svensson et al., 2000). A striking feature of FOG-2 ^{-/-} hearts is thinning of compact ventricular myocardium (Tevosian et al., 2000). Forced cardiomyocyte expression of FOG-2 in FOG-2 deficient mice rescues their cardiac and vascular defects, indicating that endogenous cardiac targets of FOG-2 signal the coronary vasculature. This finding defines an essential FOG-2-dependent role for myocardium in the program of coronary vessel development.

The MEF2 family of genes is part of the superfamily of MADS-box transcription factors that are essential for differentiation of all muscle lineages (Black and Olson, 1998). The mammalian MEF2 family includes MEF2A, MEF2B, MEF2C, and MEF2D. A, C and D members of MEF 2 family were found to be expressed in MSCs from both sources in this study, and were present in adult ventricular myocardial tissue, too. Chick MEF2A expression starts in precardiac mesoderm and continues in the heart tube, atrium, and ventricle (Buchberger and Arnold, 1999). MEF2C expression in P19 embryonic carcinoma cell line up-regulates a wide spectrum of cardiac-specific genes, which include GATA4, Nkx 2.5, cardiac alpha actin, and the myosin heavy chain (Skerjanc et al., 1998). Inactivation of the MEF 2C gene causes arrest of cardiac development in mice with lack of specification of the right ventricle and down-regulation of a number of cardiac muscle genes (Lin et al., 1997). Most notable is the absence of MHC-expressing myoblasts and differentiated muscle fibers when the MEF2 protein is not available (Bour et al., 1995). Since most of the promoters for the downregulated genes contain no or low-affinity MEF2 binding sites and they are not significantly activated by any MEF2 proteins, MEF2 may act as a cofactor (Morin et al., 2000). There is evidence that MEF2 potentiates the transcriptional activity of GATA factors.

Taken together, all the transcription factors mentioned above play critical roles in cardiomyogenesis either alone or by complex interactions that still need to be revealed.

3.6.1.5.2 Induction of Differentiation to Cardiomyocytes

Human BM MSCs (P3) and WJ MSCs (P5) were cultured for 14 days in 24 well plates in the presence of bovine insulin and valproic acid to optimize and induce cardiomyogenic differentiation. Activation of the insulin receptor (IR)/IGFR family by insulin and IGF leads to the activation of a signal transduction pathway implicated in expression of a number of cardiac specific transcription factors such as the zinc finger GATA proteins and Nkx-2.5, which are essential for heart development (Sachinidis et al., 2002). Insulin is known to act as a cardioprotectant in ischemic/reperfused heart, too (Yu et al., 2008). Histone deacetylases (HDACs) compact chromatin structure and play an important role in global gene expression. Karamboulas et al. (2006) showed that HDACs play a repressive role during the entry of mesoderm cells into the cardiac-muscle lineage and that blocking HDAC activity is sufficient to enhance the early stage of cardiomyogenesis. Valproic acid, a HDAC inhibitor, was used in our cardiomyogenic media to investigate its effect in cardiac differentiation.

Although expression of principle cardiac transcription factors GATA4, Nkx 2-5 and Tbx5 were diminished in all cultures containing either insulin or insulin and valproic acid together (Figure 3.21), immunostaining for human ventricular myosin heavy chain α/β (α/β MHC), and α -actinin was promising. α/β MHC was detected in both BM MSCs (P3) and WJ MSCs (P5) treated with insulin and valproic acid together, while α -actinin was observed only in WJ MSCs (Fig 3.22). No α/β MHC or α -actinin could be observed in cells treated with insulin only.

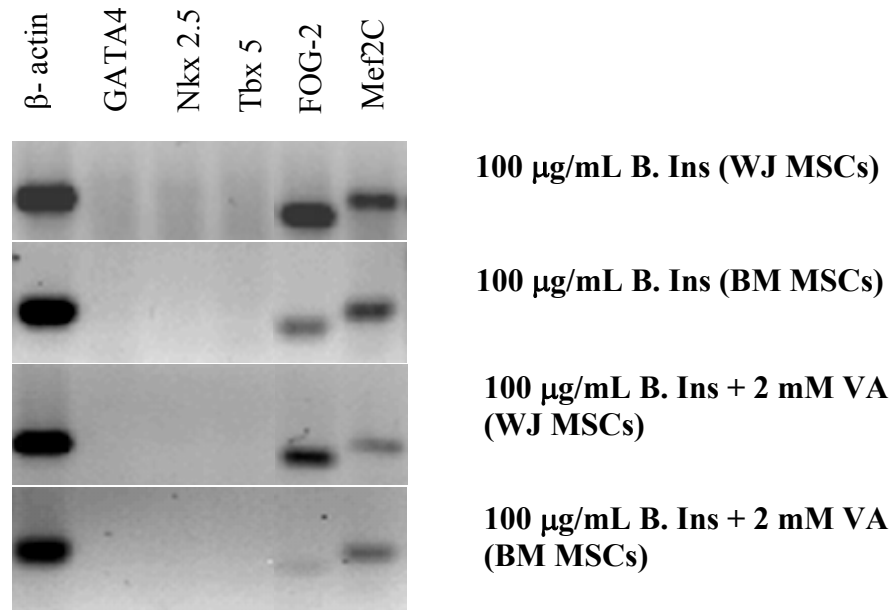


Figure 3.21 Expression of cardiac transcription factors in WJ MSCs (P5) and BM MSCs (P3) induced to differentiate into cardiomyocytes in the presence of growth factors. B. Ins: bovine insulin, VA: valproic acid.

Progress has been achieved in the generation of cardiomyocytes from both embryonic and adult stem cells. Treatment of MSCs isolated from BM with the DNA demethylating agent 5-azacytidine has been shown to induce multiple new phenotypes including cardiomyocytes (Makino et al., 1999; Hakuno et al., 2002). Xu et al. (2004) showed that 5-azacytidine can promote the differentiation of adult hBM derived MSCs into a cardiomyocyte-like phenotype, but the process was less than completely specific, as adipocyte-like cells were also observed. Myofilament-like structures were observed in electron micrographs of the differentiated myogenic cells. The mRNAs of beta-MHC, desmin, alpha-cardiac actin, and cardiac troponin T were highly expressed in the myogenic cells. These results indicate that 5-azacytidine can induce human MSCs to differentiate in vitro into cells with characteristics commonly attributed to cardiomyocytes, however no beating cells could be observed. In addition, 5-azacytidine is not preferred as differentiation inducer, since it might have genotoxic effects. It was demonstrated that it is also

possible to obtain a specific population of human cardiomyocyte-like cells (CLCs), that expresses multiple structural and myofibrillar proteins specific to cardiomyocytes, in a cardiomyogenic medium without demethylating agents or co-cultures (Shim et al., 2004). Shim et al. used insulin, dexamethasone and ascorbic acid to stimulate cardiogenic differentiation in hBM MSCs. Thin filament associated myofibrillar proteins were detected early in the cells, with cardiac troponin I, sarcomeric tropomyosin, and cardiac titin among the first expressed. Although GATA4 expression was observed, no Nkx 2.5 expression could be detected in the CLCs. Some CLCs were found to develop into a nascent cardiomyocyte phenotype with cross-striated myofibrils characterized by α -actinin-positive Z bands, which took a long time though, i.e. 4–5 passages in the differentiation culture. However, neither of differentiation attempts of human bone marrow MSCs resulted in beating cardiomyocytes.

MSCs derived from Wharton's Jelly of the human umbilical cord were investigated for their potential to differentiate into cardiomyocytes by treating them with 5-azacytidine or maintaining them in cardiomyocyte-conditioned medium and it was found that both treatments resulted in expression of the cardiomyocyte markers N-cadherin, cardiac troponin I, connexin 43, α -actinin, and desmin (Wang et al., 2004). Western blots showed that the newly extracted cells did not express N-cadherin or cardiac troponin I but that both markers were expressed in cells grown in conditioned medium and, to a lesser extent, those grown in 10% FBS. This suggested that FBS provides some differentiation factors, but not to the same extent as cardiomyocyte-conditioned medium. After 5-azacytidine treatment or culture in cardiomyocyte-conditioned media, the cells connected with adjoining cells but did not form myotubes or start spontaneous contraction.

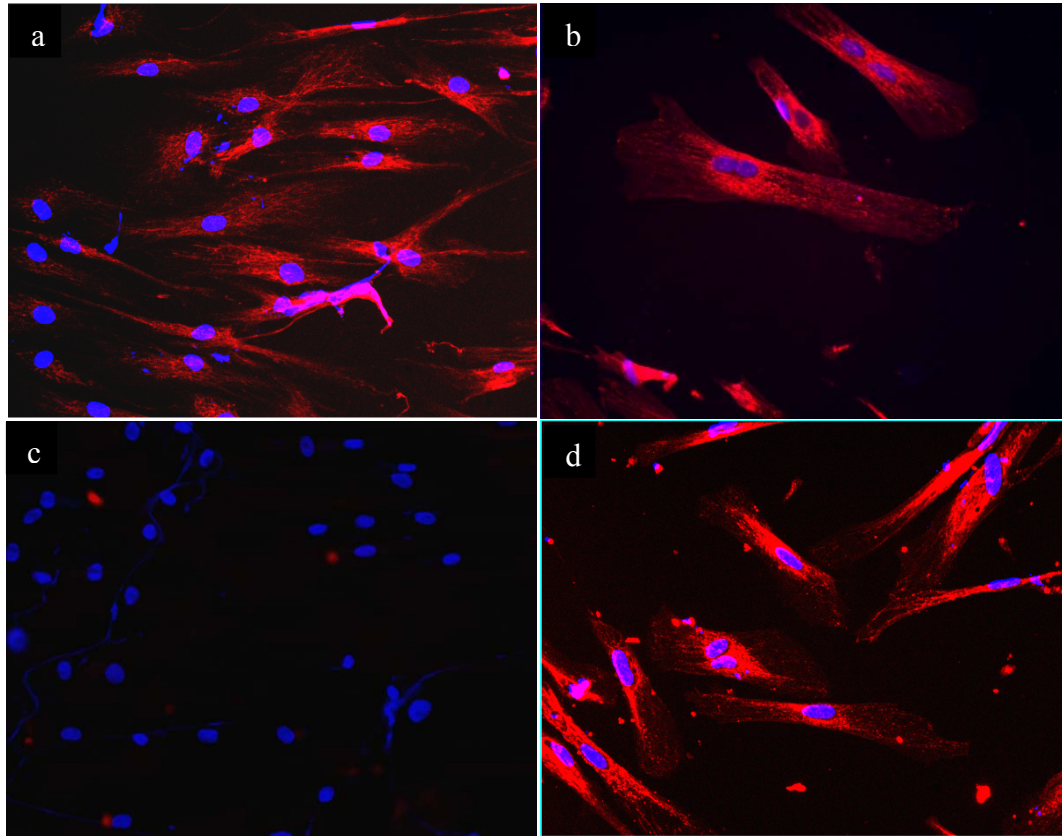


Figure 3.22 Fluorescence microscopic images of (a, c) BM and (b, d) WJ MSCs cultured for 14 days in cardiomyogenic media (B.Ins and VA) and immunostained for α/β MHC (a, b) and α -actinin (c, d) (x200). Blue: nuclei stained with DAPI, red: α/β MHC or α -actinin revealed with Cy3 labeled secondary antibody.

In our study, a profound expression of cardiac α/β MHC and α -actinin could be induced in WJ MSCs in a very short time like 2 weeks, even without the use of 5-azacytidine. In addition to expression of cardiac specific sarcomeric proteins, number of nuclei per cell was either one or two as it is expected for cardiomyocytes (Young et al., 2001) (Fig 3.22). Expression of α -actinin could not be induced in BM MSCs, suggesting the higher potential of WJ MSCs to differentiate to cardiomyocytes. It is possible that MSCs from Wharton's jelly are earlier-stage cells than MSCs from adult bone marrow. The only drawback of the induction media with valproic acid and insulin was observation of nuclei with

abnormal morphologies or nuclear fragmentation in the differentiation cultures. Unfortunately no cell beating could be observed during the culture period.

WJ MSCs were chosen as the cell source to be used in the rest of the studies because they had similar cell surface antigens and cardiomyogenic transcription factor expression with BM MSCs and also had better differentiation into cardiomyocytes.

3.6.2 Characterization of hMSC Isolated from Wharton's Jelly (TR)

hWJ MSCs were isolated from umbilical cord matrices via explant culture and the cells in the final culture were characterized in terms of their cellular morphology, growth kinetics and their ability to differentiate into cells of mesodermal lineage (osteoblasts, chondrocytes) to prove their mesenchymal origin.

3.6.2.1 Morphology of Isolated hWJ MSC

Morphology of the WJ MSCs at primary culture was examined with light microscopy (Fig 3.23). The cells grown in the two different cell culture media had a fibroblastic morphology. The cells from culture I (Primary Medium: DMEM low glucose/Ham F-12 (1:1) with 10% fetal bovine serum, 100 U/mL penicillin, 100 µg/mL streptomycin, and 1 ng/mL of bFGF) and culture II (Primary Medium: αMEM/Ham F-12 (1:1) with 2% fetal bovine serum, 100 U/mL penicillin and 100 µg/mL streptomycin) formed embryoid body like structures in their primary culture and very early passages (Figs 3.23e and 3.23f). The cells started to come out of the umbilical cord tissue after 4 days when cultured in primary medium (PM) type I, while it took 7 days to be visible when grown in PM type II. This points out the effect of FBS as a chemoattractant, the higher the FBS content of the medium the higher the cell migration rate.

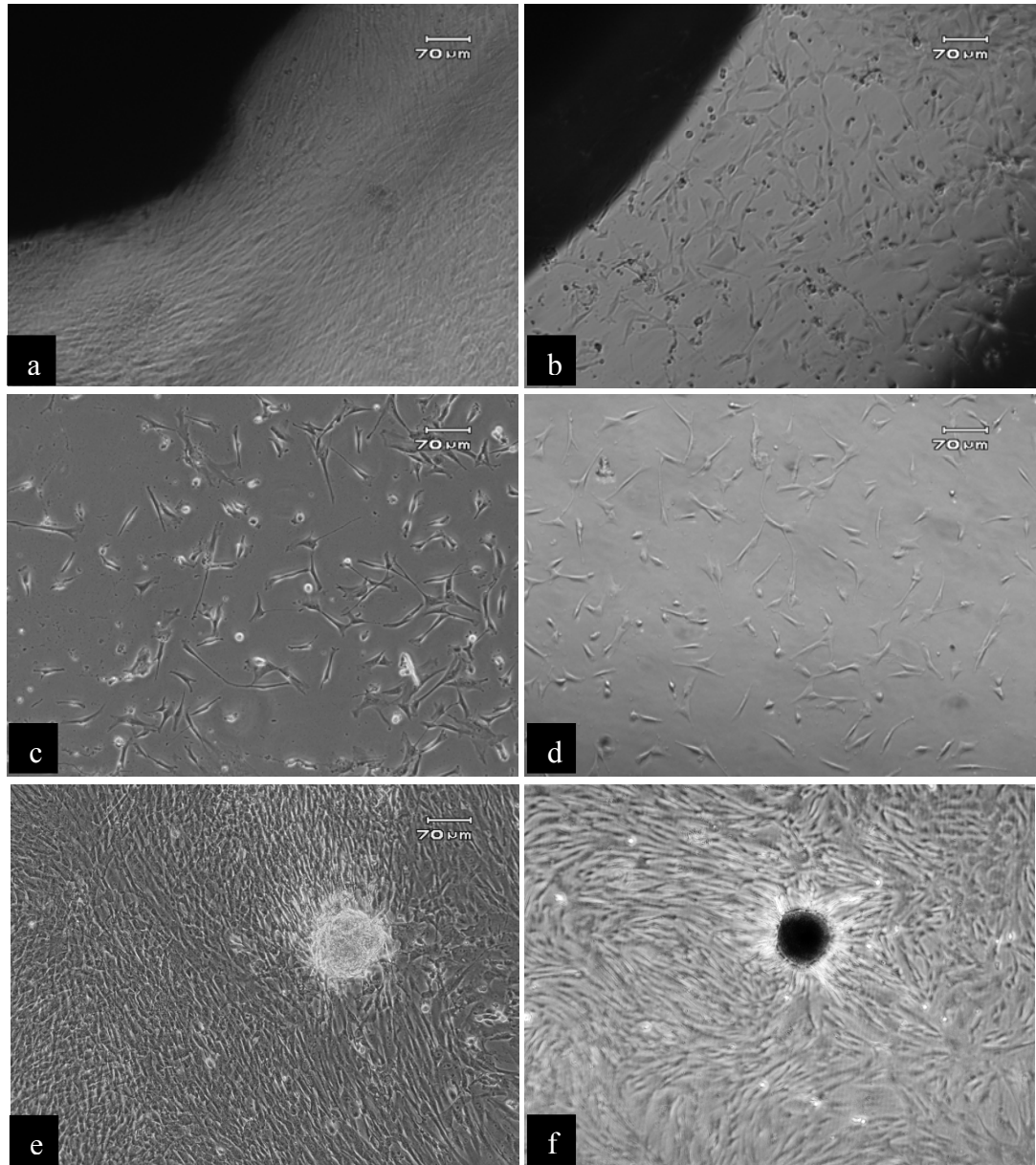


Figure 3.23 Light micrographs (10x) of primary culture hWJ MSCs grown for 17 days in PM type I (a, c, e), and PM type II (b, d, f) on TCPS. (a, b) The explant umbilical cord tissue with MSCs coming out of the tissue, (c, d) MSCs away from the tissue, (e, f) Embryoid body like structures.

Third passage cells were seeded on TCPS and collagen type I coated glass slides and grown in PM type II for several days and then fixed and stained for actin filaments and cell nuclei for morphological analysis. Two types of cells with a

different morphology were identified; one type was small in size with smaller nuclei and less profound actin filaments compared to the other type (Fig 3.24).

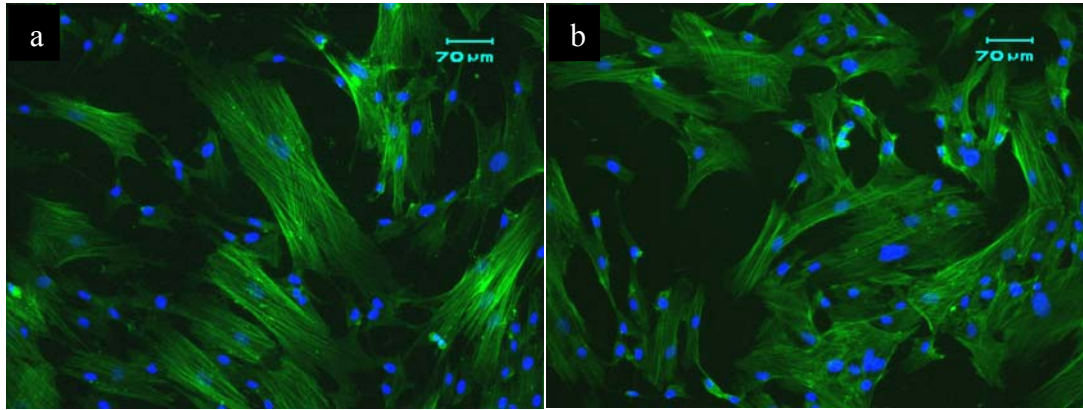


Figure 3.24 hWJ MSCs morphology revealed by fluorescence microscopy. (a) hWJ MSCs grown on glass slide, and (b) on TCPS. Green: Filamentous actin stained with FITC-Phalloidin, Blue: Cell nuclei stained with DAPI.

It was discovered previously by Karahuseyinoglu et al. (2007) that these two cell types reside at different regions of the umbilical cord; the small more fibroblastic cells are coming from the intervascular stroma of the umbilical cord, while the larger and flatter ones are from the perivascular stroma of the umbilical cord. Although they show different morphologies, both cell types were found to express the MSC marker vimentin (Karahuseyinoglu et al.,2007).

3.6.2.2 Cell Growth Kinetics: Doubling Time Determination

Doubling time of P3 hWJ MSCs grown in PM type I (DMEM low glucose/Ham F-12 (1:1) with 10% fetal bovine serum, 100 U/mL penicillin, 100 μ g/mL streptomycin, and 1 ng/mL of bFGF) was determined to be 25.73 h while the doubling time of cells grown in PM type II (α MEM/Ham F-12 (1:1) with 2% fetal bovine serum, 100 U/mL penicillin and 100 μ g/mL streptomycin) was determined as 24.08 h. Higher number of cells was obtained in culture I at the end of 240 h of growth and cell proliferation was still going on, opposed to cells in culture II, who seemed to enter the plateau (stationary) phase.

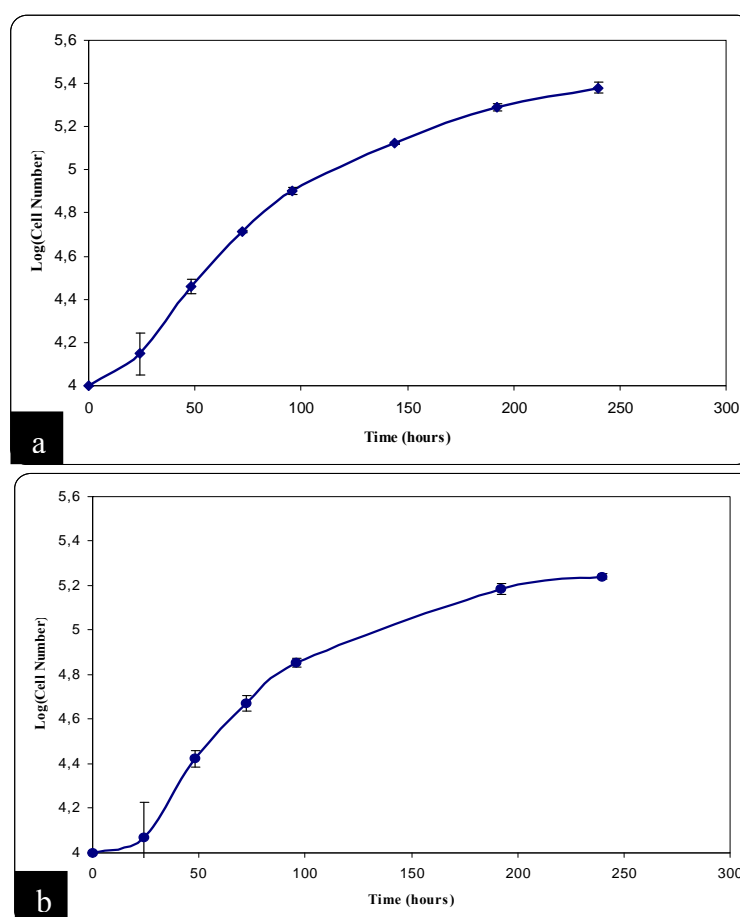


Figure 3.25 Growth curves of hWJ MSCs grown in two different cell culture media: a) PM type I and b) PM type II on TCPS.

A very similar doubling time was determined for 3rd passage hWJ MSCs grown in DMEM/Ham F-12 (1:1) with 10% fetal bovine serum, in a recent study (Karahuseyinoglu et al., 2007).

3.6.2.3 Osteogenic Induction of hWJ MSCs

In order to differentiate the WJ MSCs cultured in the two different media composition into osteoblasts they were seeded into 24-well plates in the expansion medium and after culturing in osteogenic medium for 14 days their ALP activity was tested and mineralization was observed by staining with von Kossa stain. A calibration curve of p-nitrophenol at 37 °C was used to determine the ALP enzyme activity (nanomole substrate converted to product per minute). The ALP activities of the hWJ MSCs were lower when undifferentiated than differentiated regardless of the medium type they were cultured before starting the differentiation. Also medium type did not significantly change the ALP activities; in other words medium type was not effective on ALP activity (Table 3.6). ALP activity of differentiated WJ MSCs originated from culture I was a little bit higher than the activity of those from culture II (Table 3.6) however more cell death was observed among the cells from culture I. MTS assay was performed with cells in other wells to determine the average cell number and this value was used to calculate ALP specific activity (Table 3.7).

Table 3.6 ALP activity of human Wharton's Jelly derived MSCs.

Culture Medium used before osteogenic induction	ALP Activity	
	Undifferentiated	Differentiated
Type I	0.705 ± 0.018	1.238 ± 0.344
Type II	0.714 ± 0.137	1.191 ± 0.247

* ALP Activity: nmoles substrate consumed per min

Table 3.7 ALP specific activity of hWJ MSCs taken from culture II.

Differentiation State	ALP Specific Activity ($\times 10^6$) (n=6)
Undifferentiated	4.1 ± 0.8
Differentiated	7.3 ± 1.5

* ALP Specific Activity: nmoles substrate consumed per min per cell

WJ MSCs appear to produce ALP even in their undifferentiated form, but the amount is doubled upon differentiation to osteoblasts (Table 3.7).

Von Kossa staining was applied to the undifferentiated and differentiated WJ MSCs, in order to study the mineral deposition (Fig 3.26). Cells grown in both media were found to be able to differentiate into osteoblasts because they deposited Ca-P mineral on the TCPS surface in the presence of osteogenic factors.

Osteogenic differentiation of WJ MSCs was reported to be successful by all the researchers working with WJ MSCs (Baksh et al., 2007, Wang et al., 2004, Karahuseyinoglu et al., 2007, Sarugaser et al., 2005). Ca-P mineral deposition was shown in all mentioned studies and Baksh et al. reported that osteogenic differentiation of WJ MSCs proceeded more rapidly than that of BM MSCs.

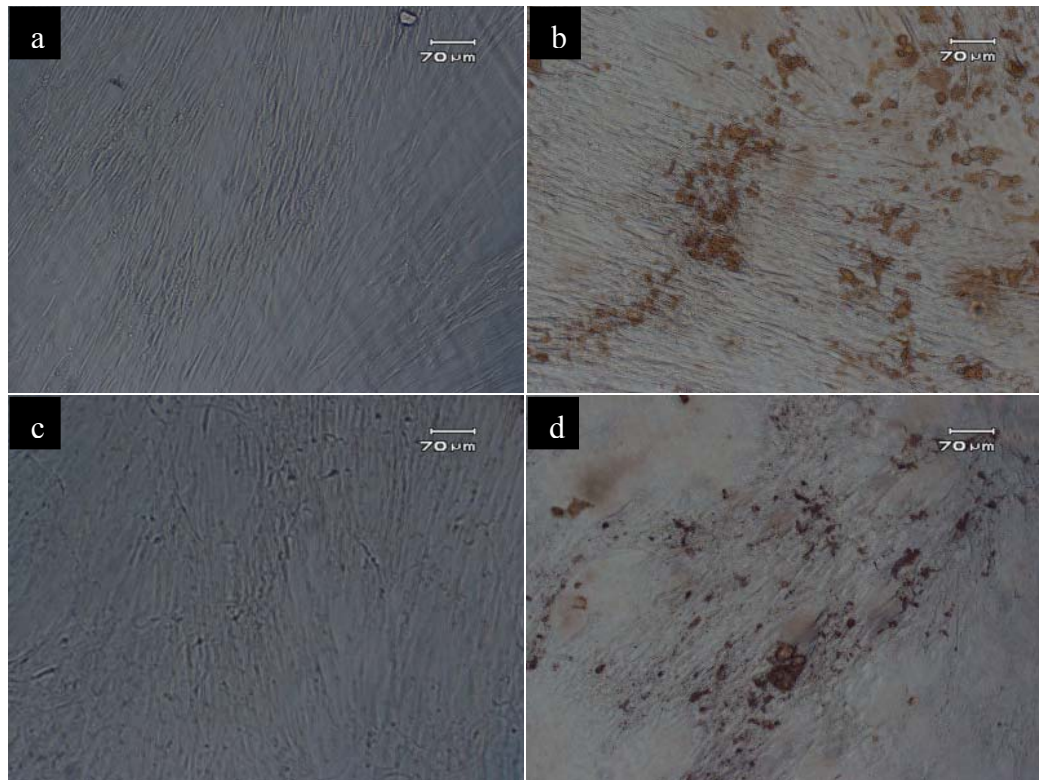


Figure 3.26 Light micrographs of (a, c) undifferentiated WJ MSCs and (b, d) WJ MSCs differentiated to bone, subjected to von Kossa staining. a, b) WJ MSCs taken from culture I and c, d) WJ MSCs taken from culture II. (x10)

3.6.2.4 Chondrogenic Differentiation of hWJ MSCs

In order to differentiate the WJ MSCs cultured in the two different media composition into chondrocytes they were seeded into 24 well plates in the expansion medium and after culturing in chondrogenic medium for 14 days their ECM was stained with Alcian blue for acid mucosubstances, like chondroitin sulfate and hyaluronic acid, and was also immunostained for Collagen type II. Alcian blue staining was positive in both the undifferentiated and differentiated WJ MSC cultures, although the latter was more intense. It is known that hyaluronic acid is present in high amounts in the umbilical cord matrix, and probably it is secreted by undifferentiated WJ MSCs in vitro, too. Collagen Type II immunostaining of ECM secreted by WJ MSCs taken from culture I revealed more intense deposition than with cells taken from culture II, both in undifferentiated and differentiated state. However more cell death with the cells from culture I was observed probably due to use of poorer media in the differentiation culture. No qualitative difference could be seen between the amount of collagen Type II secreted by undifferentiated and differentiated cells (Fig 3.27).

To elevate the sole effect of differentiation factors, no FCS was used in the following chondrocyte differentiation cultures (Fig 3.28). This time a change in cell morphology to more circular was observed in differentiated cells, and the increase in collagen Type II and mucosubstance production was more distinct, although still not satisfactory.

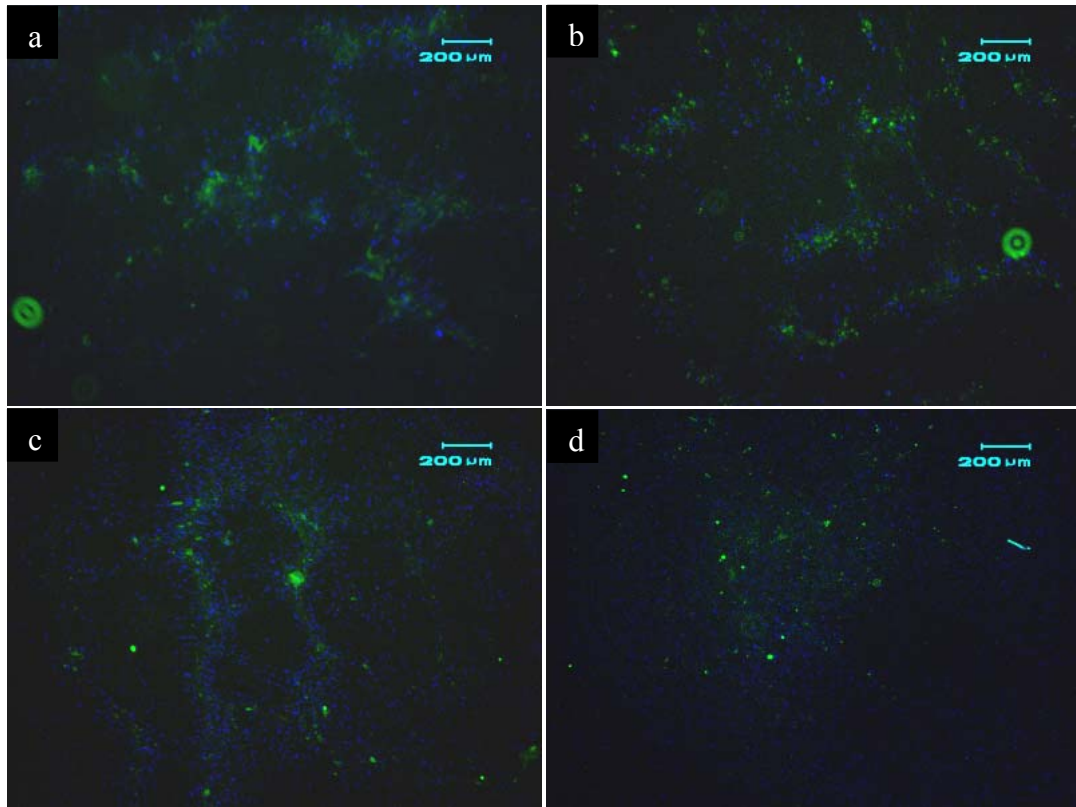


Figure 3.27 Fluorescence micrographs of undifferentiated WJ MSCs (a, c) and WJ MSCs differentiated to chondrocytes (b, d) subjected to immunostaining for Collagen Type II. a, b) WJ MSCs taken from culture I, and c, d) WJ MSCs taken from culture II (x 4). Green: Collagen Type II, blue: cell nuclei stained with DAPI.

Successful chondrogenic differentiation is reported in literature for pellet cultures of WJ MSCs (Karahuseyinoglu, 2007, Wang et al., 2004). Alcian blue staining of the extracellular matrix (ECM) was evident after chondrogenic induction in histological sections of the pellets and a type II collagen-rich ECM was demonstrated immunohistochemically by Wang et al., however, as it was observed in our study, too, the control groups were also positive for Alcian blue and type II collagen staining.

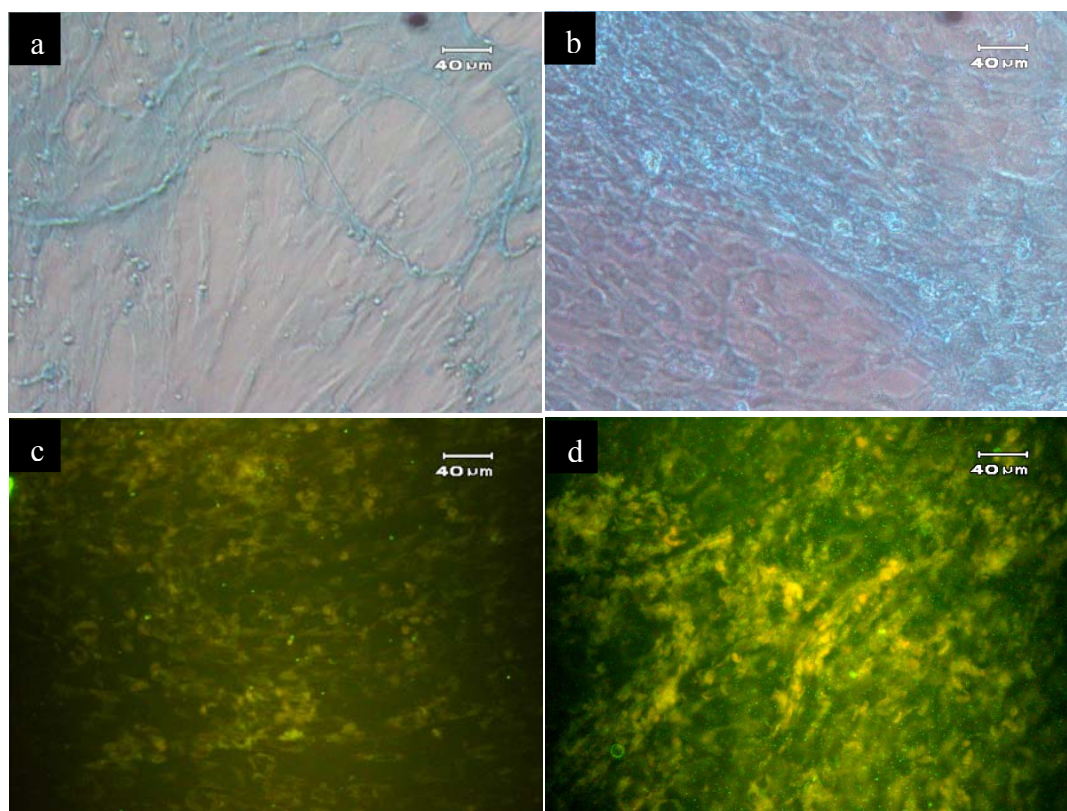


Figure 3.28 Micrographs of undifferentiated WJ MSCs (a, c) and WJ MSCs differentiated to chondrocytes (b, d) subjected to Alcian blue (a, b) and immunostaining for Collagen Type II (c, d). WJ MSCs were taken from culture II (x20). Blue: mucosubstances stained with Alcian blue, green: Collagen Type II.

3.6.3 Differentiation of hWJ MSCs to Cardiomyocytes

3.6.3.1 Gene Expression of Undifferentiated hWJ MSCs Analyzed by RT–PCR

Cardiomyogenic gene expression of third passage WJ MSCs grown in culture I and II is given in Figure 3.29. The cardiomyogenic gene expression in the two culture media differed only in terms of GATA4; GATA4 was expressed in

culture II but not in culture I. These results show the effect of growth media composition on gene expression of the WJ MSCs.

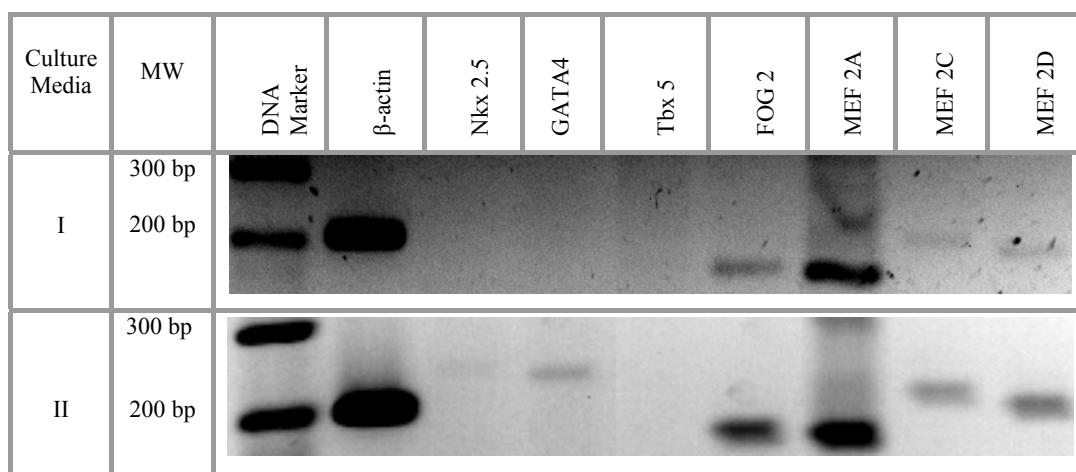


Figure 3.29 Cardiomyogenic gene expression of undifferentiated WJ MSCs grown in Culture I and Culture II.

3.6.3.2 Influence of Cardiogenic Differentiation Factors on hWJ MSCs

Valproic acid and bovine insulin were used again as cardiomyogenic factors, since they were shown to induce expression of ventricular α/β MHC and α -actinin in WJ MSCs in our previous study. In addition to these two factors, IL 1 β was used in the cardiomyogenic medium. IL 1 β is a proinflammatory cytokine that is shown to lead to hypertrophy (increased contractility) in cardiomyocytes by increasing expression of genes encoding the contractile protein MHC, and causes an approximately two fold increase in cell size (Petersen and Burleigh, 2003). It is also involved in prevention of cell apoptosis.

3.6.3.2.1 Gene Expression Analysis by RT-PCR

hWJ MSCs cultured on collagen Type I coated TCPS in the presence of differentiation factors were analyzed with RT-PCR for expression of cardiac transcription factors GATA4 and Nkx 2.5. The change of primary medium from α MEM/Ham F-12 (1:1) to a poorer medium, DMEM high glucose, diminished the expression of GATA4 (compare Figs 3.29 and 3.30); at the end of 14 day incubation period; neither GATA4 nor Nkx 2.5 were expressed. Lack of Nkx 2.5 expression is actually the effect of collagen type I; Nkx 2.5 expression was observed in DMEM high glucose media with 10% FCS. Upon addition of valproic acid to the medium expression of Nkx 2.5 was observed (Fig 3.30).

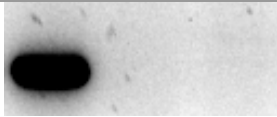
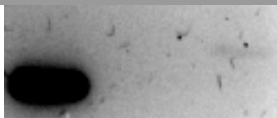
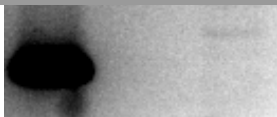
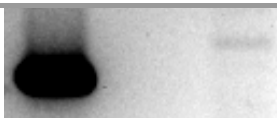
Media Composition	β -actin	GATA4	Nkx 2.5
PM			
PM+ 2mM VA			
PM+ 2mM VA+ 100 μ g/mL B. Ins			
PM+ 2mM VA+ 100 μ g/mL B. Ins + 1 ng/mL IL 1 β			

Figure 3.30 Cardiomyogenic gene expression by WJ MSCs in the presence of differentiation factors. PM: Primary Medium, B. Ins: bovine insulin, VA: valproic acid.

3.6.3.2.2 Immunostaining for ventricular α/β MHC

At the end of the 14 day incubation period the cells were immunostained for ventricular α/β MHC, a protein present in the sarcomere structure. The fluorescence micrographs obtained (Fig 3.31) were not conclusive enough to determine the most suitable growth factor cocktail for differentiation to cardiomyocytes. No significant staining for α/β MHC could be observed. Nuclear aberrations were seen in presence of insulin and IL 1 β .

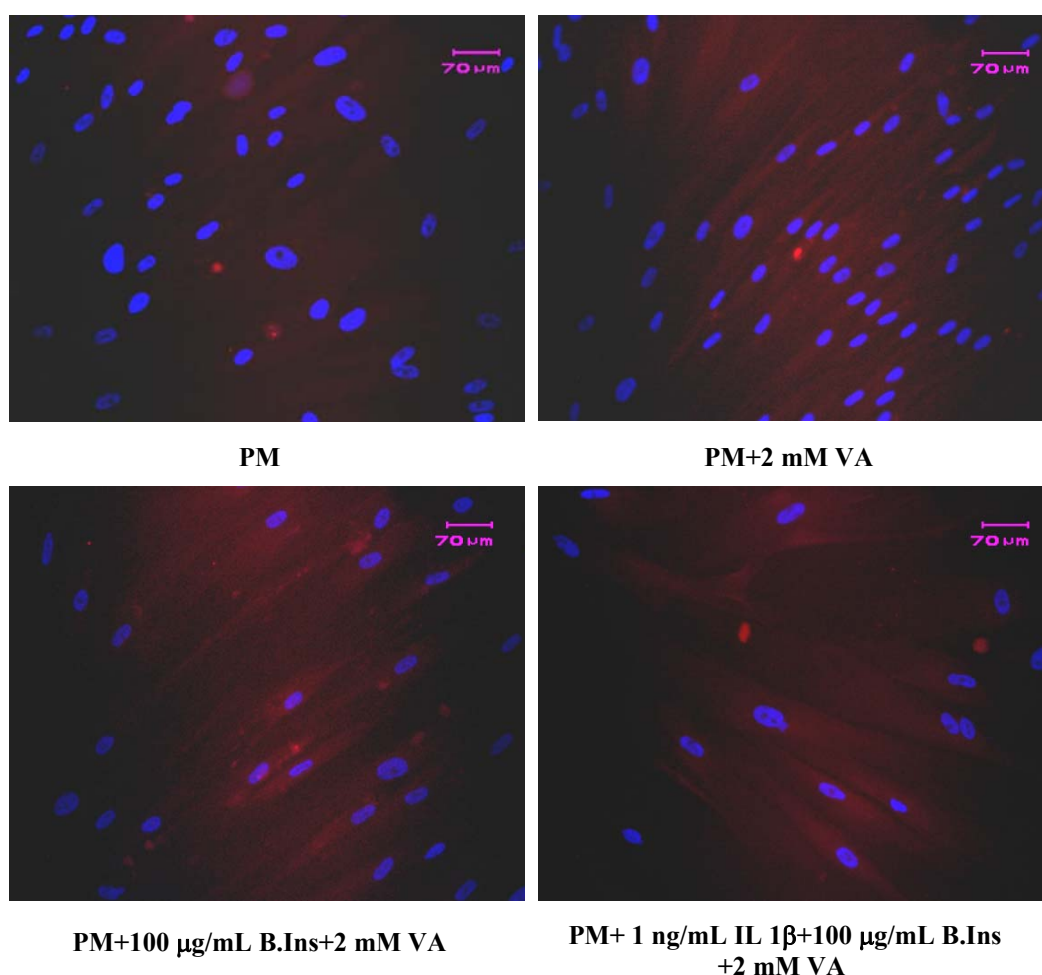


Figure 3.31 Fluorescence microscopy images of hWJ MSCs cultured for 14 days in the presence of cardiomyogenic differentiation factors, immunostained for ventricular α/β MHC (x20). PM: Primary Medium, B. Ins: bovine insulin, VA: valproic acid. Red: ventricular α/β MHC, blue: cell nuclei stained with DAPI.

These observations were not in agreement with our previous results, where valproic acid and insulin induced a profound expression of α/β MHC in WJ MSCs. This can be explained by the difference in growth media composition used for growing cells in the stock culture and difference in passage numbers of the cells, that is inability to catch the right timing for differentiation, or may be the effect of interindividual differences.

A routine cell staining for actin filaments to reveal cell morphology showed that valproic acid leads to cell enlargement and elongation and in the presence of both IL 1 β and valproic acid broader cells were obtained (Fig 3.32).

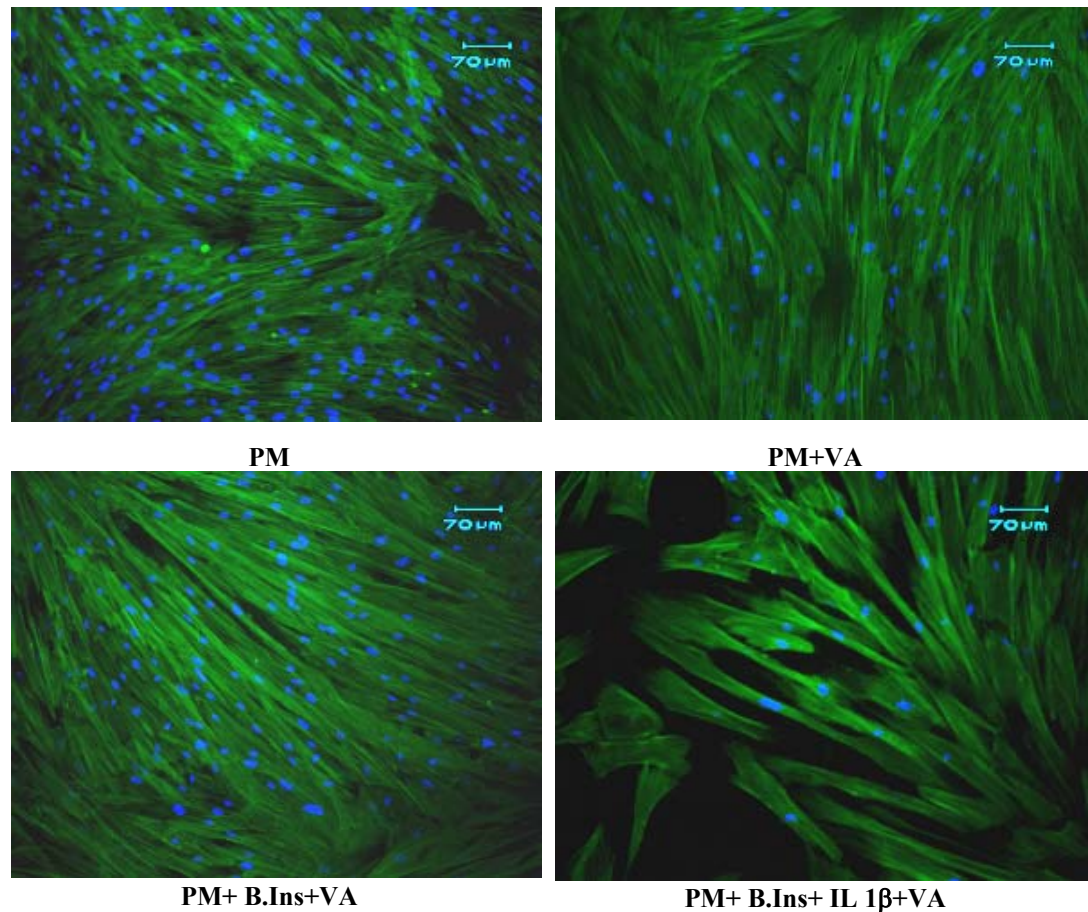


Figure 3.32 Morphology of WJ MSCs cultured for 14 days in the presence of cardiomyogenic differentiation factors, revealed by fluorescence microscopy (x10). PM: Primary Medium, B. Ins: bovine insulin, VA: valproic acid. Blue: nuclei stained with DAPI, green: actin filaments stained with FITC-Phalloidin.

3.7. Tissue Engineering on Microfiber Mats

3.7.1 Morphology of hWJ MSCs Cultured on the Unaligned and Aligned Fiber Mats

Electrospun blends of PHBV-P(L-D,L)LA:PGS (mat thickness: 12 ± 3 μm , fiber diameter 1.25 ± 0.10 μm) were tested for their suitability for attachment and alignment of WJ MSCs. Third passage WJ MSCs fed with PM type II were seeded on the UV sterilized 1×1 cm^2 dry PHBV-P(L-D,L)LA and PHBV-P(L-D,L)LA:PGS 98:2 mats. The cells were cultured on the mats for 5 days and then samples were fixed for fluorescence microscopy. Staining with FITC-Phalloidin revealed the random orientation of WJ MSC filamentous actin cytoskeleton on unaligned fiber mats and its parallel orientation in the direction of fibers when cells are cultured on the aligned fiber mats (Fig 3.33).

Third passage WJ MSCs were also grown in PM type I on 1.5×3.5 cm^2 aligned fiber mats with 1, 2 and 4% PGS content to observe cell distribution on a larger scale. The cells were cultured on the mats for 14 days and then samples were fixed for fluorescence microscopy. Staining of actin cytoskeleton showed that WJ MSCs attached very well and aligned parallel to each other in the direction of fibers on all mats (Fig 3.34). Although the cells were seeded uniformly on the mats so that a certain number of cells are delivered per unit area, the cell distribution on the mats at the end of culture period was not homogeneous (Fig 3.34). Actually the same situation was observed even on TCPS. Therefore, this nonuniform cell distribution on the mats was attributed to cellular behaviour rather than being result of material surface property.

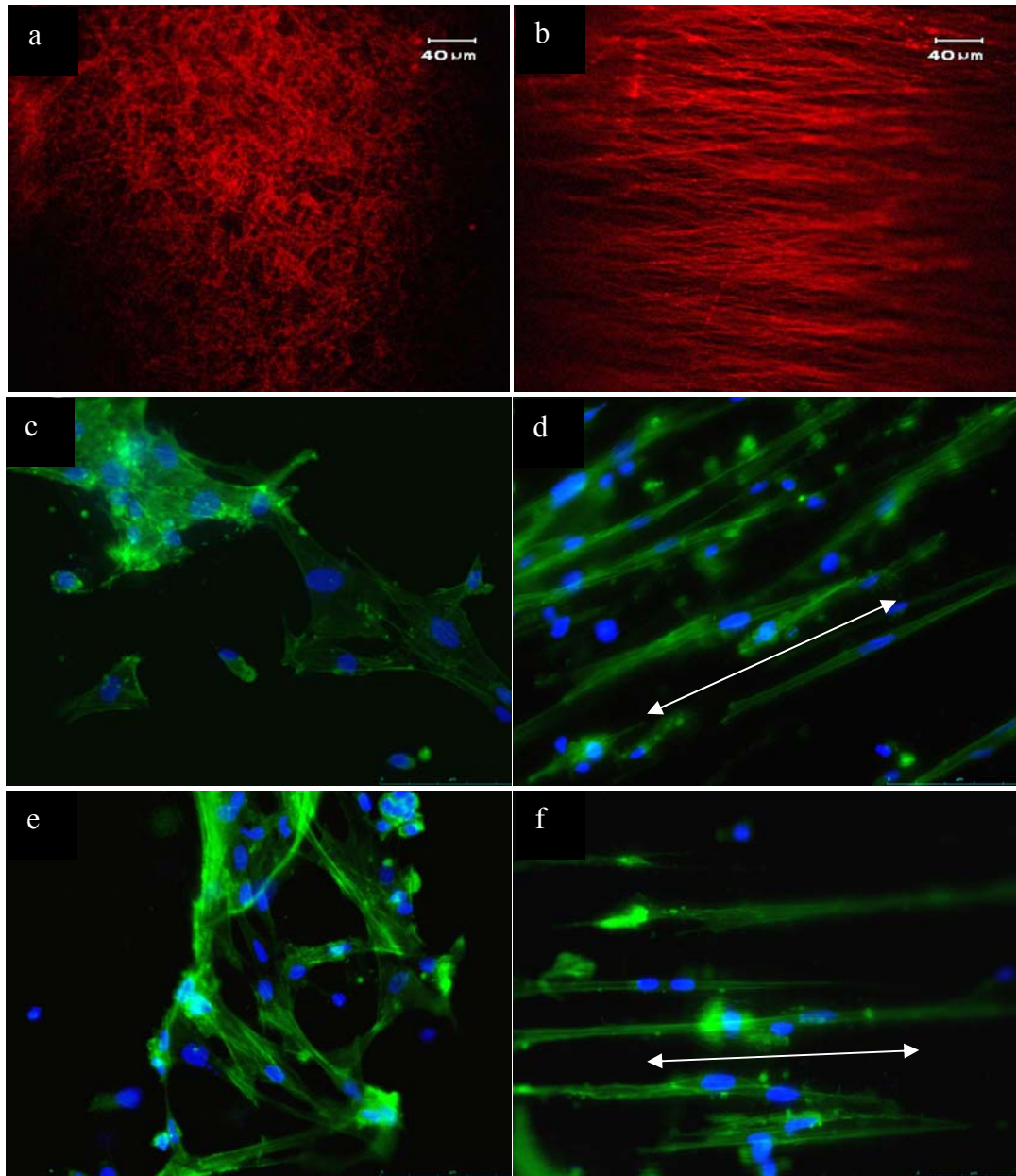
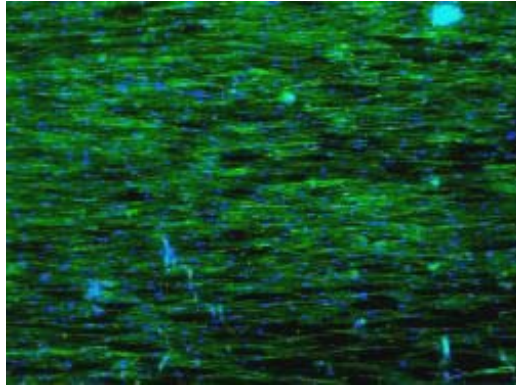
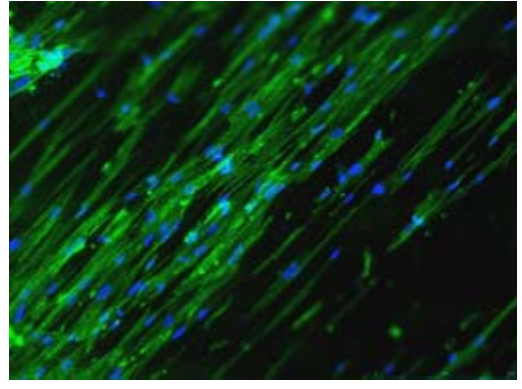


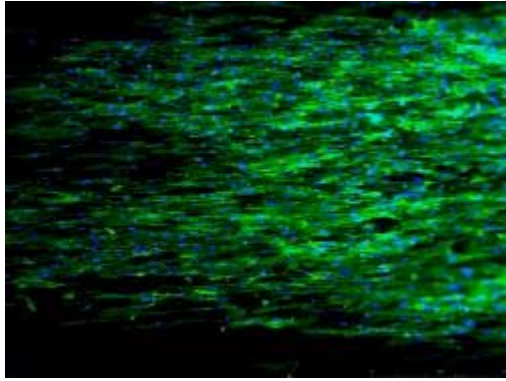
Figure 3.33 WJ MSC morphology on unaligned (a) and aligned (b) fiber mats (x20). c, d) WJ MSCs on PHBV-P(L-D,L)LA mats, e, f) WJ MSCs on PHBV-P(L-D,L)LA:PGS 98:2 mats. Red: microfibers stained with Nile Red, green: filamentous actin stained with FITC-Phalloidin, blue: cell nuclei stained with DAPI. White arrows show the direction of aligned fibers.



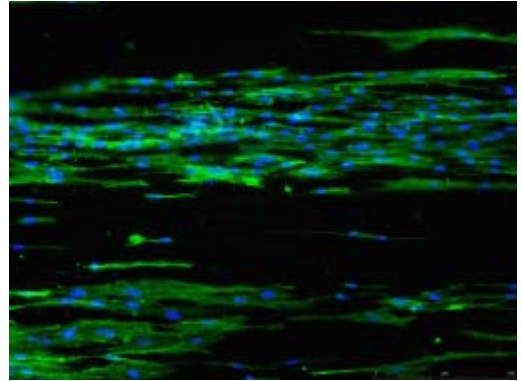
PHBV-P(L-D,L)LA:PGS (99:1) (x5)



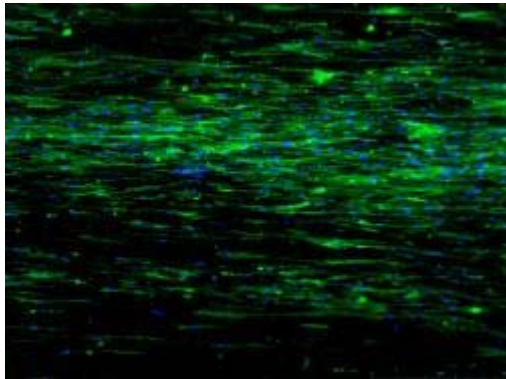
PHBV-P(L-D,L)LA:PGS (99:1) (x10)



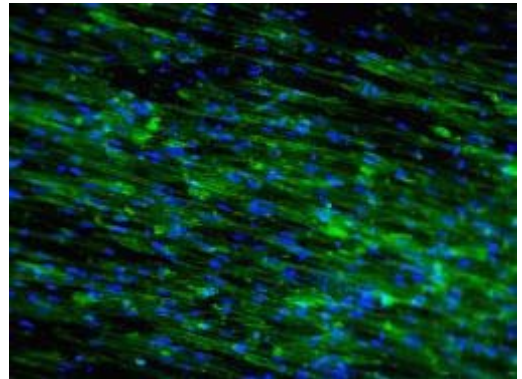
PHBV-P(L-D,L)LA:PGS (98:2) (x5)



PHBV-P(L-D,L)LA:PGS (98:2) (x10)



PHBV-P(L-D,L)LA:PGS (96:4) (x5)



PHBV-P(L-D,L)LA:PGS (96:4) (x10)

Figure 3.34 WJ MSC distribution and alignment on PHBV-P(L-D,L)LA:PGS mats ($1.5 \times 3.5 \text{ cm}^2$) after 14 days of culture. Green: filamentous actin stained with FITC-Phalloidin, blue: cell nuclei stained with DAPI.

3.7.2 hWJ MSC Proliferation on the Aligned Microfiber Mats

Electrospun aligned fiber mats of PHBV-P(L-D,L)LA and PHBV-P(L-D,L)LA:PGS blends (1x1 cm²) were seeded with WJ MSCs and then incubated for 1 and 14 days at 37 °C in the CO₂ incubator (5% CO₂), to study the effect of chemical property of mats on cell proliferation. Third passage WJ MSCs fed with PM type I were seeded on the UV sterilized 1x1 cm² dry unmodified and collagen Type I adsorbed PHBV-P(L-D,L)LA and PHBV-P(L-D,L)LA:PGS mats, and also on TCPS as positive control. MTS assay was carried out after 24h of cell seeding, to determine the number of cells attached on each sample. No significant difference could be observed in terms of cell attachment on PHBV-P(L-D,L)LA:PGS blend mats, which contained 1, 2 or 4% PGS, although the mats with 2 or 4% PGS performed better (Fig 3.35). Presence of adsorbed collagen on the mats caused a significant improvement in cell attachment.

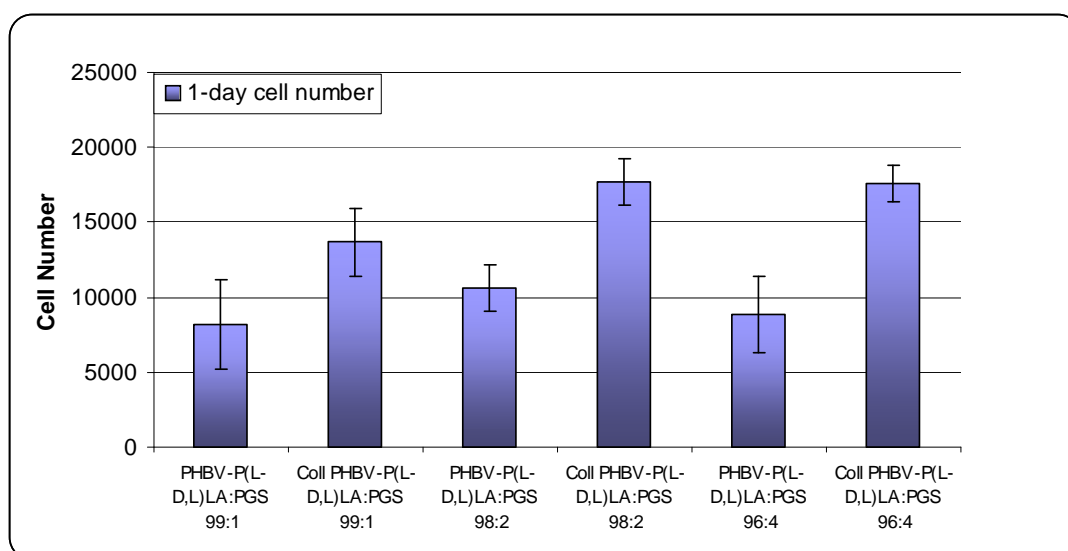


Figure 3.35 hWJ MSC attachment on aligned fiber PHBV-P(L-D,L)LA:PGS mats.

Further cell proliferation experiments were done with PHBV-P(L-D,L)LA and PHBV-P(L-D,L)LA:PGS 98:2 mats. Cell attachment on the TCPS was found to be the highest, followed by collagen adsorbed mats, especially the collagen adsorbed PHBV-P(L-D,L)LA mats (Fig 3.36). Collagen Type I is found in the ECM of many tissue types in the body, including cardiac tissue and bears the RGD (arginine - glycine - aspartic acid) amino acid sequence, an attachment site for integrins that anchor the cell to a surface. Presence of collagen on the surface improved cell attachment to the mats. In the absence of collagen, there was no significant difference in the cell attachment on PHBV-P(L-D,L)LA and PHBV-P(L-D,L)LA:PGS 98:2 mats, that is presence of 2% PGS in the polymer blend did not lead to a significant change in cell attachment.

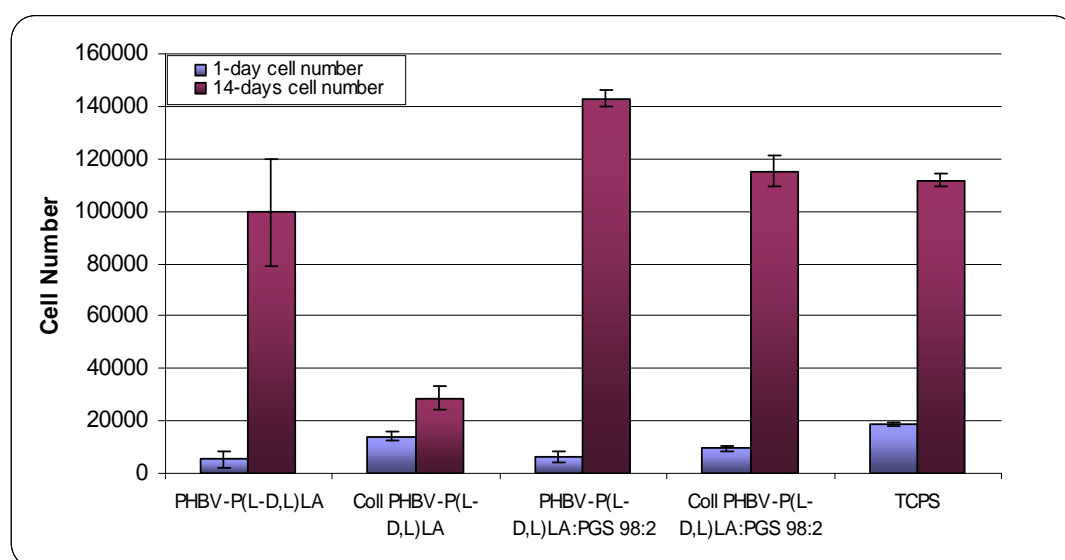


Figure 3.36 hWJ MSC proliferation on aligned fiber PHBV-P(L-D,L)LA and PHBV-P(L-D,L)LA:PGS (98:2) mats within 14 days after cell seeding.

The highest cell proliferation rate and the lowest standard deviation within 14 days were obtained on the PHBV-P(L-D,L)LA:PGS 98:2 mats, when compared to other surfaces. This value was even higher than that on TCPS. A reasonable explanation for this behavior could be that cells can penetrate easily

within the mat through the voids among the aligned fibers, therefore the mats should be considered as 3D scaffolds as opposed to 2D surface of TCPS. Presence of collagen on both types of mats significantly decreased the cell proliferation rate. RGD-integrin association is known to affect cell proliferation and/or differentiation (Kim and Mooney, 1998), and it is seen from Fig 3.36 that collagen Type I slows down the proliferation of WJ MSCs.

A significant difference in proliferation rate was observed between PHBV-P(L-D,L)LA and PHBV-P(L-D,L)LA:PGS 98:2 mats, which points out to the positive effect of more hydrophilic material on cell proliferation, either by improving cell-material interaction or cell penetration into the mat, or both.

When the whole data gathered at the end of two weeks is considered, it was deduced that presence of adsorbed collagen Type I on the aligned fiber mats had a negative effect on cell proliferation, while the presence of PGS in the bulk material, even a low amount, promoted cell proliferation.

Numerical values of the cell proliferation on PHBV-P(L-D,L)LA and PHBV-P(L-D,L)LA:PGS 98:2 mats can be found in Appendix E.

3.8. Analysis of the 3D Constructs Cultured in the Microbioreactor

The ultimate aim in this study was to obtain an artificial myocardial patch with a similar cellular organization to native tissue and macroporous tubings in between to feed the cells in the 3D construct. As a starting point, the WJ MSCs were first seeded on collagen Type I coated aligned fiber mats of PHBV-P(L-D,L)LA:PGS (98:2) (3.5 x 6 cm²) and cultured for 14 days in the CO₂ incubator, to obtain sheets of cells where cells will be aligned parallel and will be in communication with each other, as in native tissue. SEM (Fig 3.37) and confocal microscopy images (Fig 3.38) of these cell sheets were obtained to study the cell distribution and cell alignment. PHBV-P(L-D,L)LA:PGS (98:2) aligned fiber mats were used to grow the cells on, because they were shown to have less fiber fusion than PHBV-P(L-D,L)LA:PGS (96:4) mats and better supported cell proliferation compared to PHBV-P(L-D,L)LA mats.

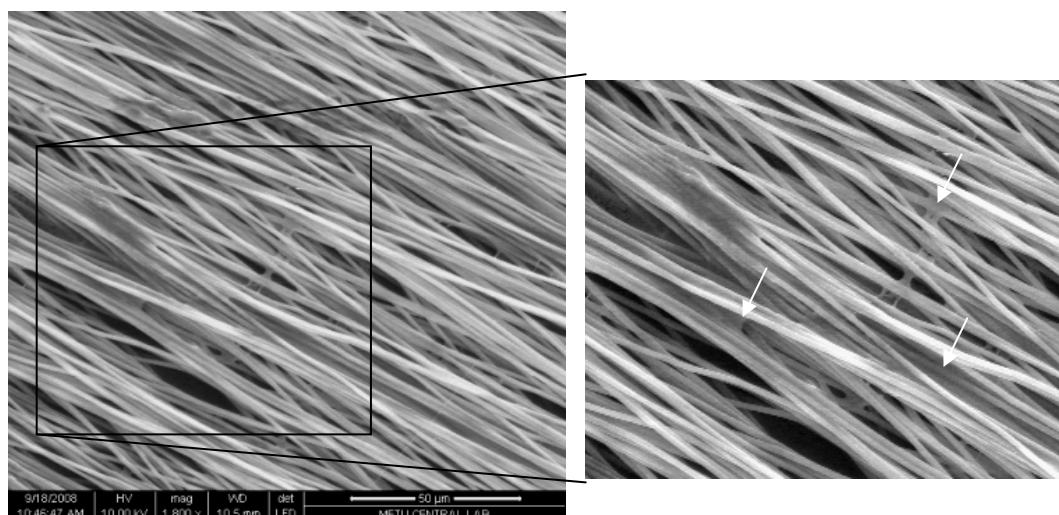


Figure 3.37 The scanning electron micrographs of WJ MSCs grown on aligned fiber PHBV-P(L-D,L)LA:PGS (98:2) mats for 14 days. White arrows on the inset point out the cells.

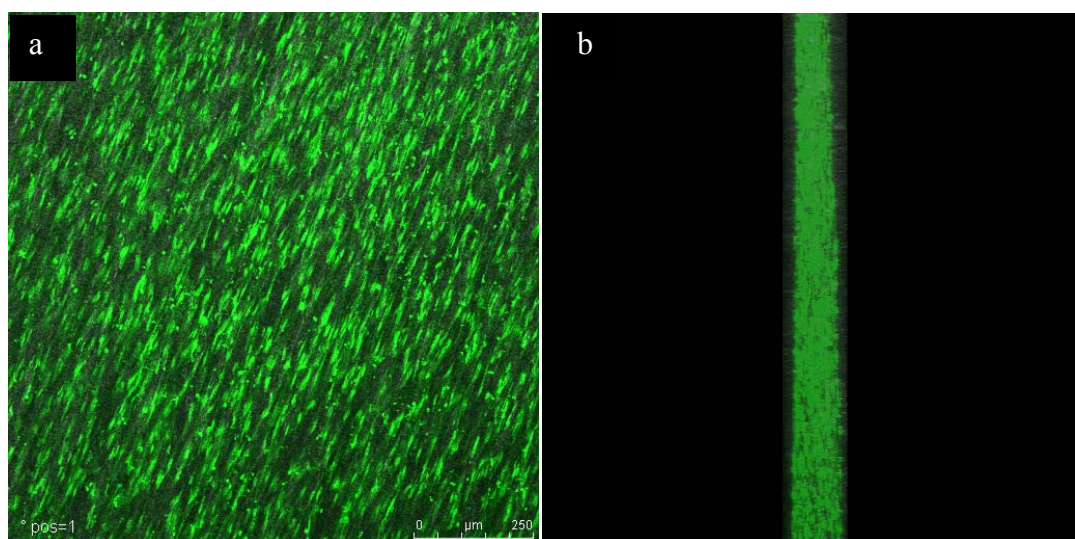


Figure 3.38 The confocal micrographs of WJ MSCs grown on aligned fiber PHBV-P(L-D,L)LA:PGS (98:2) mats for 14 days. Cells stained with Acridine Orange: a) top view, b) cross sectional view.

Although Figures 3.37 and 3.38 show essentially the same mat, the cells on the mat were almost invisible on scanning electron micrographs in contrast to their confocal micrographs. In both figures, but especially in the cross section of the mat obtained with confocal microscopy (Fig 3.38b) it is seen that cells have penetrated effectively within the mat through the fiber interstices. The cross section (Fig 3.38b) shows that at least 3-4 cell layers could be achieved with the mat used. Therefore, aligned fiber mats overcome a major problem with unaligned fiber mats, which is the inability of cells to penetrate the lower layers of the unaligned mats. With high magnification confocal images it was possible to show alignment of the cell nuclei in the direction of fibers (Fig 3.39).

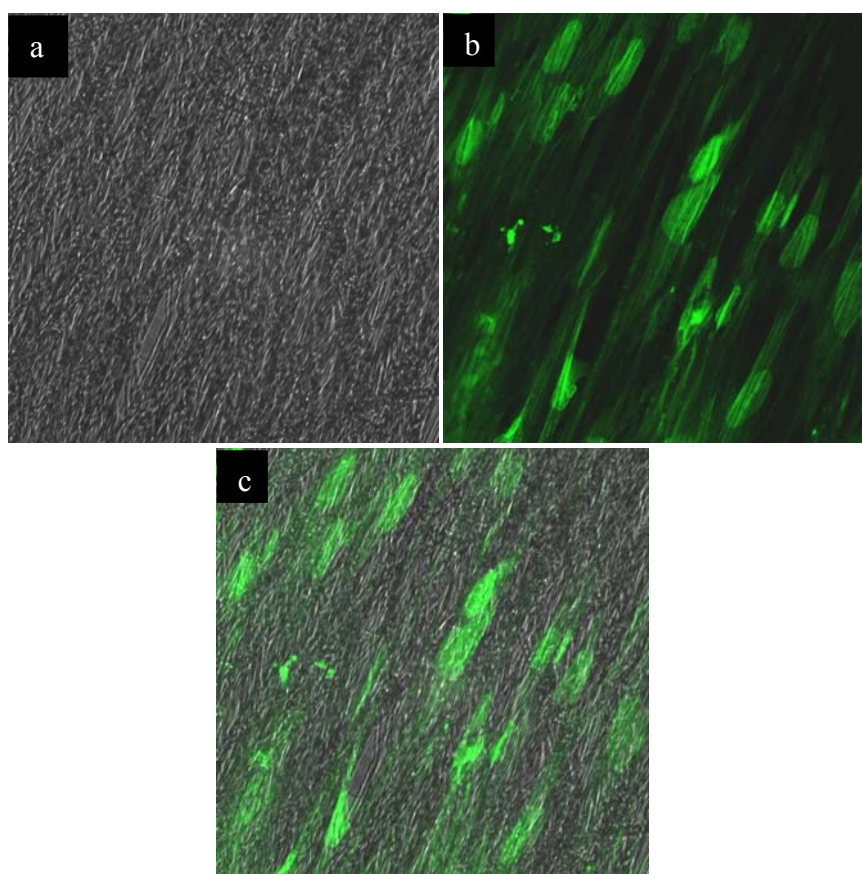


Figure 3.39 The confocal micrographs of WJ MSCs grown on aligned fiber mats of PHBV-P(L-D,L)LA:PGS (98:2) for 14 days, with an emphasis on nuclear alignment. a) Transmission image of the mat, b) WJ MSCs on the mat stained with Acridine Orange, c) overlay of the mat and the cells. (x63)

Cell growth on the thin mats caused a visible mat retraction (Fig 3.40). This shows a kind of positive achievement, since cardiomyocytes need to retract on the surface they adhere to for normal contraction, and this outcome shows that the mats are soft and flexible enough for physical retraction.

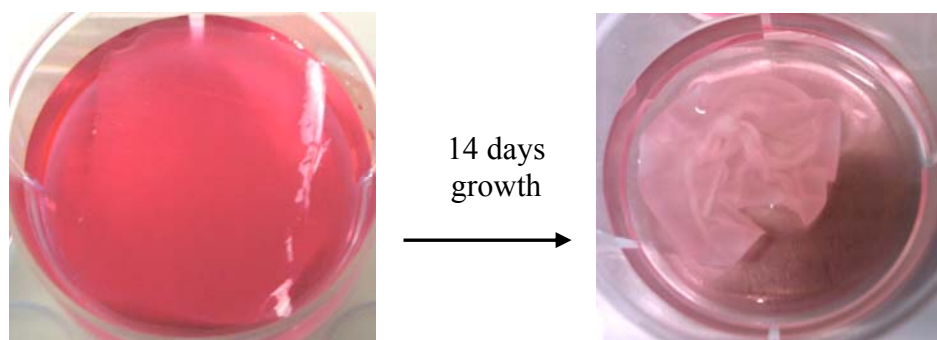


Figure 3.40 Retraction of an aligned fiber mat as a result of cell growth on it after 14 days of culture.

To assemble a 3D construct, two aligned fiber mats with WJ MSCs grown on them for 14 days were wrapped around the permeable parts of two biodegradable tubings, so that the fibers and tubings are parallel to each other. This was then placed in the PDMS chamber that was filled with growth medium. Two such cultures were prepared and one of them was kept static; the medium in the chamber was refreshed every other day (Fig 3.41). In order to see the effect of growth medium perfusion through the permeable tubings on cell survival, the nonporous parts of biodegradable tubings of the other construct were inserted to the inner side of the chamber inlets (Fig 3.42). A total of 250 μL growth medium was perfused through the construct at a rate of 100 $\mu\text{L}/\text{h}$ every other day. After 6 days of culture, the constructs were fixed with glutaraldehyde, frozen and gross sectioned with a scalpel prior to SEM analysis.

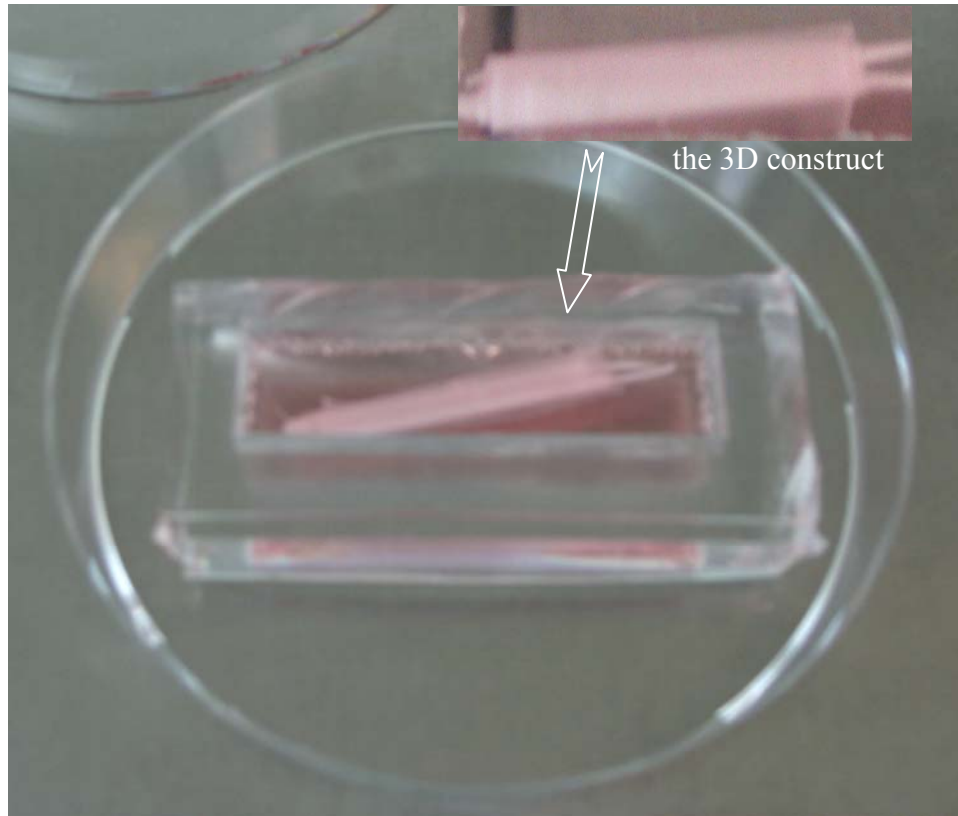


Figure 3.41 Static culture of the 3D construct. Two aligned fiber mats with WJ MSCs grown on them for 14 days were wrapped around the permeable parts of two biodegradable tubings, so that the fibers and tubings are parallel to each other to obtain the 3D construct and placed in a PDMS chamber filled with cell growth medium for further culture under static conditions.

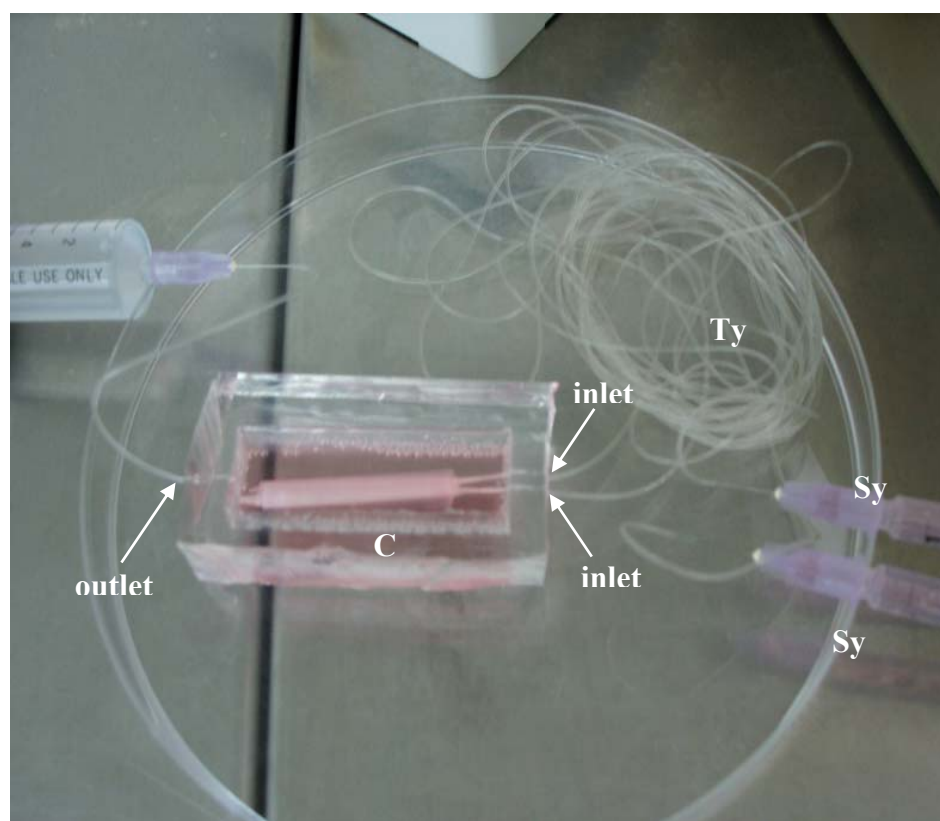


Figure 3.42 The perfused 3D construct (C). The two 1 mL syringes (Sy) on the right are used to deliver cell growth media through the Tygon tubings to the two inlets of the PDMS chamber and the medium continues to flow through the nonporous parts of the biodegradable tubings inserted at the inner holes of the inlets. Finally the medium is delivered to the cells in the mats by diffusing through the walls of macroporous portion of the tubings that are wrapped by the mats. The end of the Tygon tubing at the outlet of the chamber (occupied by another big syringe full of fluid) is opened during the medium perfusion process, to allow the outflow of excess fluid.

SEM images of sections from the 3D constructs cultured under static and medium perfused conditions for 6 days (Figs 3.43 and 3.44) revealed no interlayer cell-cell association in neither of the culture conditions, probably due to layers being not close enough to each other. Cells could not be visualized with SEM, either.

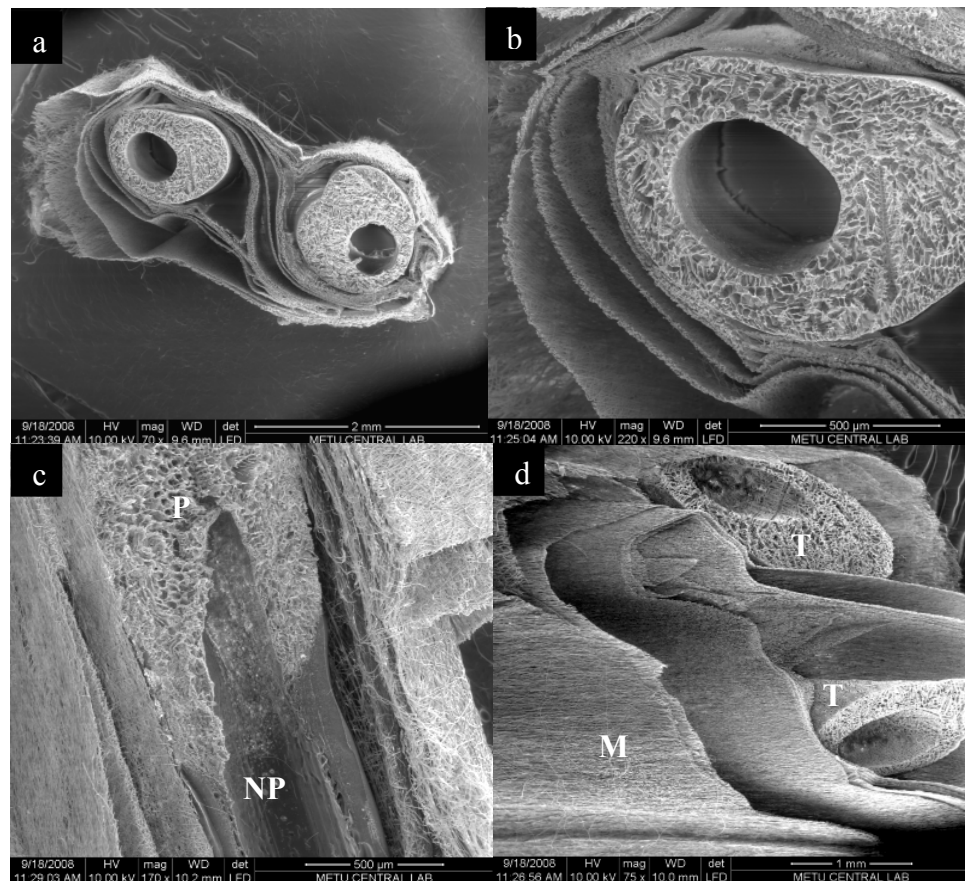


Figure 3.43 SEM images of sections from the 3D construct cultured under static conditions for 6 days. a) Cross section of the 3D construct, b) a closer view of permeable tubing surrounded by the aligned mat sheets, c) longitudinal cross section of the tubing showing both the porous (P) and nonporous (NP) parts of the structure, d) another view of the 3D construct showing the parallel arrangement of mat fibers (M) to the long axis of the tubings (T).

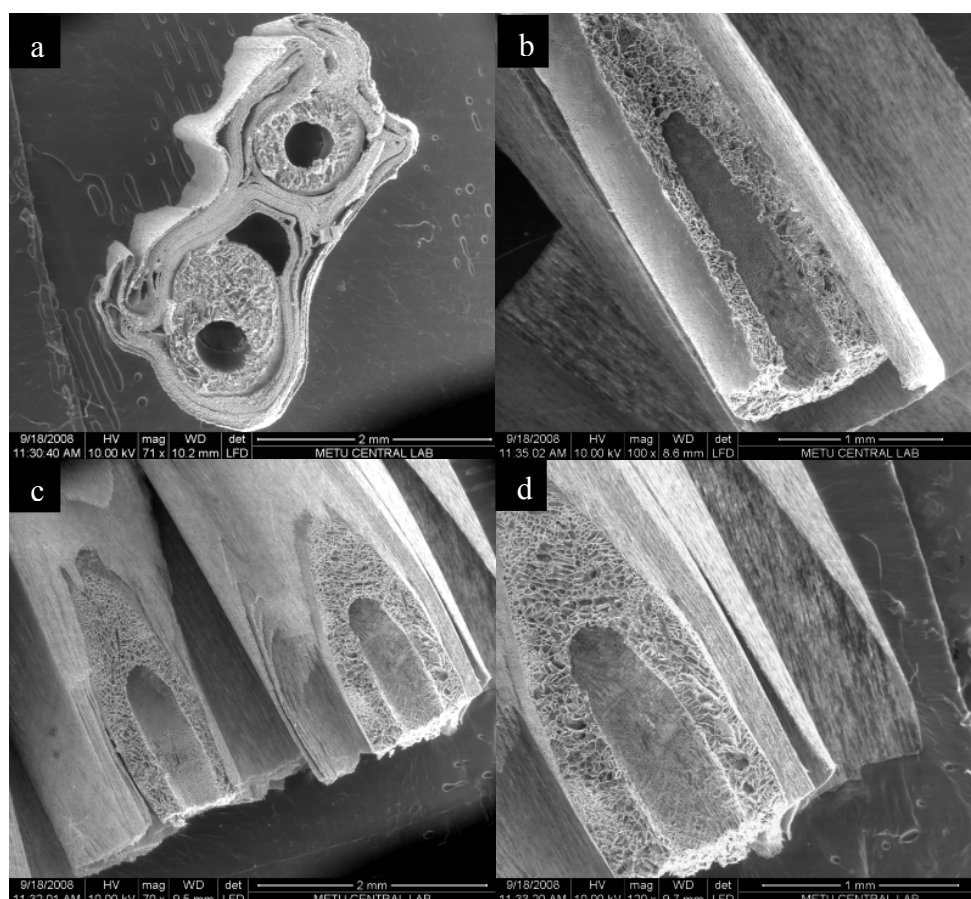


Figure 3.44 SEM images of sections from the 3D construct cultured under medium perfused conditions for 6 days. a) Cross section of the 3D construct, b) longitudinal cross section surrounded by the aligned mat sheets, c) diagonal view of the 3D construct showing the parallel arrangement of mat fibers to the long axis of the tubings and the mat-tubing association, d) a closer view of diagonally sectioned macroporous tubing surrounded by the aligned fiber mats.

The remaining cross sections of the 3D construct cultured under static conditions were stained with Acridine Orange for the cell nuclei and revealed the distribution of cells in the 3D construct (Fig 3.45).

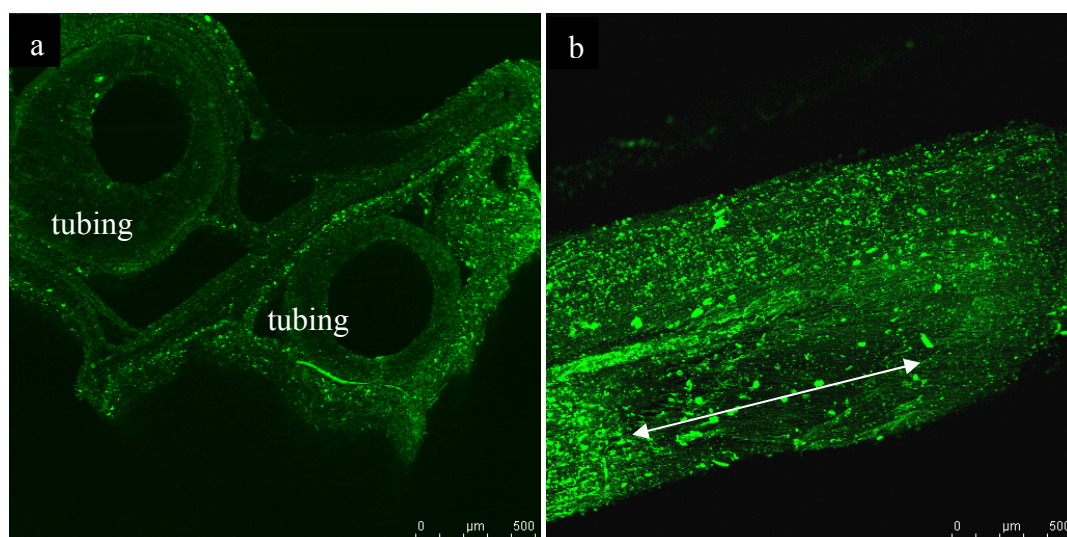


Figure 3.45 Confocal microscopy images of sections from the 3D construct cultured under static conditions for 6 days. a) Cross section of the 3D construct, b) longitudinal image of the top layer of the 3D construct. Bright green dots are the cells stained with Acridine Orange. The white arrow shows the fiber alignment direction.

The bright green dots in the confocal microscopy images in Figure 3.45 are the cells stained with Acridine Orange. The cells were found to be present at the outermost layer of the 3D construct (Fig 3.45b) cultured under static conditions and also in the layer surrounding one of the tubings (Fig 3.45a).


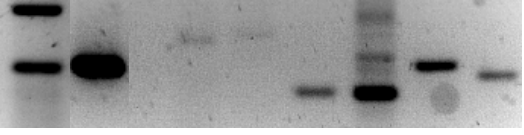

Absence of cell-cell interaction between the neighboring layers of aligned fiber mats revealed the need for a gel-like material between the mat layers to keep them closer and connected to each other and prevent unwinding after 3D construct formation. Therefore, Collagen type I gel was introduced onto the aligned mat with cells grown on its surface, before rolling around the tubing. Rest of the steps were the same. Two new 3D constructs, thus, were obtained for the static (construct dimensions: 2 mm height, 4 mm width, 3.5 cm length) and perfused (construct dimensions: 2 mm height, 3.5 mm width, 3.5 cm length) cultures. The cultures were continued for 14 days with the use of cardiomyogenic differentiation factors in the cell growth medium. At the end of culture period, the 3D constructs

were cut into 3 pieces and one piece was used for each of the following test: MTS test for cell viability determination, RT-PCR for detection of cardiomyogenic gene expression and cryosectioning for determination of cell distribution and immunostaining for cardiac specific proteins.

The viable cell number in the static culture was found as 3.7×10^5 cells, and in perfused culture as 2.5×10^5 cells. These values show that there are considerable numbers of alive cells in both constructs, but they should not be compared since the starting cell numbers were not known.

RT-PCR analysis revealed the expression of the principal cardiac transcription factor Nkx 2.5 and expression of other cardiac related genes Tbx 5, FOG 2, MEF 2A, MEF 2C and MEF 2D by the cells cultured in both the static and the perfused conditions. This was expected since they both had received the same media (Table 3.8). GATA4 expression could not be detected in neither of them. Control media contained all experimental media components except the growth factors (valproic acid, insulin and IL 1 β) and cells in this culture did not express GATA4 or Nkx 2.5.

Table 3.8 Cardiac transcription factor expression by hWJ MSCs cultured in static and perfused cultures.

Culture Type	MW	DNA Marker	β -actin	GATA4	Nkx 2.5	Tbx 5	FOG 2	MEF 2A	MEF 2C	MEF 2D
Control	300 bp									
	200 bp									
Static	300 bp									
	200 bp									
Perfused	300 bp									
	200 bp									

20 μm thick longitudinal sections of the 3D constructs from static and perfused cultures were obtained through cryosectioning and stained with Acridine Orange (Fig 3.46) and FITC-Phalloidin (Fig 3.47) to study the cell distribution and alignment within the structure. 9 to 10 layers of aligned fiber mats, with a total thickness of $\sim 500 \mu\text{m}$, could be obtained on one side of a permeable tubing (Figs 3.45b and e). It was observed that in static culture the cells on the outermost layer could survive as a continuous cell sheet and on the inner layers a very low cell density was observed (Fig 3.47). On the other hand, cell distribution in the perfused culture was distinctly more uniform among the layers and there was a cell layer formed around the medium permeable tubing at the contact site (Figs 3.46d, 3.47d and e). These images confirmed the significant effect of feeding cells from inside the 3D structure on keeping them alive. Parallel cell alignment to fiber direction was maintained within the structure, but a distinct interlayer cellular association could not be observed.

Immunostaining for ventricular myosin heavy chain revealed negative results for cells in both cultures. This was in agreement with our differentiation experiments carried out with the same differentiation media on Collagen Type I coated TCPS. Although expression of major cardiac transcription factors, except GATA4, by these cells was shown, formation of contractile machinery, that is sarcomers, could not be induced. This outcome points out to the importance of conducting immunocytochemistry besides RT-PCR for gene expression in an investigation of differentiation to a particular cell lineage.

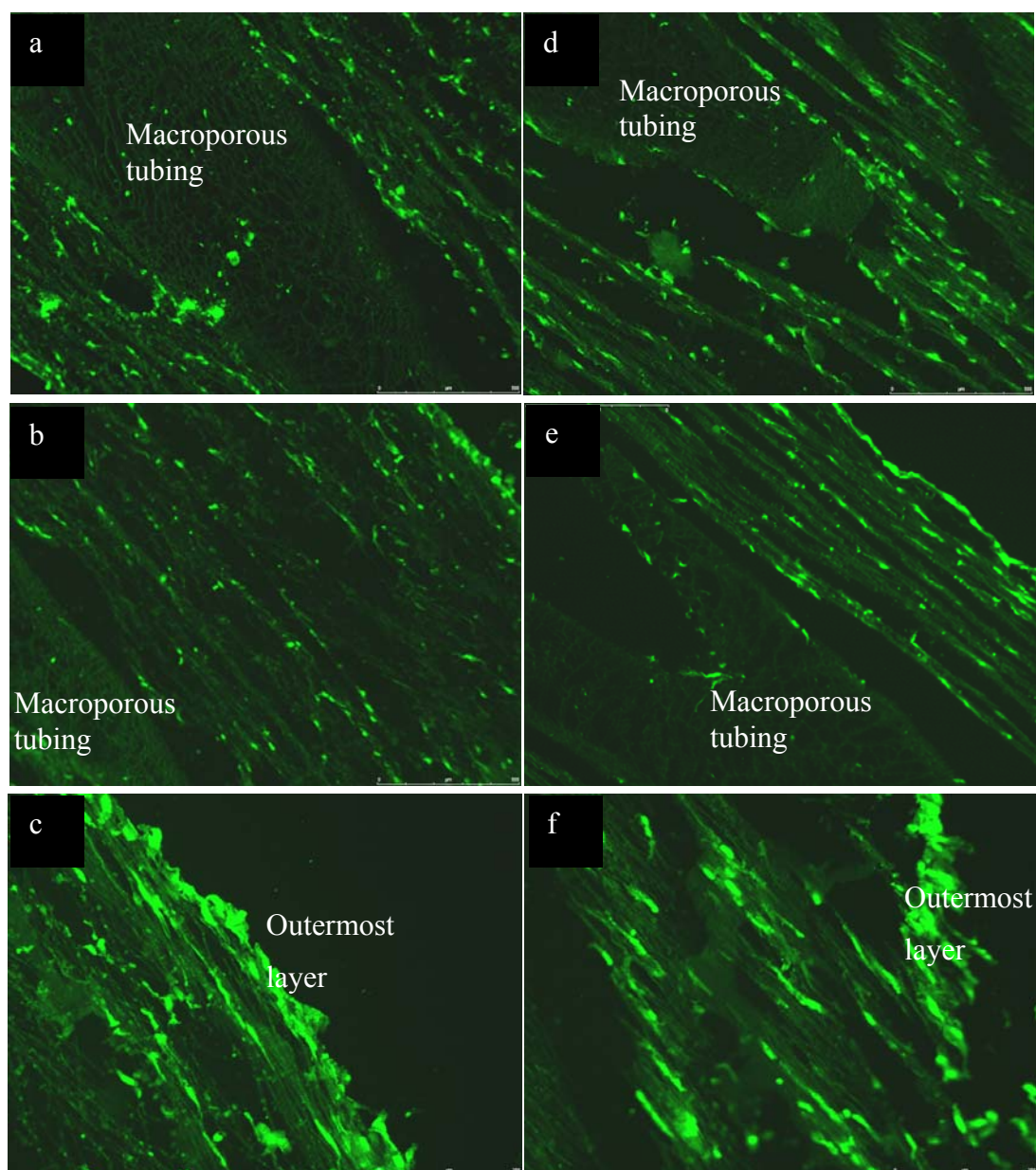


Figure 3.46 Acridine Orange stained cryosections of the 3D constructs from the static culture (a, b, c), and perfused culture (d, e, f). a, b, d, e) The macroporous tubing and the aligned fiber layers surrounding it (x5), c, f) ~ 3 layers of neighbor aligned fibers (x10). Green: cell nuclei and bodies.

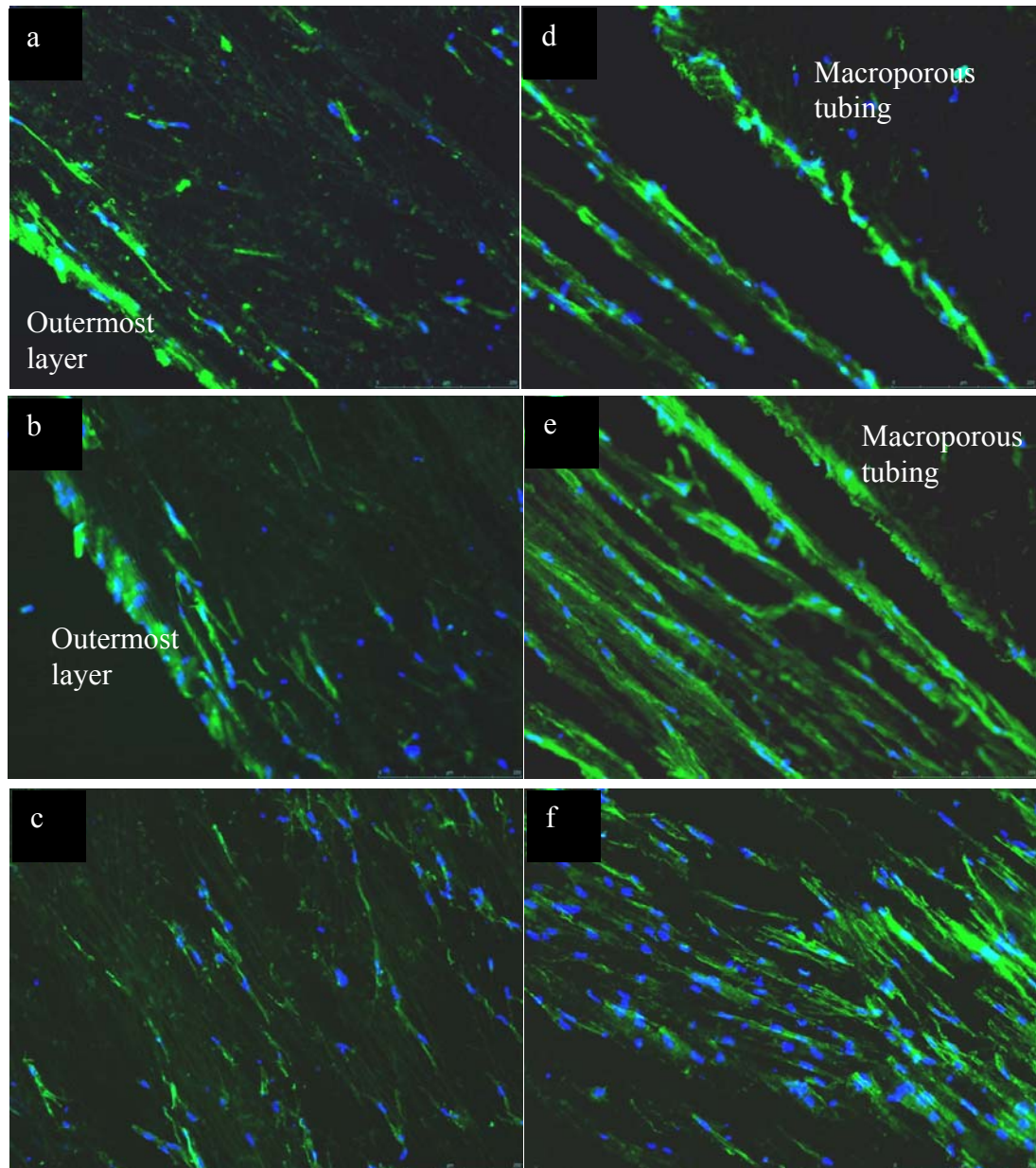


Figure 3.47 Phalloidin and DAPI stained cryosections of the 3D constructs from static culture (a, b, c), and perfused culture (d, e, f). c, f) Inner layers of the 3D construct. (x10) Green: filamentous actin, blue: cell nuclei.

5 layers of electrospun mats of poly(epsilon-caprolactone) with random, unaligned, fiber orientation that were seeded with cardiomyocytes from neonatal rats were successfully overlaid by Ishii et al. (2005) to form a 3D graft. Individual

layers adhered intimately, and morphologic and electrical communication between the layers was established, and synchronized beating was also observed. The fiber size of these mats was 250 nm, as opposed to ours (more than 1 μm), which may be the reason of not observing any interlayer cell-to-cell association. In our study, the cells resided within the mat and probably there is a need for more time for them to occupy all the available spaces and finally cover the whole mat surface to be able to associate with the cells in the neighbor layers.

Although the differentiation of WJ MSCs to functional cardiomyocytes was not successful, proof of concept was shown in terms of the 3D construct design to keep cells aligned parallel to each other in 3D and keep them homogeneously distributed and alive within the 3D structure by perfusing growth media through the macroporous tubings. The 3D construct had a relatively loose structure, which may be turned out into an advantage. The low ischemia tolerance of thick, terminally differentiated cardiac muscle samples is expected to impede their application in cardiac regeneration in vivo (Zimmermann et al., 2006). Eventually, loose, but electrically and functionally interconnected, cardiac myocyte networks with a low degree of differentiation may have a better chance to survive in vitro and after implantation in vivo.

WJ MSCs have been used in generation of living tissue engineered arteries (Hoerstrup et al., 2002) and heart valves (Schmit et al., 2005, 2006). Valve leaflets showed mature layered tissue formation and extracellular matrix production comparable with that of native tissues. Therefore, if differentiation pathways of hWJ MSCs can be elucidated, they can be used in overcoming the lack of living autologous replacements for many tissue types.

CHAPTER 4

CONCLUSIONS

Cardiac muscle contracts like a syncytium owing to the multicellular assembly of myofibers oriented parallel to each other, connected end-to-end via intercalated disks in the longitudinal direction and side-to-side in the transverse direction. It is this cellular arrangement that integrates individual contraction into a pumping action and indeed generating myofiber disarrays is known to cause arrhythmia. It was proposed in this study that it is possible to obtain in vitro a 3D cell organization similar to that of cardiomyocytes in the native myocardium by aligning the cells on aligned microfibrinous mats and subsequent stacking of these cell sheets. As one of the positive achievements of this study, electrospun, parallel microfibers of P(L-D,L)LA-PHBV:PGS polymer blends were effective in aligning the cells and were soft enough for retraction by the cell; softness of the cell carrier used in cardiac tissue engineering is of utmost importance to allow cardiomyocyte contraction. The aligned cell sheets in the fibrous mats were successfully stacked around the biodegradable macroporous tubings to obtain a 3D construct perfused with growth media from its central portion. As a proof of concept, the distinct effect of feeding cells from inside the 3D structure on keeping them alive was shown; it was possible to maintain cell viability and achieve uniform distribution of aligned cells throughout the 3D construct for 2 weeks. However, interlayer cell-to-cell interaction could not be shown.

Also for the first time human mesenchymal stem cells derived from Wharton's Jelly were proposed to serve as the cellular component of the 3D myocardial construct. To achieve this, their potential to differentiate into

cardiomyocytes had to be shown. Studies were carried out to prove the mesenchymal origin of these cells by comparing with MSCs from human bone marrow (hBM). The hBM and Wharton's Jelly MSCs expressed similar specific cell surface markers, although WJ MSCs differentiated to a lower extent into cells of mesodermal lineage. This indicates that WJ MSCs, like BM MSCs, can contribute in many ways to studies of mesenchymal cell biology, and being easy to harvest and obtain in high numbers they can be used in clinical applications, such as cell therapy and tissue engineering. Critical transitions in MSC differentiation are controlled by signaling pathways and transcriptional regulation. Attention was focused on determining the expression of transcription factors that are most likely to play an important role in development and survival of cardiac lineages. The results implied the differentiation potential of both BM and WJ derived MSCs to cardiomyocytes. RT-PCR results demonstrated that MSCs from both sources show cardiomyogenic properties by expressing specific transcription factors and proteins spontaneously, before any chemical induction. The expression of transcription factors Nkx2.5 and Tbx5 (they are considered to have a role in cardiac differentiation) by human BM and WJ MSCs in an undifferentiated state suggests that MSCs may be directed to cardiac lineage by providing the appropriate conditions.

The outcomes of this study represent an important step towards obtaining a thick autologous myocardial patch, with structure similar to native tissue and capability to grow, for ventricular restoration after a myocardial illness.

CHAPTER 5

FUTURE PROSPECTS

A 3D tissue engineered myocardial construct with cell organization similar to that of the native tissue was developed in this study. As a short term improvement there is still a need to differentiate the WJ MSCs in the structure to cardiomyocytes, either by implanting the construct to the patient in the site of myocardial infarction or in vitro via chemical induction. If in vitro differentiation can be achieved through growth factor use, these growth factors can be incorporated within or among the microfibers so that cardiomyogenic differentiation continues in vivo, too, to enrich the cardiomyocyte population at the infarct site. There is also a need to establish cell-to-cell interaction between the cell layers to achieve a syncytium, and this could be through promoting cell growth and using a gel-like material between the cell layers to keep them closer and in contact.

Permeable elastic tubings were obtained with a very simple method that can be applied to other types of 3D scaffolds, too, to ensure viability in 3D. If an endothelial cell layer is established within the tubing wall in vitro, the macroporous tubings can even serve as a real macro-vasculature in vivo, where they can be stitched to coronary arteries.

As a midterm goal, in vivo experiments in an animal model are planned to determine the feasibility of using the developed patch for restoration of ventricular function and for myocardial regeneration. The mechanism of function improvement, either cell differentiation or paracrine signaling, will be investigated. Integrity loss time of the polymer fibers and their affect on cell coupling will be determined. The patch will be optimized in accordance with the in vivo results.

Thinking of a long term development, a ventricle like tissue engineered myocardium can be obtained by incorporating the aligned cardiomyocyte sheets between two polymer pouches with macroporous tubings in between to feed the cells via growth medium perfusion. Micro and nanotechnology can be employed to get a multitype cell organization similar to native tissue. This ventricular chamber may then take the place of a deteriorating left ventricle and restore the normal heart function.

REFERENCES

Akhyari P, Fedak PW, Weisel RD, Lee TY, Verma S, Mickle DA, Li RK: Mechanical stretch regimen enhances the formation of bioengineered autologous cardiac muscle grafts. *Circulation* 2002; 106: I137-I142.

Akins RE. Can tissue engineering mend broken hearts? *Circ Res* 2002; 90: 120–2.

American Heart Association, <http://www.americanheart.org>, last access date: 02.12.08

Angelini P, Markwald RR. Stem Cell Treatment of the Heart. *Tex Heart Inst J* 2005; 32: 479-88.

Armstrong MT, Lee DY, and Armstrong PB. Regulation of proliferation of the fetal myocardium. *Dev Dyn* 2000; 219: 226–36.

Baksh D, Yao R, Tuan RS. Comparison of proliferative and multilineage differentiation potential of human mesenchymal stem cells derived from umbilical cord and bone marrow. *Stem Cells* 2007; 25: 1384 –92.

Balsam LB, Wagers AJ, Christensen JL, Kofidis T, Weissman IL, Robbins RC. Haematopoietic stem cells adopt mature haematopoietic fates in ischaemic myocardium. *Nature* 2004; 428: 668-73.

Barros D'Sa AA, Berger K, Di Benedetto G, Parenzan L, Rittenhouse EA, Mansfield PB, Smith JC, Davis CC, Hall DG, Wood SJ, Sauvage LR. A healable filamentous Dacron surgical fabric. Experimental studies and clinical experience. *Ann Surg* 1980; 192: 645–57.

Bayes-Genis A, Roura S, Soler-Botija C, Farre J, Hove-Madsen L, Llach A, Cinca J. Identification of cardiomyogenic lineage markers in untreated human bone marrow-derived mesenchymal stem cells. *Transplant Proc* 2005; 37: 4077-9.

Bieback K, Kern S, Kluter H, Eichler H. Critical parameters for the isolation of mesenchymal stem cells from umbilical cord blood. *Stem Cells* 2004; 22: 625-34.

Black BL, Olson EN. Transcriptional control of muscle development by myocyte enhancer factor-2 (MEF2) proteins. *Annu Rev Cell Dev Biol* 1998; 14: 167–96.

Blume ED, Naftel DC, Bastardi HJ, et al. Outcomes of children bridged to heart transplantation with ventricular assist devices: a multi-institutional study. *Circulation* 2006; 113: 2313–9.

Boland ED, Wnek GE, Simpson DG, Pawlowski KJ, Bowlin GL. Tailoring tissue engineering scaffolds using electrostatic processing techniques: a study of poly(glycolic acid) electrospinning. *J Macromol Sci Pure Appl Chem* 2001; 38(12): 1231–43.

Bour BA, O'Brien MA, Lockwood WL, Goldstein ES, Bodmer R, Taghert PH, Abmayr SM, Nguyen HT. Drosophila MEF2, a transcription factor that is essential for myogenesis. *Genes Dev* 1995; 9: 730–41.

Brewer AC, Alexandrovich A, Mjaatvedt CH, Shah AM, Patient RK, Pizzey JA. GATA Factors Lie Upstream of Nkx 2.5 in the Transcriptional Regulatory Cascade That Effects Cardiogenesis. *Stem Cells Dev* 2005; 14: 425–439.

Bruneau BG, Logan M, Davis N, Levi T, Tabin CJ, Seidman JG, Seidman CE. Chamber-specific cardiac expression of Tbx5 and heart defects in Holt-Oram syndrome. *Dev Biol* 1999; 211: 100-8.

Bruneau BG, Bao ZZ, Tanaka M, Schott JJ, Izumo S, Cepko CL, Seidman JG, Seidman CE. Cardiac expression of the ventricle-specific homeobox gene *Irx4* is modulated by Nkx2-5 and dHand. *Dev Biol* 2000; 217: 266-77.

Bruneau BG, Nemer G, Schmitt JP, Charron F, Robitaille L, Caron S, Conner D, Gessler M, Nemer M, Seidman CE, Seidman JG. A murine model of Holt-Oram syndrome defines roles of the T-box transcription factor Tbx5 in cardiogenesis and disease. *Cell* 2001; 106: 709-21.

Bruneau BG. Transcriptional Regulation of Vertebrate Cardiac Morphogenesis. *Circ Res* 2002; 90: 509-519.

Buchberger A and Arnold HH. The MADS domain containing transcription factor cMef2a is expressed in heart and skeletal muscle during embryonic chick development. *Dev Genes Evol* 1999; 209: 376-81.

Burlingham WJ, Jankowska-Gan E, VanBuskirk A, Orosz CG, Lee JH, Kusaka S. Loss of tolerance to a maternal kidney transplant is selective for HLA class II: evidence from trans-vivo DTH and alloantibody analysis. *Hum Immunol.* 2000; 61: 1395-402.

Bursac N, Papdaki M, Cohen RJ, Schoen FJ, Eisenberg SR, Carrier R, Vunjak-Novakovic G, and Freed LE. Cardiac muscle tissue engineering: toward an in vitro model for electrophysiological studies. *Am J Physiol Heart Circ Physiol* 1999; 277: H433-H444.

Carrier R, Papdaki M, Rupnick M, Schoen FJ, Bursac N, Langer R, Freed LE, and Vunjak-Novakovic G. Cardiac tissue engineering: cell seeding, cultivation parameters, and tissue construct characterization. *Biotechnol Bioeng* 1999; 64: 580–589.

Carrier RL, Rupnick M, Langer R, Schoen FJ, Freed LE, Vunjak-Novakovic G. Effects of oxygen on engineered cardiac muscle. *Biotechnol Bioeng* 2002; 78(6): 617–25.

Charron F and Nemer M. GATA transcription factors and cardiac development. *Semin Cell Dev Biol* 1999; 10: 85–91.

Chen J, Altman GH, Karageorgiou V, Horan R, Collette A, Volloch V, Colabro T, Kaplan DL. Human bone marrow stromal cell and ligament fibroblast responses on RGD-modified silk fibers. *J Biomed Mater Res* 2003; 67: 559–70.

Cooper DS, Jacobs JP, Moore L, Stock A, Gaynor JW, Chancy T, Parpard M, Griffin, DA, Owens T, Checchia PA, Thiagarajan RR, Spray TL, Ravishankar C. Cardiac extracorporeal life support: state of the art in 2007. *Cardiol Young* 2007; 17(Suppl. 2): 104–15.

Crawford FA Jr, Sade RM, Spinale F. Bovine pericardium for correction of congenital heart defects. *Ann Thorac Surg* 1986; 41: 602–5.

Cukierman E, Pankov R, Stevens DR, and Yamada KM. Taking cell-matrix adhesions to the third dimension. *Science* 2001; 294: 1708–12.

Dar A, Shachar M, Leor J, Cohen S: Optimization of cardiac cell seeding and distribution in 3D porous alginate scaffolds. *Biotechnol Bioeng* 2002; 80: 305–12.

David TE and Armstrong S. Surgical repair of postinfarction ventricular septal defect by infarct exclusion. *Semin Thorac Cardiovasc Surg*. 1998; 10(2): 105–10.

Dengler TJ and Katus HA. Stem cell therapy for the infarcted heart ('cellular cardiomyoplasty'). *Herz* 2002; 27: 598-610.

Denker HW. Potentiality of embryonic stem cells: an ethical problem even with alternative stem cell sources. *J Med Ethics* 2006; 32: 665-71.

Di Eusanio M and Schepens MA. Left atrial thrombus on a Teflon patch for ASD closure. *Eur J Cardiothorac Surg* 2002; 21: 542.

Dor V, Sabatier M, Montiglio F, Civaia F, DiDonato M. Endoventricular patch reconstruction of ischemic failing ventricle. a single center with 20 years experience. advantages of magnetic resonance imaging assessment. *Heart Fail Rev* 2004; 9(4): 269–86.

Duncan BW. Pediatric mechanical circulatory support in the United States: past, present, and future. *ASAIO J* 2006; 52: 525–9.

Durocher D and Nemer M. Combinatorial interactions regulating cardiac transcription. *Dev Genet*. 1998; 22: 250–62.

Endo S, Saito N, Misawa Y, Sohara Y. Late pericarditis secondary to pericardial patch implantation 25 years prior. *Eur J Cardiothorac Surg* 2001; 20: 1059–60.

Engelmayr GC Jr, Cheng M, Bettinger CJ, Borenstein JT, Langer R, Freed LE. Accordion-like honeycombs for tissue engineering of cardiac anisotropy. *Nat Mater* 2008; 7(12): 1003-10.

Evans HJ, Sweet JK, Price RL, Yost M, Goodwin RL. Novel 3D culture system for study of cardiac myocyte development. *AJP-Heart Circ Physiol* 2003; 285: 570-8.

Fang X and Reneker DH. DNA fibers by electrospinning. *J Macromol Sci Phys* 1997; B36(2): 169–73.

Fedak PWM, Weisel RD, Verma S, Mickle DAG, Li R-K. Restoration and Regeneration of Failing Myocardium with Cell Transplantation and Tissue Engineering. *Seminars in Thoracic and Cardiovascular Surgery* 2003; 15(3): 277-286.

Ferrero Jr JM. *Wiley Encyclopedia of Biomedical Engineering*: John Wiley & Sons Inc, 2006.

Foley A and Mercola M. Heart Induction: Embryology to Cardiomyocyte Regeneration. *Trends Cardiovasc Med* 2004; 14: 121–5.

Forrester JS, Price MJ, Makkar RR: Stem cell repair of infarcted myocardium: an overview for clinicians. *Circulation* 2003; 108: 1139-45.

Fossett N and Schulz RA. Conserved cardiogenic functions of the multitype zinc-finger proteins: U-shaped and FOG-2. *Trends Cardiovasc Med* 2001; 11: 185–90.

Giraud MN, Armbruster C, Carrel T, Tevæearai HT. Current state of the art in myocardial tissue engineering. *Tissue Eng* 2007; 13(8): 1825-36.

Hakuno D, Fukuda K, Makino S, Konishi F, Tomita Y, Manabe T, Suzuki Y, Umezawa A, Ogawa S. Bone marrow-derived regenerated cardiomyocytes (CMG Cells) express functional adrenergic and muscarinic receptors. *Circulation* 2002; 105(3): 380-6.

Harding SE, Ali NN, Martins M, Gorelik J. The human embryonic stem cell-derived cardiomyocyte as a pharmacological model. *J Pharm Ther* 2007; 113: 341–53.

Harken DE. Heart valves: ten commandments and still counting. *Ann Thorac Surg* 1989; 48(3 Suppl): S18-9.

Hatcher CJ, Goldstein MM, Mah CS, Delia CS, Basson CT. Identification and localization of TBX5 transcription factor during human cardiac morphogenesis. *Dev Dyn* 2000; 219: 90–5.

He JQ, Ma Y, Lee Y, Thomson JA, Kamp TJ. Human embryonic stem cells develop into multiple types of cardiac myocytes: action potential characterization. *Circ Res*. 2003; 93(1): 32-9.

Heikinheimo M, Scandrett JM, Wilson DB. Localisation of transcription factor GATA-4 to regions of the mouse embryo involved in cardiac development. *Dev Biol* 1994; 164: 361-73.

Hiroi Y, Kudoh S, Monzen K, Ikeda Y, Yazaki Y, Nagai R, Komuro I. Tbx5 associates with Nkx2–5 and synergistically promotes cardiomyocyte differentiation. *Nat Genet* 2001; 28: 276–80.

Hoerstrup SP, Sodian R, Daebritz S, Wang J, Bacha EA, Martin DP, Moran AM, Guleserian KJ, Sperling JS, Kaushal S, Vacanti JP, Schoen FJ, Mayer JEt Jr. Functional Living Trileaflet Heart Valves Grown In Vitro. *Circulation* 2000; 102[suppl III]: III-44-49.

Hoerstrup SP, Kadner A, Breymann C, Maurus CF, Guenter CI, Sodian R, Visjager JF, Zund G, Turina MI. Living, autologous pulmonary artery conduits tissue engineered from human umbilical cord cells. *Ann Thorac Surg* 2002; 74: 46–52.

Holland SJ, Yasin M, Tighe B. Polymers for biodegradable medical devices VII. Hydroxy butyrate–hydroxyvalerate copolymers: degradation of copolymers and their blends with polysaccharides under in vitro physiological conditions. *Biomaterials* 1990; 11: 206–15.

Huang L, Apkarian RP, Chaikof EL. High-resolution analysis of engineered type I collagen nanofibers by electron microscopy. *Scanning* 2001; 23(6): 372–5.

Hubbell JA. Materials as morphogenetic guides in tissue engineering. *Curr Opin Biotechnol* 2003; 14(5): 551–8.

Ishii O, Shin M, Sueda T, Vacanti JP. In vitro tissue engineering of a cardiac graft using a degradable scaffold with an extracellular matrix-like topography. *J Thorac Cardiovasc Surg* 2005; 130(5): 1358-63.

Jamali M, Rogerson PJ, Wilton S, Skerjanc IS. Nkx2–5 Activity Is Essential for Cardiomyogenesis. *J Biol Chem* 2001; 276(45): 42252–8.

Jawad H, Ali NN, Lyon AR, Chen QZ, Harding SE, Boccaccini AR. Myocardial tissue engineering: a review. *J Tissue Eng Regen Med* 2007 Sep-Oct;1(5):327-42.

Jawad H, Lyon AR, Harding SE, Ali NN, Boccaccini AR. Myocardial tissue engineering. *Br Med Bull* 2008; 87: 31-47.

Jia H, Zhu G, Vugrinovich B, Kataphinan W, Reneker DH, Wang P. Enzyme-carrying polymeric nanofibers prepared via electrospinning for use as unique biocatalysts. *Biotechnol Prog* 2002; 18(5): 1027–32.

Karahuseyinoglu S, Cinar O, Kilic E, Kara F, Gumus Akay G, Özel Demiralp D, Tukun A, Uckan D, Can A. Biology of Stem Cells in Human Umbilical Cord Stroma: In Situ and In Vitro Surveys. *Stem Cells* 2007; 25: 319-31.

Karamboulas C, Swedani A, Ward C, Al-Madhoun AS, Wilton S, Boisvenue S, Ridgeway AG and Skerjanc IS. HDAC activity regulates entry of mesoderm cells into the cardiac muscle lineage. *J Cell Sci* 2006; 119 (20): 4305-14.

Kasahara H, Wakimoto H, Liu M, Maguire CT, Converso KL, Shioi T, Huang W-Y, Manning WJ, Paul D, Lawitts J, Berul CI, Izumo S. Progressive atrioventricular conduction defects and heart failure in mice overexpressing a mutant Csx/Nkx2.5 homeoprotein. *J Clin Invest.* 2001; 108: 189–201.

Kassiri Z, Khokha R. Myocardial extra-cellular matrix and its regulation by metalloproteinases and their inhibitors. *Thromb Haemost* 2005; 93: 212-9.

Kehat I, Kenyagin-Karsenti D, Snir M, Segev H, Amit M, Gepstein A, Livne E, Binah O, Itskovitz-Eldor J, Gepstein L. Human embryonic stem cells can differentiate into myocytes with structural and functional properties of cardiomyocytes. *J Clin Invest* 2001; 108: 407–14.

Kehat I, Gepstein A, Spira A, Itskovitz-Eldor J, Gepstein L. High-resolution electrophysiological assessment of human embryonic stem cell-derived cardiomyocytes: a novel in vitro model for the study of conduction. *Circ Res* 2002; 91: 659–61.

Kehat I, Khimovich L, et al. Electromechanical integration of cardiomyocytes derived from human embryonic stem cells. *Nat Biotech* 2004; 22: 1282–9.

Khil MS, Cha DI, Kim HY, Kim IS, Bhattarai N. Electrospun nanofibrous polyurethane membrane as wound dressing. *J Biomed Mater Res* 2003; 67B(2): 675–9.

Kikuchi A, Kobayashi E, and Okano T. Polysurgery of cell sheet grafts overcomes diffusion limits to produce thick, vascularized myocardial tissues. *FASEB J*. 2006; 20(6): 708-10.

Kim B-S., Mooney D.J. Development of biocompatible synthetic extracellular matrices for tissue engineering. *TIBTECH* 1998; 16: 224-30.

Kim J, Reneker DH. Mechanical properties of composites using ultrafine electrospun fibers. *Polym Composites* 1999; 20: 124–31.

Kim K, Yu M, Zong X, Chiu J, Fang D, Seo YS, et al. Control of degradation rate and hydrophilicity in electrospun non-woven poly(D,L-lactide) nanofiber scaffolds for biomedical applications. *Biomaterials* 2003; 24(27): 4977–85.

Kloner RA and Jennings RB. Consequences of Brief Ischemia: Stunning, Preconditioning, and Their Clinical Implications: Part 1. *Circulation* 2001; 104: 2981-9.

Klouda L, Vaz CM, Mol A, Baaijens FPT, Bouten CVC. Effect of biomimetic conditions on mechanical and structural integrity of PGA/P4HB and electrospun PCL scaffolds *J Mater Sci: Mater Med* 2008; 19: 1137–44.

Kofidis T, Akhyari P, Wachsmann B, Boublik J, Mueller-Stahl K, Leyh R, Fischer S, Haverich A. A novel bioartificial myocardial tissue and its prospective use in cardiac surgery. *Eur J Cardiothorac Surg* 2002; 22(2): 238-43.

Kofidis T, Akhyari P, Boublik J, Theodorou P, Martin U, Ruhparwar A, Fischer S, Eschenhagen T, Kubis HP, Kraft T et al. In vitro engineering of heart muscle: artificial myocardial tissue. *J Thorac Cardiovasc Surg* 2002, 124: 63-9.

Kofidis T, Lenz A, Boublik J, Akhyari P, Wachsmann B, Stahl KM, Haverich A, Leyh RG. Bioartificial grafts for transmural myocardial restoration: a new cardiovascular tissue culture concept. *Eur J Cardiothorac Surg* 2003, 24: 906-11.

Kofidis T, Lenz A, Boublik J, Akhyari P, Wachsmann B, Mueller-Stahl K, Hofmann M, Haverich A. Pulsatile perfusion and cardiomyocyte viability in a solid threedimensional matrix. *Biomaterials* 2003; 24: 5009-14.

Kofidis T, Lee CN. From vision to mission in myocardial restoration. *Asian Cardiovasc Thorac Ann* 2008; 16(2): 91-2.

Laflamme MA, Gold J, et al. Formation of human myocardium in the rat heart from human embryonic stem cells. *AJP* 2005; 167: 663–71.

Leor J, Aboulafia-Etzion S, Dar A, Shapiro L, Barbash IM, Battler A, Granot Y, Cohen S: Bioengineered cardiac grafts: a new approach to repair the infarcted myocardium? *Circulation* 2000, 102: III56-III61.

Leor J, Gerecht-Nir S, et al. Undifferentiated human embryonic stem cells are not guided to form new myocardium by transplantation into normal and infarcted heart. *J Am Coll Cardiol* 2005; 45: 151A–151A.

Leor J, Rozen L, Zuloff-Shani A, Feinberg MS, Amsalem Y, Barbash IM, Kachel E, Holbova R, Mardor Y, Daniels D, Ocherashvili A, Orenstein A, Danon D. Ex vivo activated human macrophages improve healing, remodeling, and function of the infarcted heart. *Circulation* 2006; 114(1 Suppl): I94-100.

Li WJ, Laurencin CT, Catterson EJ, Tuan RS, Ko FK. Electrospun nanofibrous structure: a novel scaffold for tissue engineering. *J Biomed Mater Res* 2002; 60(4): 613–21.

Liberatore CM, Searcy-Schrick RD, Yutzey KE. Ventricular expression of *tbx5* inhibits normal heart chamber development. *Dev Biol* 2000; 223: 169–80.

Lin Q, Schwarz J, Bucana C, Olson EN. Control of mouse cardiac morphogenesis and myogenesis by transcription factor MEF2C. *Science* 1997; 276: 1404–7.

Lu LL, Liu YJ, Yang SG et al. Isolation and characterization of human umbilical cord mesenchymal stem cells with hematopoiesis-supportive function and other potentials. *Haematologica* 2006; 91: 1017–26.

Lyons I, Parsons LM, Hartley L, Li R, Andrews JE, Robb L, Harvey RP. Myogenic and morphogenetic defects in the heart tubes of murine embryos lacking the homeo box gene *Nkx2-5*. *Genes Dev* 1995; 9: 1654–66.

Makino S, Fukuda K, Miyoshi S et al. Cardiomyocytes can be generated from marrow stromal cells in vitro. *J Clin Invest* 1999, 103: 697–705.

Martin-Rendon E, Sweeney D, Lu F, Girdlestone J, Navarrete C, Watt SM. 5-Azacytidine-treated human mesenchymal stem/progenitor cells derived from umbilical cord, cord blood and bone marrow do not generate cardiomyocytes *in vitro* at high frequencies. *Vox Sanguinis* 2008; 95: 137–48.

Matthews JA, Wnek GE, Simpson DG, Bowlin GL. Electrospinning of collagen nanofibers. *Biomacromolecules* 2002; 3(2): 232–8.

Mauney JR, Volloch V, Kaplan DL. Matrix-mediated retention of adipogenic differentiation potential by human adult bone marrow-derived mesenchymal stem cells during ex vivo expansion. *Biomaterials* 2005; 26: 6167-75.

McDevitt TC, Woodhouse KA, Hauschka SD, Murry CE, Stayton PS Spatially organized layers of cardiomyocytes on biodegradable polyurethane films for myocardial repair. *J Biomed Mater Res A* 2003; 66(3): 586-95.

Menasche P. Myoblast-based cell transplantation. *Heart Fail Rev* 2003; 8: 221-227.

Min BM, Lee G, Kim SH, Nam YS, Lee TS, Park WH. Electrospinning of silk fibroin nanofibers and its effect on the adhesion and spreading of normal human keratinocytes and fibroblasts in vitro. *Biomaterials* 2004; 25(7-8): 1289–97.

Mirensky TL and Breuer CK. The Development of Tissue-Engineered Grafts for Reconstructive Cardiothoracic Surgical Applications. *Pediatr Res* 2008; 63 (5): 559-68.

Mohri H, Barnes RW, Rittenhouse EA, Reichenback DD, Dillard DH, Merendino KA. Fate of autologous pericardium and Dacron fabric used as substitutes for total atrial septum in growing animals. *J Thorac Cardiovasc Surg* 1970; 59: 501–11.

Morin S, Charron F, Robitaille L, Nemer M. GATA-dependent recruitment of MEF2 proteins to target promoters. *EMBO J* 2000; 19: 2046–55.

Mummery C. Cardiomyocyte differentiation of mouse and human embryonic stem cells. *J Anat* 2002; 200: 233–42.

Mummery C, Ward-van Oostwaard D, Doevendans P, Spijker R, van den Brink S, Hassink R, van der Heyden M, Opthof T, Pera M, de la Riviere AB, Passier R, Tertoolen L. Differentiation of human embryonic stem cells to cardiomyocytes: role of coculture with visceral endoderm-like cells. *Circulation* 2003; 107: 2733–40.

Murry CE, Soonpaa MH, Reinecke H, Nakajima H, Nakajima HO, Rubart M, Pasumarthi KB, Virag JJ, Bartelmez SH, Poppa V et al. Haematopoietic stem cells do not transdifferentiate into cardiac myocytes in myocardial infarcts. *Nature* 2004; 428: 664–8.

Nakamura T, Schneider MD. The way to a human's heart is through the stomach: visceral endoderm-like cells drive human embryonic stem cells to a cardiac fate. *Circulation* 2003; 107: 2638–9.

National Heart Lung and Blood Institute, <http://www.nhlbi.nih.gov>, last access date: 04.12.08

National Heart Lung and Blood Institute, Diseases and Conditions Index, Congenital Heart Defects, http://www.nhlbi.nih.gov/health/dci/Diseases/chd/chd_all.html, last access date: 04.12.08

National Heart Lung and Blood Institute, Diseases and Conditions Index, Heart Attack, http://www.nhlbi.nih.gov/health/dci/Diseases/HeartAttack/HeartAttack_WhatIs.html, last access date: 04.12.08

Orlic D, Kajstura J, Chimenti S, Jakoniuk I, Anderson SM, Li B, Pickel J, McKay R, Nadal-Ginard B, Bodine DM et al.: Bone marrow cells regenerate infarcted myocardium. *Nature* 2001; 410:701-5.

Ozawa T, Mickle DA, Weisel RD, Koyama N, Ozawa S, Li RK: Optimal biomaterial for creation of autologous cardiac grafts. *Circulation* 2002, 106: I176-I182.

Park H, Radisic M, Lim JO, Chang BH, Vunjak-Novakovic G. A novel composite scaffold for cardiac tissue engineering. *In Vitro Cell Dev Biol Anim* 2005; 41(7): 188-96.

Parker KK and Ingber DE. Extracellular matrix, mechanotransduction and structural hierarchies in heart tissue engineering. *Phil Trans R Soc B* 2007; 362: 1267–79.

Passier R and Mummery C. Origin and use of embryonic and adult stem cells in differentiation and tissue repair. *Cardiovasc Res* 2003, 58: 324-35.

Passier R, Ward-van Oostwaard D, Snapper J, Kloots J, Hassink RJ, Kuijk E, Roelen B, de la Riviere AB, Mummery C. Increased Cardiomyocyte Differentiation from Human Embryonic Stem Cells in Serum-Free Cultures, *Stem Cells* 2005; 23: 772–80.

Peter S. Pericardial patch for atrial septal defect closure. *Ann Thorac Surg* 1999; 67: 573–4.

Petersen CA and Burleigh BA. Role for Interleukin-1 β in *Trypanosoma cruzi*-Induced Cardiomyocyte Hypertrophy. *Infect Immun* 2003; 71(8):4441-7.

Pham QP, Sharma U, Mikos AG. Electrospinning of Polymeric Nanofibers for Tissue Engineering Applications: A Review. *Tissue Eng* 2006; 12(5): 1197-211.

Pires AC, Saporito WF, Cardoso SH, Ramaciotti O. Bovine pericardium used as a cardiovascular patch. *Heart Surg Forum* 1999; 2: 60–9.

Pittenger MF and Martin BJ. Mesenchymal stem cells and their potential as cardiac therapeutics. *Circ Res* 2004; 95: 9-20.

Planat-Bénard V, Menard C, André M, Puceat M, Perez A, Garcia-Verdugo J-M, Pénicaud L, Casteilla L. Spontaneous Cardiomyocyte Differentiation From Adipose Tissue Stroma Cells. *Circ Res* 2004; 94: 223-9.

Radisic M, Euloth M, Yang L, Langer R, Freed LE, Vunjak-Novakovic G. High density seeding of myocyte cells for tissue engineering. *Biotechnol Bioeng* 2003; 82: 403-14.

Radisic M, Park H, Shing H, Consi T, Schoen FJ, Langer R, Freed LE, Vunjak-Novakovic G. Functional assembly of engineered myocardium by electrical stimulation of cardiac myocytes cultured on scaffolds. *PNAS* 2004; 101(52): 18129–134.

Radisic M, Yang L, Boublik J, Cohen RJ, Langer R, Freed LE, Vunjak-Novakovic G. Medium perfusion enables engineering of compact and contractile cardiac tissue. *Am J Physiol Heart Circ Physiol* 2004; 286(2) H507-16.

Radisic M, Malda J, Epping E, Geng W, Langer R, Vunjak-Novakovic G. Oxygen gradients correlate with cell density and cell viability in engineered cardiac constructs. *Biotechnol Bioeng* 2006; 93(2): 332–43.

Radisic M, Park H, Chen F, Salazar-Lazzaro JE, Wang Y, Dennis R, Langer R, Freed LE, Vunjak-Novakovic G. Biomimetic approach to cardiac tissue engineering: oxygen carriers and channeled scaffolds. *Tissue Eng* 2006; 12(8): 2077-91.

Radisic M, Park H, Martens TP, Salazar-Lazaro JE, Geng W, Wang Y, Langer R, Freed LE, Vunjak-Novakovic G. Pre-treatment of synthetic elastomeric scaffolds by cardiac fibroblasts improves engineered heart tissue. *J Biomed Mater Res A* 2008; 86(3): 713-24.

Rittenhouse EA, Sauvage LR, Stamm SJ, Mansfield PB, Hall DG, Herndon PS. Radical enlargement of the aortic root and outflow tract to allow valve replacement. *Ann Thorac Surg* 1979; 27: 367–73.

Rosenzweig A. Cardiac cell therapy – mixed results from mixed cells. *N Engl J Med* 2006; 355: 1274–7.

Sachinidis A, Kolossov E, Fleischmann BK, Hescheler J. Generation of Cardiomyocytes from Embryonic Stem Cells *Herz* 2002; 27: 589–97.

Sarugaser R, Lickorish D, Baksh D et al. Human umbilical cord perivascular (HUCPV) cells: A source of mesenchymal progenitors. *Stem Cells* 2005; 23: 220-9.

Schachinger V, Erbs S, et al. Intracoronary bone marrow derived progenitor cells in acute myocardial infarction. *N Engl J Med* 2006; 355: 1210–11.

Schmidt D, Mol A, Neuenschwander S, Breymann C, Gössi M, Zund G, Turina M, Hoerstrup SP. Living patches engineered from human umbilical cord derived fibroblasts and endothelial progenitor cells. *Eur J Cardiothorac Surg* 2005; 27(5): 795-800.

Schmidt D, Mol A, Odermatt B, Neuenschwander S, Breymann C, Gössi M, Genoni M, Zund G, Hoerstrup SP. Engineering of biologically active living heart valve leaflets using human umbilical cord-derived progenitor cells. *Tissue Eng* 2006; 12(11): 3223-32.

Sekine H, Shimizu T, Yang J, Kobayashi E, Okano T. Pulsatile Myocardial Tubes Fabricated With Cell Sheet Engineering. *Circulation* 2006; 114[suppl I]: I-87–I-93.

Sekine H, Shimizu T, Hobo K, Sekiya S, Yang J, Yamato M, Kurosawa H, Kobayashi E, Okano T. Endothelial cell coculture within tissue-engineered cardiomyocyte sheets enhances neovascularization and improves cardiac function of ischemic hearts. *Circulation* 2008; 118(14 Suppl): S145-52.

Shim WS, Jiang S, Wong P, Tan J, Chua YL, Tan YS, Sin YK, Lim CH, Chua T, Teh M, Liu TC, Sim E. Ex vivo differentiation of human adult bone marrow stem cells into cardiomyocyte-like cells. *Biochem Biophys Res Commun* 2004; 324: 481-8.

Shimizu T, Yamato M, Akutsu T, Shibata T, Isoi Y, Kikuchi A, Umezumi M, Okano T: Electrically communicating three dimensional cardiac tissue mimic fabricated by layered cultured cardiomyocyte sheets. *J Biomed Mater Res* 2002, 60: 110-17.

Shimizu T, Yamato M, Isoi Y, Akutsu T, Setomaru T, Abe K, Kikuchi A, Umezumi M, Okano T. Fabrication of pulsatile cardiac tissue grafts using a novel 3-dimensional cell sheet manipulation technique and temperature-responsive cell culture surfaces. *Circ Res* 2002; 90(3): e40-e48.

Shimizu T, Yamato M, Kikuchi A, Okano T. Cell sheet engineering for myocardial tissue reconstruction. *Biomaterials* 2003; 24: 2309-16.

Shimizu T, Sekine H, Isoi Y, Yamato M, Kikuchi A, Okano T. Long-Term Survival and Growth of Pulsatile Myocardial Tissue Grafts Engineered by the Layering of Cardiomyocyte Sheets. *Tissue Eng* 2006; 12(3): 499-507.

Shrivastava S and Radhakrishnan S. Infective endocarditis following patch closure of ventricular septal defect: a cross-sectional Doppler echocardiographic study. *Int J Cardiol* 1989; 25: 27–32.

Skerjanc IS, Petropoulos H, Ridgeway AG, Wilton S. Myocyte enhancer factor 2C and Nkx2-5 up-regulate each other's expression and initiate cardiomyogenesis in P19 cells. *J Biol Chem* 1998; 273(52): 34904–10.

Smit TH, Thomas KA, Hoogendoorn RJ, Strijkers GJ, Helder MN, Wuisman PI. Sterilization and strength of 70/30 polylactide cages: e-beam versus ethylene oxide. *Spine* 2007; 32(7): 742-7.

Sodian R, Hoerstrup SP, Sperling JS, Martin DP, Daebritz S, Mayer JE Jr, Vacanti JP. Evaluation of biodegradable, three-dimensional matrices for tissue engineering of heart valves. *ASAIO J* 2000; 46(1): 107-10.

Solloway MJ and Harvey RP. Molecular pathways in myocardial development: a stem cell perspective. *Cardiovasc Res* 2003; 58: 264–77.

Sutton MGSJ and Sharpe N. Left Ventricular Remodeling After Myocardial Infarction : Pathophysiology and Therapy. *Circulation* 2000; 101: 2981-8.

Svensson EC, Huggins GS, Lin H, Clendenin C, Jiang F, Tufts R, Dardik FB, Leiden JM. A syndrome of tricuspid atresia in mice with a targeted mutation of the gene encoding Fog-2. *Nat Genet* 2000; 25: 353–6.

Tanaka M, Chen Z, Bartunkova M, Yamazaki N, Izumo S. The cardiac homeobox gene *Csx/Nkx2.5* lies genetically upstream of multiple genes essential for heart development. *Development* 1999; 126: 1269–80.

Tevosian SG, Deconinck AE, Tanaka M, Schinke M, Litovsky SH, Izumo S, Fujiwara Y, Orkin SH. FOG-2, a cofactor for GATA transcription factors, is essential for heart morphogenesis and development of coronary vessels from epicardium. *Cell* 2000; 101: 729–39.

Tribak M, Marmade L, El Kouache M, El Moktadir K, Abdallah H, Maghraoui SA, Baghdadi K, Laaroussi M, Moughil S, Bensouda A, Benomar M. Results of the surgical closure of ventricular septal defects of various ages: report of 30 cases. *Ann Cardiol Angeiol (Paris)* 2008; 57(1): 48-51.

Uemura R, Xu M, Ahmad N, Ashraf M. Bone marrow stem cells prevent left ventricular remodeling of ischemic heart through paracrine signaling. *Circ Res* 2006; 98: 1414-21.

University of Guelph, Developmental Biology Online, Muscle Tissue, <http://www.uoguelph.ca/zoology/devobio/210labs/muscle1.html>, last access date: 05.12.08

Van de Graaff K.M. *Human Anatomy*. Fifth Ed., Weber State University, The McGraw-Hill Companies Inc. 1998

Vander AJ, Sherman JH, Luciano DS. *Human Physiology*. Sixth Edition, McGraw-Hill Inc. 1994

Vunjak-Novakovic G, Radisic M, Obradovic B. Cardiac tissue engineering: effects of bioreactor flow environment on tissue constructs. *J Chem Technol Biotechnol* 2006; 81(4): 485–490.

Vural KM. Ventricular assist device applications. *Anadolu Kardiyol Derg* 2008; 8 (Suppl 2): 117-30.

Wagner W, Wein F, Seckinger A, Frankhauser M, Wirkner U, Krause U, Blake J, Schwager C, Eckstein V, Ansorge W, Ho AD. Comparative characteristics of mesenchymal stem cells from human bone marrow, adipose tissue, and umbilical cord blood. *Exp Hematol* 2005; 33: 1402-16.

Wang HS, Hung SC, Peng ST, Huang CC, Wei HM, Guo YJ, Fu YS, Lai MC, Chen CC. Mesenchymal stem cells in the Wharton's jelly of the human umbilical cord. *Stem Cells* 2004; 22(7): 1330-7.

Wang Y, Ameer GA, Sheppard BJ, Langer R. A tough biodegradable elastomer. *Nat Biotechnol* 2002; 20(6): 602-6.

Weiss ML, Medicetty S, Bledsoe AR, Rachakatla RS, Choi M, Merchav S, Luo Y, Rao MS, Velagaleti G, Troyer D. Human umbilical cord matrix stem cells: preliminary characterization and effect of transplantation in a rodent model of Parkinson's disease. *Stem Cells* 2006; 24: 781-92.

Wu KH, Lu XD, Liu YL. Recent progress of pediatric cardiac surgery in China. *Chin Med J (Engl.)* 2006; 119 (23): 2005–12.

Wu KH, Zhou B, Yu CT, Cui B, Lu SH, Han ZC, Liu YL. Therapeutic potential of human umbilical cord derived stem cells in a rat myocardial infarction model. *Ann Thorac Surg.* 2007 Apr;83(4):1491-8.

Xu CY, Inai R, Kotaki M, Ramakrishna S. Aligned biodegradable nanofibrous structure: a potential scaffold for blood vessel engineering. *Biomaterials* 2004; 25(5): 877–86.

Xu C, Police S, Rao N, Carpenter MK. Characterization and enrichment of cardiomyocytes derived from human embryonic stem cells. *Circ Res*. 2002; 91(6): 501-8.

Xu W, Zhang X, Qian H, Zhu W, Sun X, Hu J, Zhou H, Chen Y. Mesenchymal stem cells from adult human bone marrow differentiate into a cardiomyocyte phenotype in vitro. *Exp Biol Med* 2004; 229: 623-31.

Yang S, Leong KF, Du Z, Chua CK. The design of scaffolds for use in tissue engineering. Part I. Traditional factors. *Tissue Eng*. 2001; 7(6): 679-89.

Yi F, LaVan DA. Poly(glycerol sebacate) Nanofiber Scaffolds by Core/Shell Electrospinning. *Macromol Biosci*. 2008; 8(9): 803-6.

Young HE, Steele TA, Bray RA, Hudson J, Floyd JA, Hawkins K, Thomas K, Austin T, Edwards C, Cuzzourt J, Duenzl M, Lucas PA, and Black AC. Human Reserve Pluripotent Mesenchymal Stem Cells Are Present in the Connective Tissues of Skeletal Muscle and Dermis Derived From Fetal, Adult, and Geriatric Donors. *Anat Rec* 2001; 264: 51–62.

Yu QJ, Si R, Zhou N, Zhang HF, Guo WY, Wang HC, Gao F. Insulin inhibits beta-adrenergic action in ischemic/reperfused heart: a novel mechanism of insulin in cardioprotection. *Apoptosis* 2008; 13(2): 305-17.

Zammaretti P and Jaconi M. Cardiac tissue engineering: regeneration of the wounded heart. *Curr Opin Biotechnol* 2004; 15: 430–34.

Zimmermann WH, Schneiderbanger K, Schubert P, Didie M, Munzel F, Heubach JF, Kostin S, Neuhuber WL, Eschenhagen T: Tissue engineering of a differentiated cardiac muscle construct. *Circ Res* 2002; 90: 223-30.

Zimmermann WH, Eschenhagen T. Cardiac tissue engineering for replacement therapy. *Heart Fail Rev* 2003; 8: 259-69.

Zimmermann WH, Melnychenko I, Eschenhagen T: Engineered heart tissue for regeneration of diseased hearts. *Biomaterials* 2004; 25: 1639-47.

Zimmermann WH, Didie M, Döker S, Melnychenko I, Naito H, Rogge C, Tiburcy M, Eschenhagen T. Heart muscle engineering: an update on cardiac muscle replacement therapy. *Cardiovasc Res* 2006; 71(3): 419-29.

Zong X, Bien H, Chung C-Y, Yin L, Fang D, Hsiao BS, Chu B, Entcheva E. Electrospun fine-textured scaffolds for heart tissue constructs. *Biomaterials* 2005; 26: 5330–38.

Zong XH, Ran SF, Fang DF, Hsiao BS, Chu B. Control of structure, morphology and property in electrospun poly(glycolide- co-lactide) non-woven membranes via post-draw treatments. *Polymer* 2003; 44(17): 4959–67.

Zong XH, Li S, Chen E, Garlick B, Kim KS, Fang DF, et al. Prevention of postsurgery-induced abdominal adhesions by electrospun bioabsorbable nanofibrous poly(lactide-co-glycolide)- based membranes. *Ann Surg* 2004; 240(5): 910–5.

Zund G, Breuer CK, Shinoka T, Ma PX, Langer R, Mayer JE, Vacanti JP: The in vitro construction of a tissue engineered bioprosthetic heart valve. *Eur J Cardiothorac Surg* 1997; 11: 493-497.

APPENDIX A

MATERNAL CONSENT

MATERNAL CONSENT

I am willing to consent to:

1. The collection and storage of umbilical cord after delivery of my baby.
2. Use the umbilical cord for research projects at Middle East Technical University, Department of Biological Sciences, Biotechnology Research Unit.

Mother's Name: Albana Ndreu

Mother's Signature:



Witness Name: Deniz Yücel

Witness Signature:



Date: 04 / 01 / 2007

APPENDIX B

GPC DISTRIBUTION PLOTS

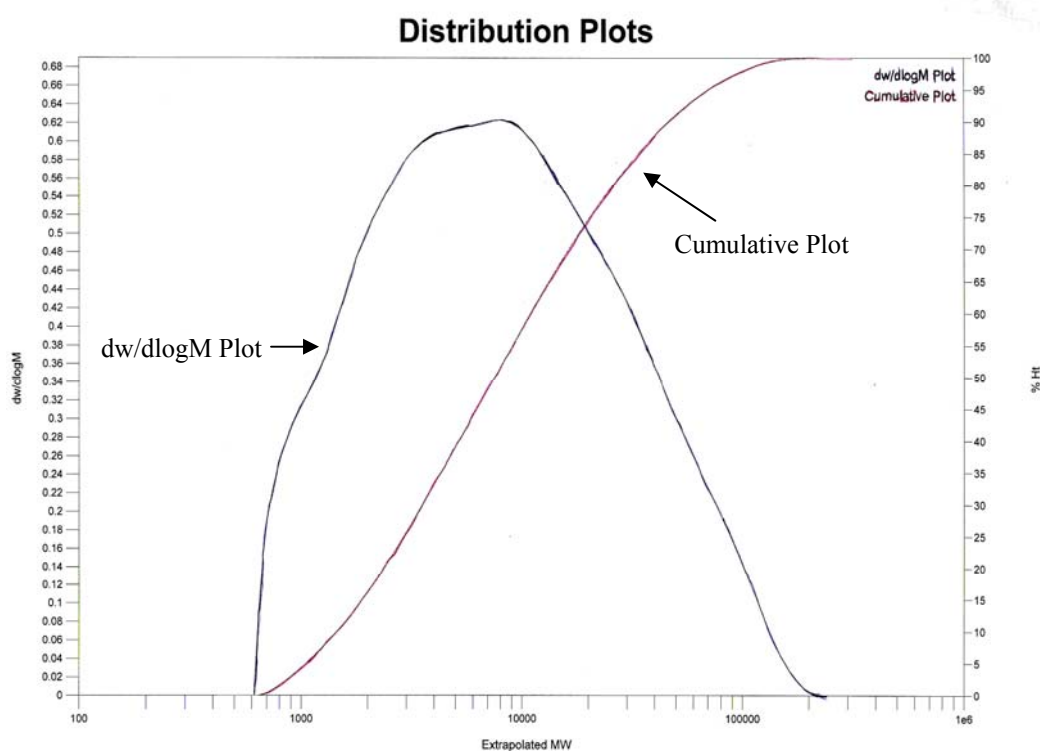


Figure B.1 GPC molecular weight distribution plot of PGS prepolymer polymerized under vacuum for 24h (1st run). (Mw: 16 727 Da).

APPENDIX C

FIBER DIAMETERS OF THE MICROFIBROUS MATS

Table C 1 Fiber diameters of microfibrinous mats obtained by electrospinning from PHBV-P(L-D,L)LA:PGS polymer blends.

PGS content & solvent composition	Fiber diameter (μm)
PGS1%, Chl:DMF 95:5	1.34 ± 0.09
PGS2%, Chl:DMF 95:5	1.25 ± 0.10
PGS4%, Chl:DMF 95:5	1.37 ± 0.08
PGS1%, Chl:DMF 10:1	1.16 ± 0.13
PGS2%, Chl:DMF 10:1	1.16 ± 0.07
PGS4%, Chl:DMF 10:1	1.27 ± 0.10

Chl: Chloroform, DMF: N,N-dimethylformamide

APPENDIX D

LOAD- EXTENSION CURVE

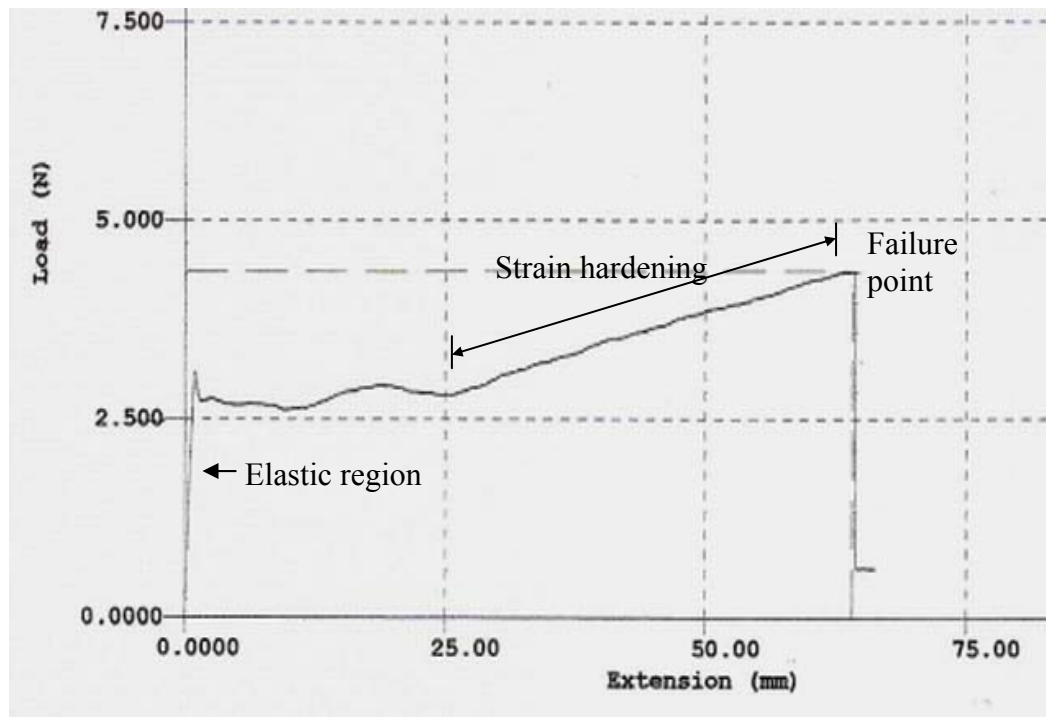


Figure D.1 Load-Extension Curve of a nonporous P(L-D,L)LA-PGS (96:4) tubing, with designations for elastic region, strain hardening and failure point.

APPENDIX E

WJ MSC PROLIFERATION ON ALIGNED FIBER MATS

Table E.1 hWJ MSC numbers on aligned fiber mats after 1 and 14 days of culture.

Sample Type	1-day cell number	14-days cell number
PHBV-P(L-D,L)LA	5333 \pm 3161	99519 \pm 20479
Coll PHBV-P(L-D,L)LA	14141 \pm 1877	28442 \pm 4487
PHBV-P(L-D,L)LA:PGS 98:2	6115 \pm 2103	143000 \pm 3067
Coll PHBV-P(L-D,L)LA:PGS 98:2	9410 \pm 1207	115154 \pm 5874
Tissue Culture Polystyrene	18813 \pm 815	111599 \pm 2496

CURRICULUM VITAE

PERSONAL INFORMATION

Surname, Name: Kenar, Halime

Nationality: Turkish (T.C.)

Date and Place of Birth: 9 July 1977, Choumen, Bulgaria

Phone: +90 312 210 5341

Fax: +90 312 210 1542

E-mail: hkenar@metu.edu.tr, kenarhalime@yahoo.com

EDUCATION

Degree	Institution	Year of Graduation
MS	METU Biotechnology Department	2003
BS	METU Biology Department	2001
High School	Mimar Kemal High School	1995

ACADEMIC EXPERIENCE

Year	Place	Enrollment
2001-2008	METU Dept. of Biological Sciences	Research Assistant
2005-2006	Massachusetts General Hospital, Harvard Medical School Tufts University	Visiting Researcher

FOREIGN LANGUAGES: Advanced English, Intermediate Bulgarian

PUBLICATIONS

1. H. Kenar, A. Kocabas, A. Aydinli, V. Hasirci. Chemical and topographical modification of PHBV surface to promote osteoblast alignment and confinement. *J Biomed Mater Res A*. 85(4), 1001-10 (2008)
2. V. Hasirci, H. Kenar. Novel surface patterning approaches for tissue engineering and their effect on cell behavior. *Nanomedicine* 1(1), 83–100 (2006)
3. H. Kenar, G. Torun Köse, and V. Hasirci. Tissue Engineering Of Bone On Micropatterned Biodegradable Polyester Films. *Biomaterials* 27, 885–895 (2006)
4. H. Göktaş, G. Oke, H. Kenar, and V. Hasırcı, Plasma Based Electron Beam Generator and Its Nanobiomaterial Related Applications. Book chapter in *Plasma Polymers and Related Materials (COST Action 527)*, Hacettepe University Press, Ed. in chief. Mehmet Mutlu, Eds. George Dinescu, Renate Förch, Jose Miguel Martin-Martinez, and Jiri Vyskocil, (2005)
5. G. Torun Köse, H. Kenar, N. Hasırcı, V. Hasırcı, Macroporous poly(3-hydroxybutyrate-co-3-hydroxyvalerate) matrices for bone tissue engineering, *Biomaterials*, 24(11), 1949-1958 (2003)